AN INVESTIGATION INTO THE INFLUENCE OF BOND DEFECTS ON THE BEHAVIOUR OF RC BEAMS STRENGTHENED WITH CFRP

mgr inż. RAFAŁ BIAŁOZOR

Department of Structural Engineering
Faculty of Civil Engineering

Supervisors: prof. dr hab. inż. Jan Kubica
dr inż. Marcin Górski, prof. PŚ

Silesian University of Technology

March 2023

This page intentionally left blank

ACKNOWLEDGMENTS

ABSTRACT

The use of Carbon Fiber Reinforced Polymer (CFRP) is one of the most popular methods of strengthening existing reinforced concrete structures nowadays. Many civil engineering structures are strengthened this way. After many years of using CFRP strengthening techniques, more and more concerns are dictated by its lifetime durability, gradual deterioration as well as quality assessment of the bond between composite and concrete. Whenever any kind of defect is detected in the bond, there is no simple answer to how it affects the structural member. That is why the fundamental aim of the thesis is to investigate the behaviour of reinforced concrete beams strengthened using CFRP strips with existing defects in the bond.

For the purpose of a better understanding of relevant factors affecting the studied strengthening system and phenomena governing its behaviour, a brief literature review was presented based on available data. Previously conducted studies concerning 'the effect of the defects' were used as a reference to further work.

The experimental part of the thesis consisted of two series of RC beams strengthened with CFRP strips, with a different number of stirrups. As a result, the influence of defects on predicted failure mode was analysed. In each series, three selected defects locations along the beam, on ultimate load also were studied. To observe the influence of the defect size ratio, an additional specimen with a relatively large defect was introduced. Experimental work was preceded by an investigation of materials.

To verify the predictive possibilities of numerical simulations, an additional part of the study was dedicated to finite element analysis. This part focused on the selected strategy for numerical modelling of strengthened RC beams with the initiated defects. The data obtained from the experimental study allowed for the validation of numerical calculations. For an additional level of verification of FE simulations, an independent numerical tool was developed based on fibre-beam analysis and strain limitation concept. Thanks to the extended numerical study, the relationship between the midspan defect size ratio and the ultimate load was determined for the adopted beam geometry. Additionally, more insightful observations were made on the damage initiation criterion and damage evolution along the beam. Numerical calculations show that the damage is initiated discretely around the defects, in the proximity of the point load and at the ends of the strip in the case of the conducted four-point bending test.

Received conclusions and observations from the study can be useful as a base for further work in the point of view of formulating guidelines and simplified procedures for dealing with defects that are detected during the inspection of passive strengthened structural members in bending with the use of CFRP strips.

CONTENTS

SYMBOLS

In this study, the most commonly appearing symbols were presented below.

GREEK LETTERS

Δ_{eff}		strengthening efficiency
Δ_{red}	-	capacity reduction factor
ε_c	-	strain of concrete
ε_{cu}	-	ultimate concrete strain
ε_f	-	strain of CFRP
ε_s	-	strain of steel
ε_y	-	yield strain
κ	-	curvature
λ	-	load increment
φ	-	creep coefficient
$\sigma_1, \sigma_2, \sigma_3$	-	principle stress directions
σ_{fd}	-	stress in CFRP due to ultimate load
τ_{max}	-	maximal shear stress
ν	-	Poisson's ratio

LATIN LETTERS

A_{def}	-	area of the defect
A_{tot}	-	area of total bonded CFRP strip
A_{s1}	-	the cross-section area of bottom steel reinforcement in the RC beam
A_{s2}	-	the cross-section area of top steel reinforcement in the RC beam
b_c	-	width of concrete beam
b_f	-	width of CFRP strip
d_c / d_t		CDP concrete damage parameter in compression/tension
D	-	damage evolution variable of CFRP-concrete interface
E_{cm}	-	elastic modulus of concrete
E_s	-	elastic modulus of steel
E_{sh}	-	hardening modulus of steel
E_f	-	elastic modulus of CFRP
f_{ck}	-	characteristic compressive strength
f_{cm}	-	mean compressive strength value
f_{ck}	-	characteristic compressive strength
f_{ctm}	-	mean tensile strength value
f_y	-	yield strength of steel

$2F\ (2P)$	-	the total value of acting point loads in four-point bending tests
G_f	-	fracture energy of the concrete-CFRP interface
k_b	-	width coefficient
l_{Eb}	-	effective bond length
L	-	length
$M\ /\ M_{Ed}$	-	value of bending moment/design value of bending moment
$M_{Rk}\ /\ M_{Rd}$	-	characteristic / design value of bending moment capacity
P_u	-	ultimate load
Q	-	variable of damage initiation criterion
R	-	radius
s_f	-	ultimate slip
t_f	-	the thickness of the CFRP strip
u	-	mid-span deflection
u_x, u_y, u_z	-	displacement in x,y and z direction

MATRIXES AND TENSORS SYMBOL:

$\boldsymbol{D}$	-	elasticity matrix
$\boldsymbol{\varepsilon}$	-	strain tensor
$\boldsymbol{\varepsilon}^p$	-	plastic strain tensor
$\boldsymbol{\sigma}$	-	stress tensor

IMPORTANT ABBREVIATIONS:

CAD	-	Computer-Aided design
CCS	-	Concrete cover separation failure mode
CFRP	-	Carbon Fiber Reinforced Polymer
EBR	-	Externally bonded reinforcement
EXP	-	Experimental results
FB	-	Fibre-beam analysis
FEA	-	Finite element analysis
FIT	-	The function of least-squares approximation
GFR	-	Gauge factor
IC	-	Intermediate crack debonding failure mode
IRT	-	Infrared thermography
PE	-	Plate end debonding failure mode
RC	-	Reinforced concrete

1. BACKGROUND AND MOTIVATION

1.1. INTRODUCTION TO THE RESEARCH

Nowadays, the technology of strengthening and rehabilitation existing reinforced concrete (RC) structures is a widely used practice in the civil engineering industry, especially when more and more focus is put on sustainable development. So far, it is still economically and environmentally justified to strengthen existing structures rather than demolish old ones and build new ones. Externally bonded reinforcement (EBR) in the form of steel plates was a popular type of strengthening of structures since the mid-20th century [100]. In the early '80s, the building industry draws more attention to lighter and non-metallic materials in the form of fibre-reinforced polymers (FRP). Today, it is almost three decades since the first industrial use of carbon fibre-reinforced polymers (CFRP) took place in Switzerland to strengthen a Rhine bridge [26]. From that time a large amount of theoretical and applied research all around the world was dedicated to the description of mechanical behaviour and the application of such strengthening systems in various types of structures. Among others: RC, steel [86], masonry [91] and wooden [159] structural members in bending, shear [77] and torsion [42] were investigated. As a consequence, it resulted in the formulation of a few guidelines and standards for design purposes [N1][N5][N9][N10][N17], especially in RC structures. After many years of using CFRP strengthening techniques, more and more concerns are dictated by its lifetime durability, gradual deterioration as well as quality assessment of the bond between composite and concrete.

1.2. OUTLINE OF THE PROBLEM

In the strengthening life cycle, there are two basic scenarios when a current state of strengthening needs to be verified. Firstly, quality control is required to be done right after strengthening execution. The surface of structural members prepared in a regardless way can result in hidden defects or voids as well as discontinuities between concrete – adhesive or adhesive - CFRP interface. Bond quality control does not refer only to the construction stage but also is required during periodic inspections of existing structures [N18]. Rapid technological progress in recent years led to the development of various non-destructive evaluations (NDE) of strengthening systems that can deliver detailed data about the state of strengthening and the potential defects. Discontinuities revealed in the bond, imply the need for the correct assessment of the structural performance of strengthened members. This type of issue has to be subjected to engineering judgment and leads to the fundamental conundrum - what actions need to be taken, what criteria for acceptable defect level have to be chosen or how member capacity should be estimated taking

revealed bond defects into account. There is a natural presumption that voids result in local delamination of the strengthening composite material (especially in the case of passive strengthening), which may lead to a stage where the bond does not meet the required criteria anymore. Simplified calculation methods of CFRP strengthened members usually assume a perfect bond between composite and concrete. That is why, a more complex approach needs to be taken, given that the crucial aspect of the effectiveness of this kind of strengthening lies in adhesive bond. Although available manufacturers' design guidelines for nondestructive evaluation of strengthened RC structures indicate possible inspection methods, in the practice, they are limited mainly to visual inspection and tap test [N18]. So far, it is not clear if any acceptable level of defect size in FRP-bonded members exists, thus if any air voids or delamination are detected, (which is based usually on the worker's perception) laminate should be replaced with the new one [128]. The lack of qualitative and quantitative guidelines for acceptable defect levels may lead to conservative conclusions and unnecessary economic loss.

1.3. WORKFLOW CONCEPT

Many studies are dedicated to the constant development of existing NDE techniques in a more and more automated manner. This creates new opportunities for a more convenient way to go through the decision-making process during inspections. An investigation into the structural performance of strengthened structural members with bond defects is also a part of a wider concept of the automated diagnostic workflow. An attempt to create such a workflow is a subject of research at Silesian University Technology [1][9][37][46]. The main goal of this research is to develop a tool for the diagnostic of strengthened engineering structures even in hardly accessible places, that gives information on the structural performance of the structure as feedback (*see Fig. 1.1*).
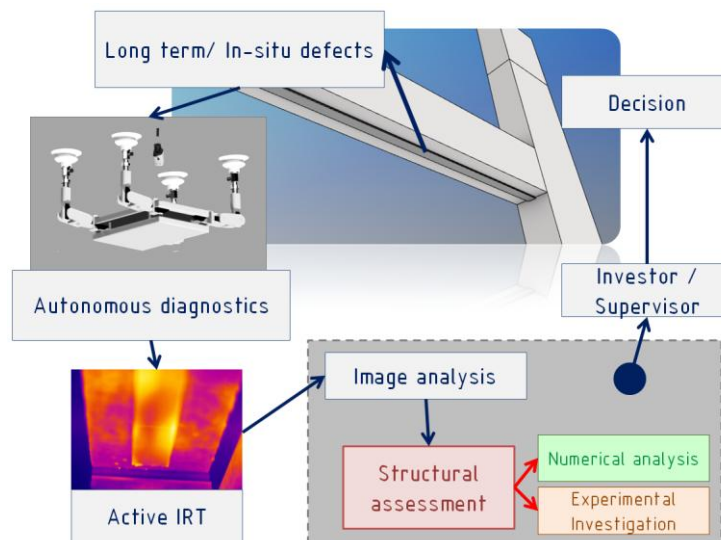
Fig. 1.1. General workflow concept

The creation of an effective workflow is a multilevel challenge where a wide range of engineering branches need to be involved. There are many steps to develop: robotics, data acquisition, reliable defects detection method, data conversion as well as structural analysis assessment that answers if the defect level is acceptable. Although this research focuses mostly on the influence of defects on structural performance, a brief description of the whole concept was presented below.

1.3.1.   DEFECTS AND SELECTED NDE METHOD

Precise FRP strengthening quality control not only requires information if a defect exists or not but also information about its size and localization. For inspections of composite structures, a few non-destructive methods are used such as dynamic [112], acoustic, radiographic [159] and ultrasonic testing [126]. Among them, a method of infrared thermography (IRT) can be found that seems to have the required potential. A wide range of studies was dedicated to thermal diagnostics and defects identification in the bond between CFRP and concrete [109][148][151][155]. In the active infrared thermography pulse, pulse-phase and transient methods can be distinguished depending on how the spatial temperature field is treated during the experiment. An example of IRT diagnostic measurement was presented in Fig. 1.2.
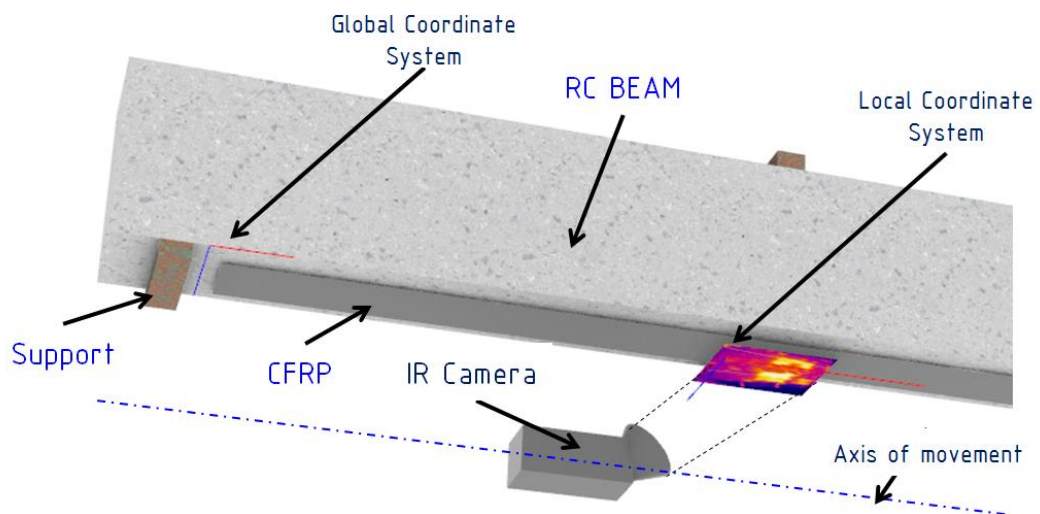
Fig. 1.2. General diagnostic measurement setup for IRT NDE

The transient technique gives results that are independent of the local emissivity based on the inverse analysis, applied to retrieve the values of the thermal resistance between the CFRP and the concrete [1]. The studies show that temperature response over time is higher in defective areas in comparison to non-defective ones [134][143]. As a result of using this method, an image of the bond with potential defects can be received.

1.3.2. AUTOMATED DATA ACQUISITION

Data (image) acquisition can be processed manually but also in an automated manner. The second way is especially important in non-accessible places or areas where access generates high-cost eg. in the middle of the span of the bridge or inside girders. For this reason, robotic devices and drones are more and more often developed and used (*see Fig. 1.3*) where track drive, wheel drive vehicles and drones can be distinguished depending on specific use [37][51]. The recorded data via a thermographic camera is transferred to the local PC via a set of microcontrollers and sensors installed on the device. In the case of external FRP flexural strengthening which is mostly applied linearly, the important issue is to keep track of coordinates according to the chosen reference point. Thermographic images need to be taken the required number of times depending on strengthening length and coordinates to allow localising defects along strengthening.

a)   b)
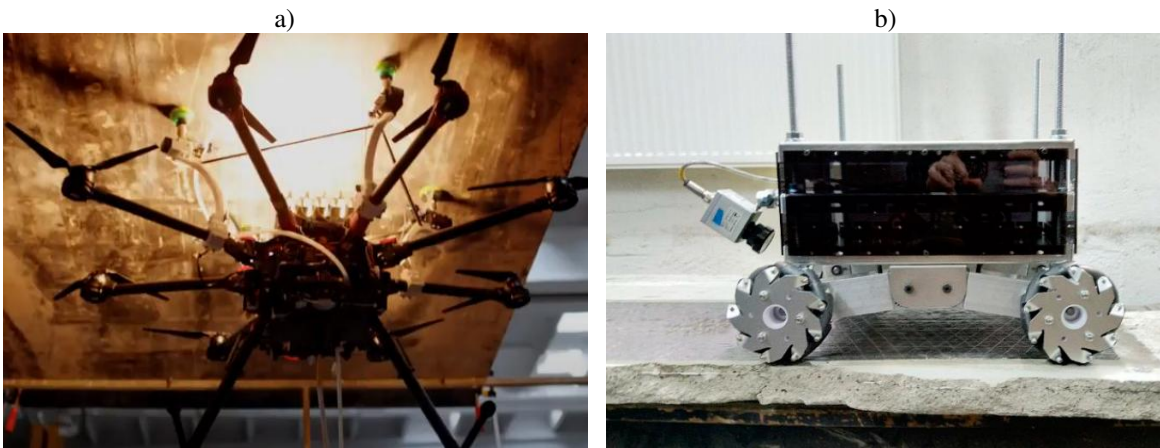
Fig. 1.3. Aerial device a) and wheel drive vehicle b) for top and bottom surface inspection [37]

1.3.3. IMAGE TO CAD CONVERSION

Images created in the previous step are a powerful database about the structure not only when it comes to visual checks but also for digital or numerical investigation. Each image in its digital representation is formulated as a grid of pixels with a specified size depending on its resolution (*see Fig. 1.4*). Each pixel handles information about its colour. In the case of an RGB pallet, it is defined by numbers that take values from 0 to 255 in three-dimensional space. Converting images from colour to monochrome, numeric representation is reduced to one dimension which is much more convenient for retrieving extreme temperature areas. For this purpose, an author developed a python script that has been used for analysing images pixel by pixel where a two-dimensional matrix of numbers is created as a result. Numeric boundaries of the created matrix are remapped based on the max/min boundaries of the temperature scale of the input image.
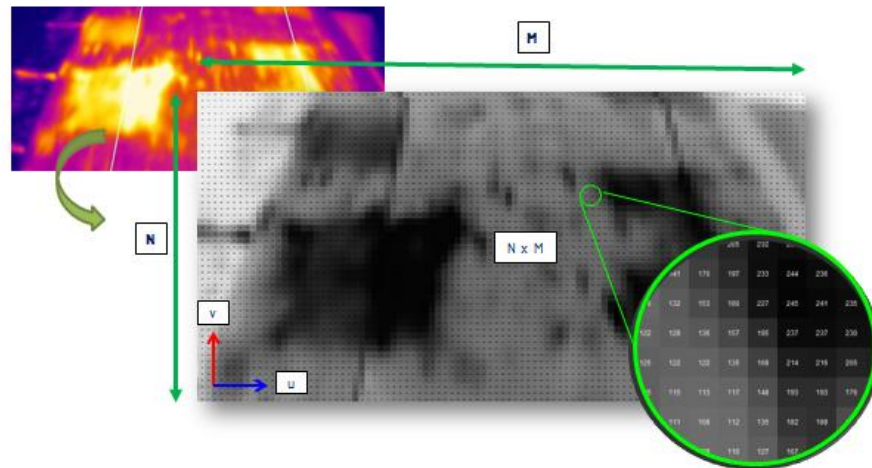
Fig. 1.4. Image transformation and its numeric representation.

Usually, the camera is not directed perpendicular to the surface because of the reflecting phenomenon. For this reason, the image is somehow distorted. However, when the distance range from the camera to the object is relatively small, this issue can be neglected. In the general case, the image geometry should be transformed with an assumed level of acceptance of its representation in perpendicular projection, knowing the distance from the camera to the object and its inclination.

In addition to information about colour, each pixel has its own coordinates (u,v) based on which the point object can be defined in scaled 2D image space.

By filtering out the assumed temperature level which is considered a defect of photography (*Fig. 1.5a*), shapes in form of point clouds are created (*Fig. 1.5b*). The outline of the defect is received by solving the mathematical convex hull problem. As a consequence approximation of the defect outline is obtained as a polyline in CAD representation (*Fig. 1.5c*). At this point, such representation can be used to estimate the revealed defect area and compare values to acceptable defect levels if a proper nomogram or guidelines will be available. On the other hand, it can be stored in a digital model of structure (digital twin concept) or can be used for advanced numerical analysis.
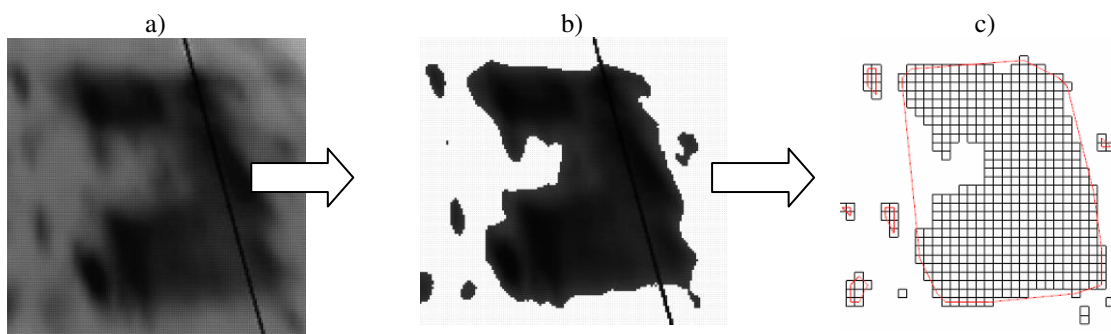
Fig. 1.5. a) image from IR camera, b) filtered temperature range,
c) automated CAD approximation of the defect (red line).

1.3.4. FROM ALGORITHM TO DIGITAL MODEL

For described workflow, a complementary feature can be added to increase automation of the structural analysis of strengthened structures where defects could be taken into account until specific guidelines for defects will be created. To perform analysis, the numerical model is generated, which is a digital representation of the existing structure that includes all of the data of material models, geometry and boundary conditions (*Fig. 1.6a*). Usually, the numerical model is created manually in the target FEA software each time. However, the design process of reinforced concrete members such as beams or slabs is repetitive to some extent. By recreating and properly composing structural rules, an algorithm could be defined (*Fig. 1.6b*) that generates structural member geometry as an output.
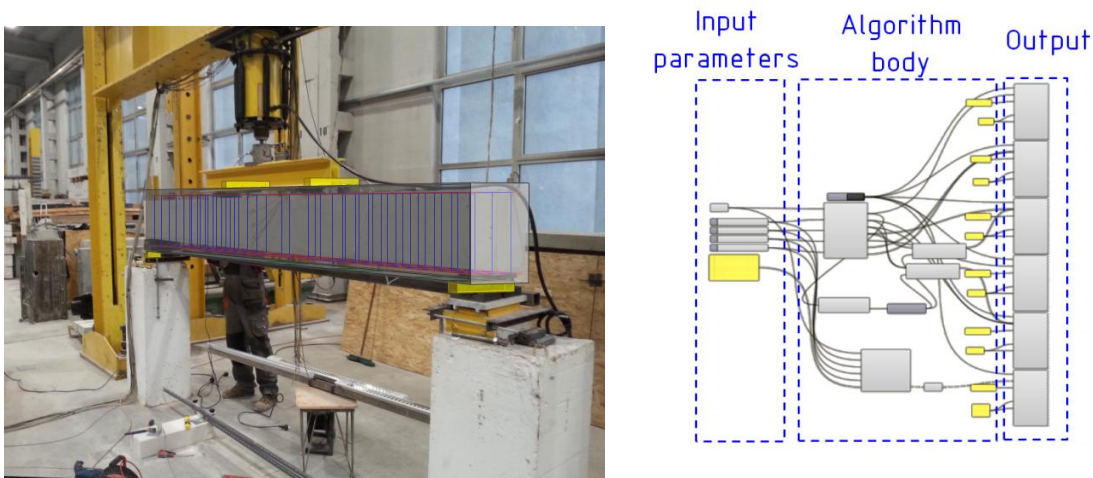
Fig. 1.6. a) Laboratory and digital RC beam models investigations b) block representation of the algorithm of RC beam in the parametric design concept.

As a result, from one properly prepared and developed algorithm, an adaptable numerical model is obtained whenever the algorithm is called by changing input parameters. This is known as the concept of parametric design [10][13][28]. Parameters can be different in various strengthening scenarios. In the simplest case, rectangular beam cross-section dimensions, beam length, main reinforcement spacing, stirrups spacing, strengthening geometry and most important: defect geometry and position along the beam, can be set as input parameters in the algorithm. Most of the input data for the algorithm is used to be available in the design reports as structural data of the existing structure.

1.4. RESEARCH AIM AND SCOPE, OBJECTIVES AND LIMITATIONS

Regardless of how the quality control is carried out (manually or automatically), the problem remains the same - how to estimate the load capacity of a component with present defects? Very limited research in this civil engineering field pays attention to defects' influence on strengthened beams. Some of them indicate that the structural performance of passive flexural strengthening may vary depending on the location of the defect and some cases can be neglected. As far as known, there are more parameters influencing the behaviour of flexural strengthening RC beams [N5] and failure modes [81] that should be taken into account to create more general quantitative guidelines to support engineering judgment. Engineering research usually starts from scientific curiosity accelerated by doubts and questions that occur in engineering practice and cannot be answered in a satisfactory manner with the current state of knowledge. In considered context, such questions that this study is going to answer can be formulated as follows:

- Is it always necessary to replace applied CFRP laminate no matter how big the defect or air void is detected in the bond?
- Is it possible to arrange and classify geometrical properties of air voids (dimension, quantity, percentage, distance) based on which it can be decided that the laminate safety level is no longer acceptable?
- Can failure mode be controlled by the bond defect regardless of the predicted failure mode with the perfect bond or can failure mode be changed?
- Is it possible to estimate the flexural capacity of CFRP-strengthened RC members based on records of bond defects detected along the laminate?
- Can the behaviour of the flexural strengthened members with defects in the bond be satisfactorily represented in the numerical simulations?

Given the above, the main aim of this study is to investigate the influence of bond defects on the behaviour of CFRP flexural strengthened RC beams in both laboratory tests and numerical simulations.

Considering that the investigation deals with the safety aspect, conclusions based on this study should be formulated in a gentle and careful manner. It is necessary to set the limitations of this study that need to be taken into account:

- Only flexural passive strengthening of rectangular RC beams with the use of CFRP strips is considered,
- The study is limited to strengthened beams with defects subjected to monotonic load only.

1.5. ORGANIZATION OF THE THESIS

The thesis consist of six chapters described briefly below.

- **CHAPTER 01 – BACKGROUND AND MOTIVATION** – description of the background and motivation of this study, the problem definition, aim and scope as well as its limitations.

- **CHAPTER 02 - INTRODUCTION** - presents an overview of issues related to passive CFRP strengthening. Attention is focused on parameters affecting strengthening, failure modes and defects which leads to a better understanding of crucial aspects from the point of view of this study when defects are taken into account.

- **CHAPTER 03 - EXPERIMENTAL PLAN, RANGE AND METHODOLOGY** - presents an experimental plan and assumptions that have been made. It provides details of test specimens, experimental setup, test procedures and measurements used in tests.

- **CHAPTER 04 – EXPERIMENTAL INVESTIGATION** - In this chapter, an experimental study is presented. Work starts from the investigation of materials used in the research, through the results of full-scale beam specimens with applied defects.

- **CHAPTER 05- NUMERICAL ANALYSIS** - deals with numerical modelling of the structural response of CFRP-strengthened RC beam with bond defects. A review of the numerical methods used in the research also was briefly presented. The experimental findings, received in the previous chapter, are used as a reference for the validation of models.

- **CHAPTER 06 - SUMMARY** - discuss the findings of the research presented in the previous chapters. Conclusions, as well as recommendations for further research, are formulated.

2. INTRODUCTION TO CFRP STRENGTHENING

2.1. BRIEF INTRODUCTION TO FRP MATERIALS

FRP is a group of composite materials consisting of the polymer matrix and a wide range of fibres, composed and manufactured for many purposes. Many fields including aerospace, aircraft, railway, automotive, sport, and even the clothing industry are direct recipients of FRP materials, mainly because of their high strength-to-mass ratio. The building industry uses FRP as an externally bonded reinforcement (EBR), an internal reinforcement as rebars [45], and directly as prefabricated structural members [135]. Nevertheless, still, the most recognized application of the FRP in the civil engineering environment seems to be the technology of strengthening and rehabilitation existing reinforced concrete (RC) structures (*see examples presented in Fig. 2.1).* There are many reasons that RC structures may require the use of strengthening including:

- increase of the load capacity as a consequence of functionality change,
- insufficient reinforcement in case of design or construction in-situ mistakes,
- structural alterations as a supplementary reinforcement,
- structural damage or to improve seismic resistance,
- repair deteriorated structural members.

a)   b)
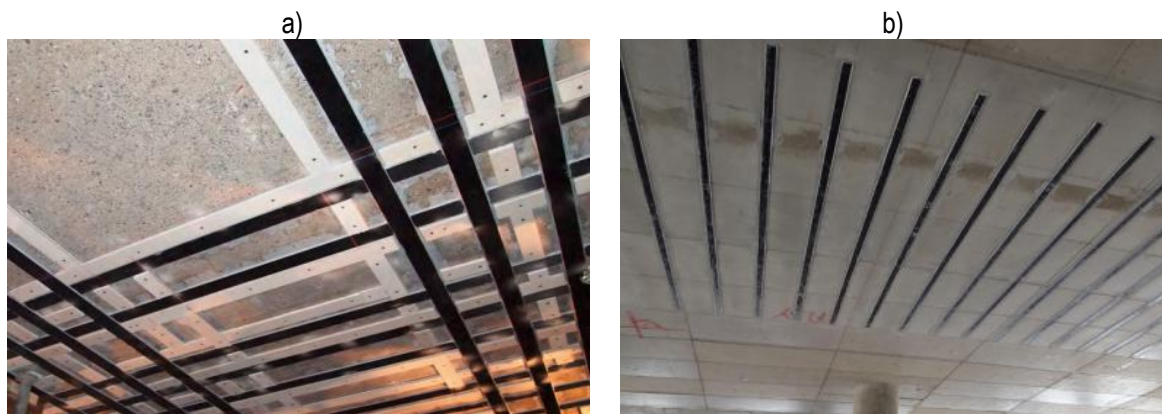
Fig. 2.1 Examples of FRP strengthening application [128] I two a) and one direction b)

FRP material consists of fibres, resin matrix, and adhesive. For FRP materials a wide group of fibres can be used where glass, aramid, basalt or carbon fibres are most common. Different kinds of fibres have different sets of mechanical properties and tolerance for environmental influences (*see Table 2.1 and Fig. 2.2a*) [74][159]. In this study, only carbon fibres will be further taken into consideration.

Table 2.1. Mechanical properties of selected fibres according to [N5]

	Young's modulus [GPa]	Tensile strength [MPa]	Ultimate tensile strength [%]
Aramid	70 - 130	3500 - 4100	2.5 - 5.0
Carbon	215 – 700	2100 - 6000	0.2 - 2.3
Glass	70 - 90	1900 - 4800	3.0 - 5.5
Basalt	80 - 90	2500 - 3200	3.0 - 3.5
Natural	30 - 70	500 - 1500	1.5 – 4.0

Depending on a destination, there are several types of CFRP strengthening: wet lay-up systems, systems based on prefabricated elements and also special systems (e.g prestressed or near-surface mounted etc). A strengthening system based on pre-cured strips with unidirectional fibres is usually recommended for straight and plane surfaces. Wet lay-up systems in form of sheets or fabrics with one- or two-directional fibres are more flexible and applicable also to out-of-plane surfaces.
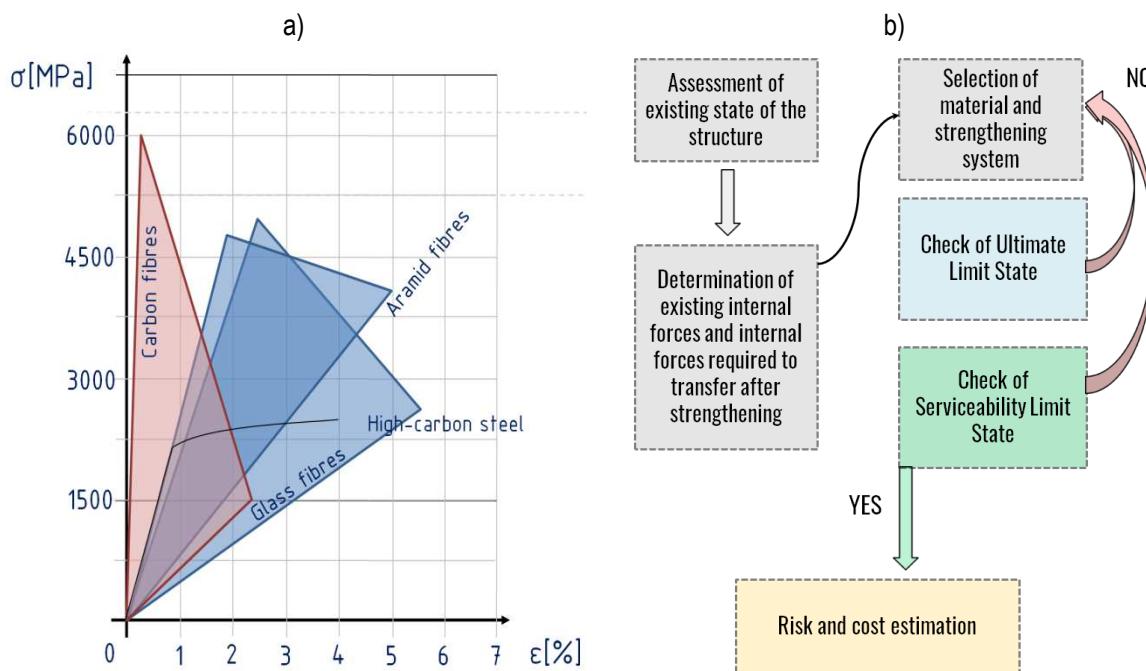
Fig. 2.2 a) Comparison of fibres' mechanical properties ranges (based on [42])
b) flowchart of the design of the strengthening system (based on [100])

CFRP strengthening system is typically manufactured in a pultrusion process [44]. Direct use of CFRP materials, is proceeded by the design stage where the pros and cons of strengthening material choice in a particular case are considered. An example of a flow chart formulated for the design process of strengthening [N17][100], is presented in Fig. 2.2b.

2.2. THE GENERAL BEHAVIOUR OF CFRP-STRENGTHENED RC BEAMS IN BENDING

Understanding the behaviour of CFRP strengthening and its limitations are crucial steps in understanding undertaken design solutions and utilizing them for the right application, as well as in the context of this study. Over the years, many studies were conducted to recognize CFRP strengthening behaviour mainly on RC beams in bending where various factors and boundary conditions have been taken into account. A general trend in load - mid-span deflection response of idealised CFRP strengthened RC beam based on laboratory four-point bending tests under incremental load was presented in Fig. 2.3.
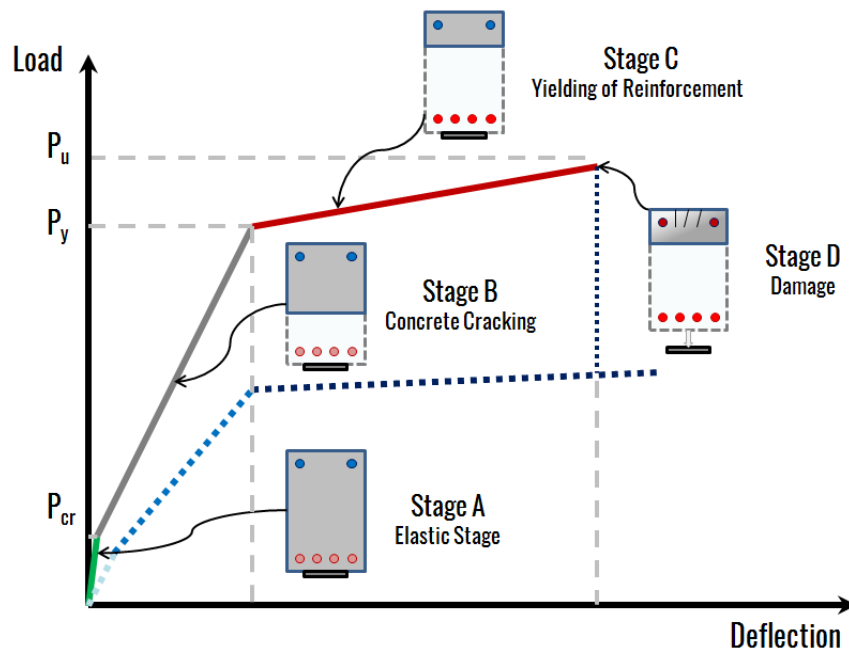
Fig. 2.3 Typical flexural stages of CFRP strengthened RC members until failure (based on [14])

In reference to non-strengthened RC members, a few similar phases can be distinguished in the full load range. At the very beginning, the strengthened RC beam remains fully in the elastic range (stage A), until the concrete reaches its tensile strength. After the load reached a certain value corresponding to the cracking moment, the structural member in the crucial section enters stage B. In this stage, developing cracks cause a weakening tension zone of concrete and cause a movement of the neutral axis in the beam cross-section. Moreover, forming cracks leads to loss of initial stiffness of concrete which results in higher deflection of the cracked beam in comparison to an idealised uncracked beam with the same load level. A decrease in stiffness can be observed as a more horizontal slope on the load-deflection plot. The next phase (phase C) is initiated by exceeding reinforcement yield strength in a critical cross-section followed by increasing plastic strains of reinforcement due to increasing load level until failure. However, depending on the geometry, properties of used materials and their application, failure (phase D) can occur after as

well as before phase C. Nevertheless, such ductile behaviour where yield strength of reinforcement is reached and followed by damage due to concrete crushing or delamination of composite is usually considered a desirable failure in terms of safety in both RC and CFRP-strengthened members. The different forms of damage are usually described in the literature under the term 'failure modes'. On the whole, there are a few failure modes that were observed in laboratory tests of strengthened beams [81][141]. They can be divided into two main categories:

- where composite action between concrete and strengthening remains,
- where the loss of composite action of strengthening occurs.

2.3. FULL COMPOSITE ACTION

In the first group concrete crushing in the compressive zone (*Fig. 2.4a*) and laminate rupture (*Fig. 2.4b*) without debonding can be distinguished, preceded or followed by steel yielding. However, in the case of carbon-based composite fibres, rupture failure is hardly ever observed due to its high tensile strength [87].
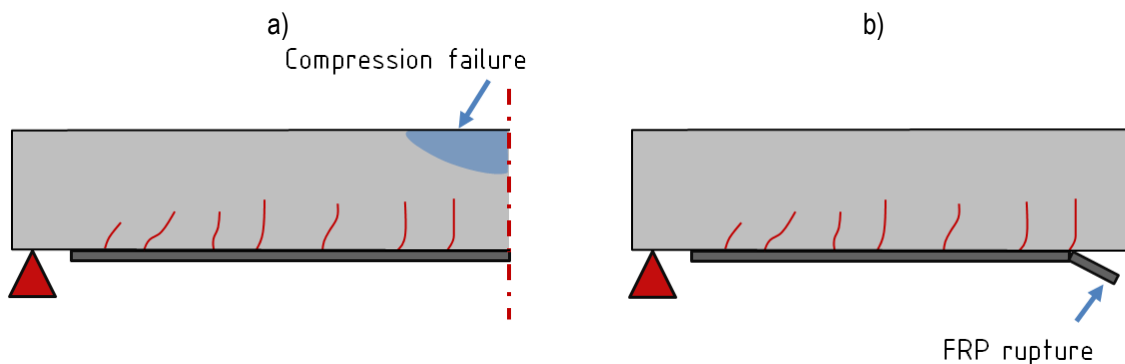
Fig. 2.4 Failure modes with remained CFRP – concrete bond
a) failure at concrete compression zone b) CFRP rupture

When full composite action remains, basic simplified principles of design of the cross-section in bending strengthened with externally bonded CFRP composites are quite similar to the traditional elastic design of reinforced concrete structures in bending [N4][N5]. Hence, the main assumptions are: the plane section remains plain before and after bending as well as tensile stress acting on concrete is neglected. The major principle is an assumption of the perfect bond between steel reinforcement and concrete and crucial from point of view of this study - full composite action between the CFRP and the concrete substrate. The estimation of the capacity of the strengthening section is based on the strain limitation of section components.
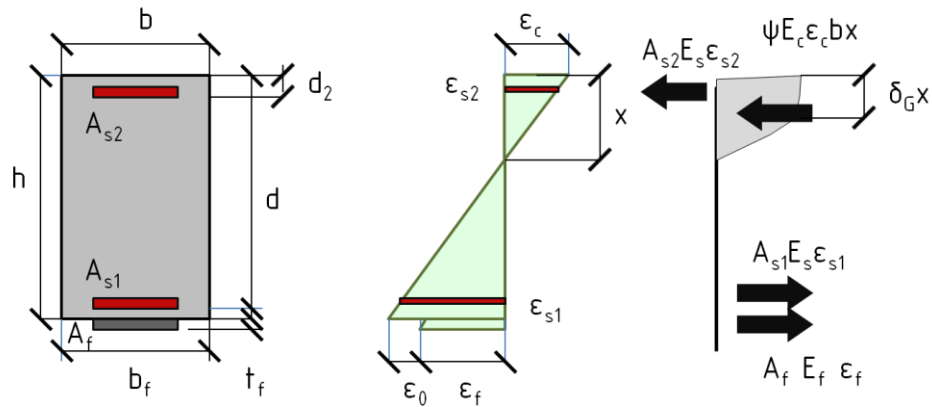
Fig. 2.5 General case of analytical method of cross-section design

In the analytical approach, the design moment resistance can be obtained from moment equilibrium. A few design cases need to be considered, depending on the failure mode. Then strain quantities in Fig. 2.5 are replaced by proper limit values (for an explanation of the symbols see the list at beginning of the thesis). The most desired failure is the yielding of the tensile steel reinforcement and crushing of concrete when CFRP bond interaction with concrete is still maintained [N5]. Neutral axis depth x and flexural resistance of cross-section can be calculated from strain compatibility and internal force equilibrium. Then calculated strain values in internal steel reinforcement and external composite reinforcement are compared with adequate ultimate strain values. A compressive zone can be limited with the use of coefficients ψ and δ_G [N5]. Additionally, initial strain ε_0 need to be taken into account when strengthened structural member was not fully unloaded before strengthening.

Nevertheless, for the flexural design of the RC strengthened section, a more general numerical-iterative approach based on fibre-beam elements and the same ultimate strain concept of materials can also be used [142][27]. It is a direct result of the mechanical properties and generalization of previously introduced principles of the cross-section design method of RC structural members. An advantage of such an iterative approach is the possibility of applying the nonlinear stress-strain relationship of material used as cross-section components. It is particularly important in the case of brittle-plastic materials like concrete where tensile and compressive behaviour can be taken into account. In this study, this method was used as another level of verification of the main numerical analysis and the procedure was described in Appendix A. The main numerical analysis using the finite element method also can be used for calculations of strengthened members in both cases: full composite action and when composite action loss is expected. Finite element analysis (FEA) was presented and described in chapter 5.

2.4. LOSS OF COMPOSITE ACTION

Apart from design based on full composite action, it is required to prevent occurring debonding failure modes. That is why bond plays a crucial role in externally bonded strengthening systems. The most observed type of failure is the loss of composite action due to debonding. Debonding is understood as a failure that may be initialised at different interfaces (*see Fig. 2.6*).
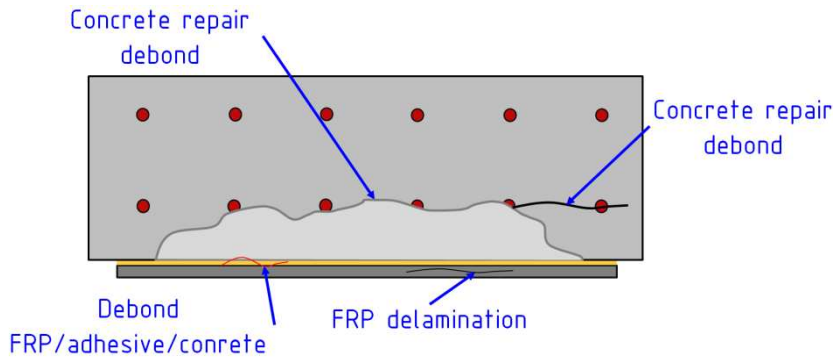
Fig. 2.6 Various bond interface debonding (based on [46])

In the case of RC beam strengthening, various failure modes related to debonding can be found in the literature depending on the initiation point alongside the structural member [81][141]. Hence, two main types can be distinguished: those induced away from the ends of the CFRP (also known as intermediate crack debonding - *Fig. 2.7a*) and those associated with high interfacial stresses near the ends of the bonded plate in a high-shear, low-moment region: (*Fig. 2.7b*) at the level of concrete cover or at the level of bond interface between concrete and CFRP (*Fig. 2.7c*). Some studies, classify the peeling-off of the CFRP due to the unevenness of the concrete surface in this group (Fig. 2.7d).
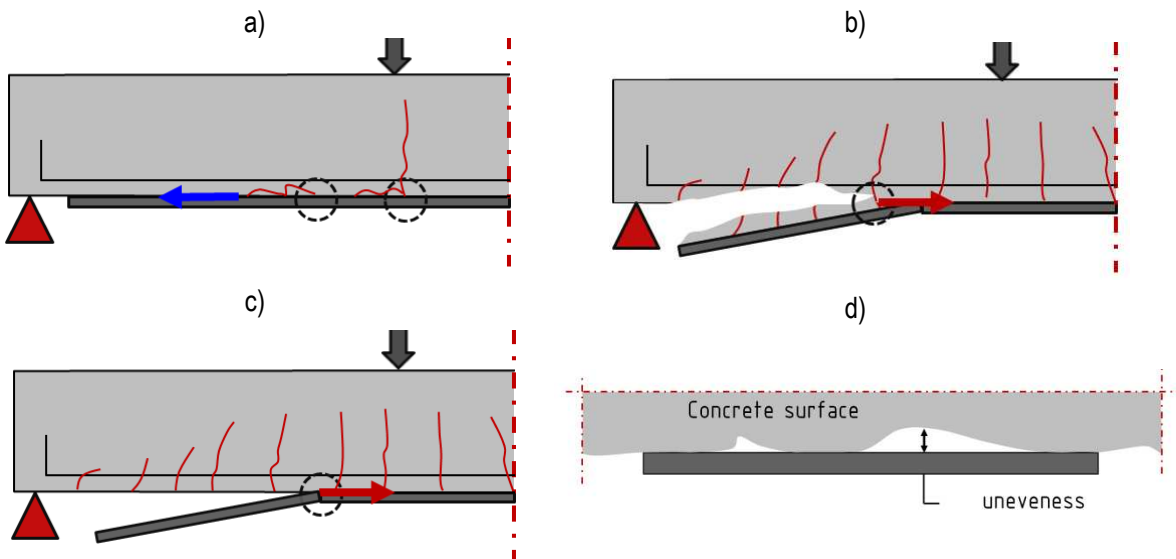
Fig. 2.7 Failure modes due to loss of composite action: end debonding a) concrete cover separation b) intermediate crack debonding c) debonding due to unevenness

2.4.1.   INTERMEDIATE CRACK DEBONDING (IC)

It occurs as a result of the bond interfacial shear stress effects in form of flexural as well as shear-flexural cracks along the RC beam. Debonding is initialised by the cracks bridged by the CFRP and it propagates in a thin layer of concrete towards the end of the CFRP strip. It was noted that the formation of critical initiating cracks can be affected by the loading pattern. According to [N8], for design consideration simplified stress/strain limitation approach can be taken. Then stress and corresponding strain need to be limited and the following criteria need to be met:

$$\sigma_{Ed} < \sigma_{fd} = \min (f_{fbd.IC} , f_{fd}) \tag{2.1}$$

$$\varepsilon_{Ed} < \varepsilon_{fd} = \min (\frac{f_{fbd.IC}}{E_f} , \frac{f_{fd}}{E_f}) \tag{2.2}$$

$$f_{fbd.IC} = \frac{k_{cr.k} k_k k_b \sqrt{\frac{2E_f}{t_f} f_{cm}^{\frac{2}{3}}}}{\gamma_{fb}} \tag{2.3}$$

where:

f_{fd}	-	*the design stress limit value for composite*
$f_{fbd.IC}$	-	*the design value of FRP bond strength corresponding to IC debonding failure mode:*
f_{cm}	-	*mean compressive strength value*
$k_k = 0.17$	-	*coefficient obtained from the statistical procedure as a 5% characteristic value*
$k_{cr.k} = 1.8$	-	*empirical coefficient*
k_b	-	*width coefficient (see 2.5.6)*
$\sigma_{Ed}/\varepsilon_{Ed}$	-	*the design value of stress/strain*
$\gamma_{fb} = 1.5$	-	*safety factor*

A more accurate approach based on the analysis of concrete segments between cracks can be found in [N8].

2.4.2.   END INTERFACIAL DEBONDING/PLATE END DEBONDING (PE)

In this case debonding is associated with high interfacial shear and normal stresses near the ends of the bonded plate (*see Fig. 2.8*). This stress in RC beams is related to the sudden ending of the CFRP strip and it is induced by the curvature of the beam under loading [79]. Failure is initiated at the near plate end and propagates towards the mid-span region. According to [154], this failure mode is most likely to occur with a low plate-width to beam-width ratio. This failure mode occurs usually at the end of CFRP and runs along the beam in a thin layer of concrete near the surface of the composite due to the typical lower tensile strength of concrete in comparison to the adhesive.
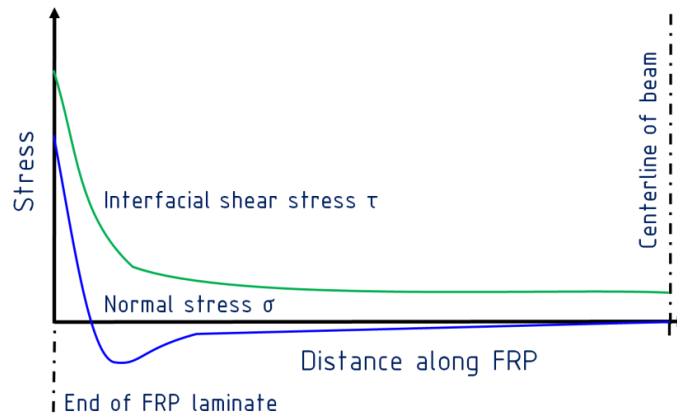
Fig. 2.8 Distribution of bond stress on the surface of the CFRP-strengthened beam

A design indication for avoiding this type of failure is to ensure the required curtailment of CFRP [N8] or to strengthen the anchorage zone.

2.4.3. CONCRETE COVER SEPARATION (CCS)

Unlike plate-end debonding this failure mode usually occurs at the level of bottom internal steel reinforcement due to a shear crack in the end region of CFRP which is related to the low shear strength of strengthened RC element [41]. Failure is initiated at the end of CFRP and propagates towards the middle of the span. Usually, a part of the concrete cover remains at a detached CFRP plate after failure. There are a few different approaches like concrete tooth models or interfacial stress-based models in dealing with CCS failure mode. Most simple and preferred by guidelines CCS design check, based on Jansze's shear strength capacity model and strut and tie (truss) concept [47]. The target truss is set up as a combination of two systems: an unstrengthened member with internal reinforcement only and a member with externally bonded reinforcement [N8]. Failure mode occurs when a tie in the concrete generated due to force in the strip can not be carried by concrete strength due to a missing shear tie between external composite and internal steel reinforcement.

Fig. 2.9 Tuss analogy – strut and tie concept (based on [N8])

Thus, if shear occurs at the end of support (V_{Ed}) exceed shear resistance ($V_{Rd.c.fe}$), additional shear reinforcement at the end of the CFRP strip should be provided:
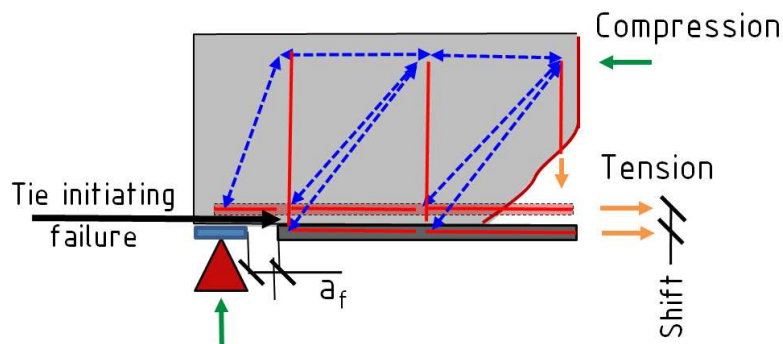
$$V_{Ed} \le V_{Rd.c.fe} = 0.75 \left[1 + \frac{19.6(100\rho_s)^{0.15}}{a_f} \right] V_{Rd.c} \qquad (2.4)$$

where:

a_f	-	*distance between support and end of CFRP strip in mm*
ρ_s	-	*steel reinforcement ratio*
$V_{Rd.c}$	-	*a design shear capacity value of the member without shear reinforcement according to [N4]*

2.4.4. DEBONDING DUE TO UNEVENNESS

It is mostly related to the proper preparation of concrete surface prior to strengthening as well as during the installation process. Again, in FIB90 Builettin [N8] it was mentioned that it is unlikely to cause total debonding. On the other hand, it is recommended to reduce risk by proper treatment of concrete surface that prevents a reduction of internal force transfer due to accidental surface defects. Acceptable values of unevenness (*see also Fig. 2.7*) at the concrete surface (measured from the perfect geometry of the CFRP strip before the application) were presented in Table 2.2.

Table 2.2. Acceptable values of unevenness at strengthened element concrete surface [N5]

Precured CFRP thickness	On a 2.0m base (mm)	On a 0.3m base (mm)
> 1mm	10	4
< 1mm	6	2

2.4.5. BOND STRENGTH

The bond is responsible for transferring forces between all related components - concrete, adhesive and composite. Bond strength is usually determined in shear lap tests (*see Fig. 2.10b*). Mathematically, bond behaviour is usually expressed by a bond-slip relationship which describes the shear stress transfer τ_b and the corresponding slip. The area under the bond-slip curve defines the fracture energy (G_f) of the concrete – CFRP interface (see *Fig. 5.16*). Many bond models have been described [118]. They can be used for the estimation of anchoring forces, crack formations, numerical analysis etc. [N5]. A wide review of advanced bond strength models can be found in [79].
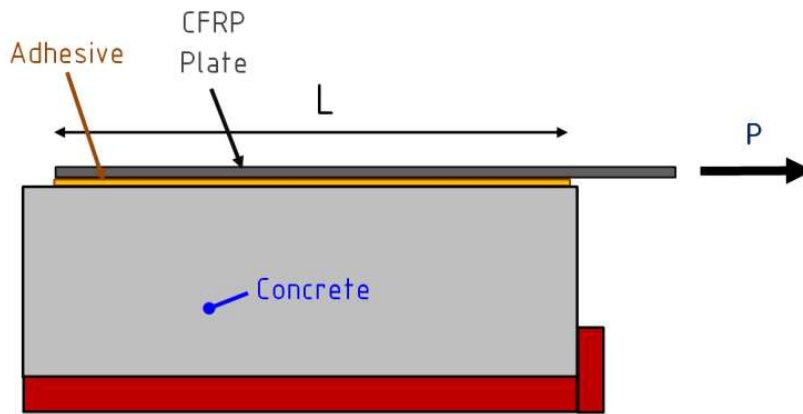
Fig. 2.10 Single shear-lap test setup (based on [130])

2.5. GENERAL FACTORS AFFECTING CFRP FLEXURAL STRENGTHENING

DESIGN RELATED FACTORS

2.5.1. MEMBER GEOMETRY, STEEL, AND CFRP REINFORCEMENT RATIO

When the design of the strengthening of existing members using CFRP is required, data on member geometry, steel reinforcement ratio and material properties usually should be known. Those factors affect own bending capacity of the beam even if it is non-strengthened. By increasing member cross-section size and steel reinforcement ratio, its capacity even without strengthening also increases and as a result the capacity after strengthening increases. That is why it is used to consider quantity like strengthening efficiency instead of direct member's bending capacity. A study conducted by Kamińska and Kotynia [67][82] revealed that the effectiveness of CFRP strengthening of RC beams is higher for the lower value of the steel reinforcement ratio. A higher value of bending moment capacity can be achieved by increasing the CFRP reinforcement ratio (see *Fig. 2.11a*). However, it can be done up to the moment when the value of strain in concrete exceeds the value of the ultimate strain of concrete usually equal to 3,5‰. It has been noted that the debonding process of CFRP starts when strain achieves a value of about 5,0‰. A further study based on a vast numerical parametric study proceeded with laboratory tests [79] shows a clear distinction between failure modes of IC debonding and concrete failure in compressive zone depending on those factors. The relationship was expressed through strengthening efficiency as a function of CFRP reinforcement ratio concrete grade and steel reinforcement.
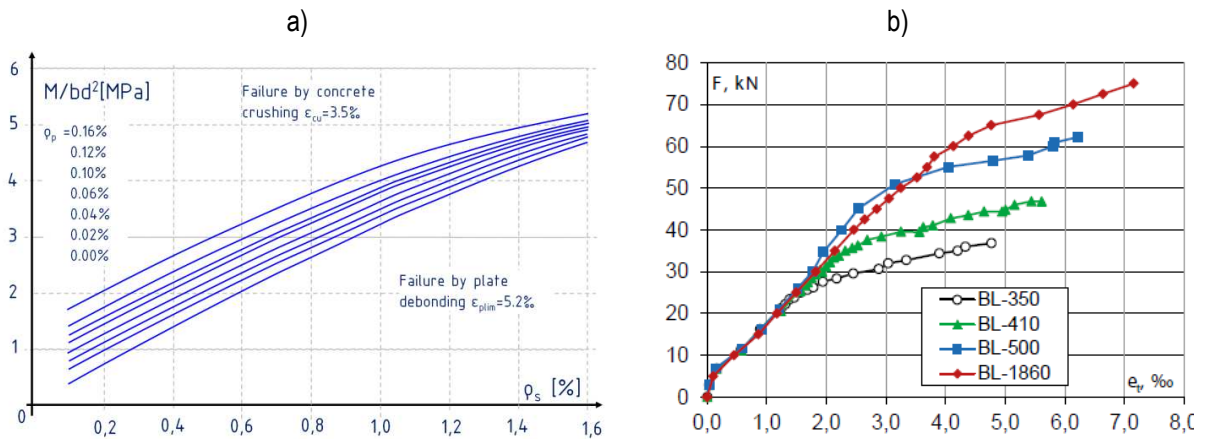
Fig. 2.11 a) steel and composite area ratio relationship for strengthened RC beams in bending (based on [67]) b) load – CFRP strain relationship for different steel grades [12]

2.5.2.   STEEL GRADE

An investigation [12] on strengthened RC beams in bending with different steel grades of internal steel reinforcement confirmed the relationship resulting directly from the mechanical properties of materials. Results in form of a relationship between the applied load of the beams and recorded CFRP strain for different yield strengths of internal steel reinforcement were shown in Fig. 2.11. For reinforcing steel of a yield strength of 360-520 MPa ultimate strain of CFRP was recorded in the range of 4,8-6,2‰. For steel of yield strength, equal 1860MPa recorded ultimate strain value was 7.16‰. The lower value of the steel yield strength for the same steel reinforcement ratio, the lower value of ultimate load and the ultimate strain in CFRP were observed in the study when a relatively low value of concrete strength was used (cubic concrete strength varied from 17.6 to 24 MPa).

2.5.3.   PRELOADING EFFECT AND INITIAL STRAIN PRIOR TO CFRP STRENGTHENING

CFRP strengthening is rarely designed for newly raised RC structures and its most common application is to retrofit existing structures to elongate their life cycle in terms of ultimate and serviceability states of design. Structural members of such structures undergo certain load history and they have some current load and strain states which should be taken into account during the design stage. Several studies have been conducted to investigate the importance of the preloading effect in the flexural strengthening of existing RC structural members [4][49][96][152]. General conclusions from those investigations can be formulated as follows: the higher value of the sustaining load during strengthening application, the lower value of the ultimate load at failure. Moreover, in the study [152] it was noted, that there is no significant difference in the ultimate capacity of strengthened beams when the initial load is the same for specimens with different load histories prior to strengthening. In design considerations, the effect of preloading resulting in initial

strain in strengthened members is commonly taken into account by reducing the CFRP strain by the value equal to the existing concrete strain during the application of composite [87][100] or by assuming initial curvature along strengthened cross-section [79]. Thanks to this approach, the calculated force acting inside the CFRP laminate decrease respectively, but it can influence the serviceability limits of the strengthened member [15]. Guidelines [N9] indicate that initial strain can be neglected in the case when the existing load causes a bending moment that is smaller than the cracking moment of the structural member.

2.5.4. EFFECT OF LOAD DISTRIBUTION

Research on strengthened beams is usually conducted in the point-loading test instead of a uniformly distributed load which usually fits more to the real design cases. A study [40] performed on beams in the flexural test with a different number of loading points revealed an increasing value of the ultimate bending moment at failure with the increasing number of loading points used in the test and simultaneously, more regions with local debonding were observed prior to the ultimate failure and critical crack was observed closer to the midspan. Obtained conclusions in this study indicate that developed debonding strength models based on beams tested in three- or four-point bending can be conservative for design use in the case of beams under uniformly distributed loading schemes.

2.5.5. EFFECTIVE BOND LENGTH

The effective-bond length concept of CFRP strips can be understood in a similar manner to reinforcing bar anchorage length in RC structures. It is a minimum length capable to transfer the required maximal tensile force between the strengthened member and EBR. Increasing the value of effective bond length does not result in an increased possibility of greater stress transfer due to the limitation of fracture energy in the bond. It is determined mostly in the pull-off test [17][76]. In a simply supported beam, it is related to an uncracked zone beyond the outermost crack (*see Fig. 2.12*). That is why it is required to determine the critical section (where the bending moment value is lower than the cracking moment M_{cr}) from which the anchorage needs to be provided.
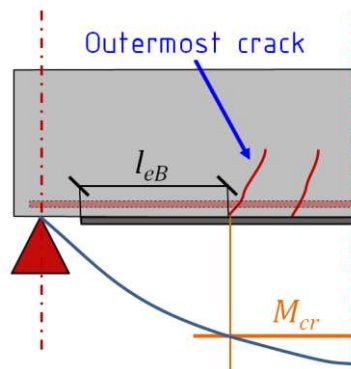

Fig. 2.12 An effective length concept (based on [15])

Over the years different empirical formulas for the minimal effective bond length were proposed (*see Table 2.3*). It can be noted that most of them depend on strengthening as well as concrete mechanical properties.

Table 2.3. Selected formulas for effective bond lengths

HOLZENKÄMPFER [54] (1994)	$l_{Eb} = \sqrt{\dfrac{E_f \cdot t_f}{2 \cdot E_{cm}}}$	(2.5)
CHEN & TENG [17] (2001)	$l_{Eb} = \sqrt{\dfrac{E_f \cdot t_f}{\sqrt{f_{cm}}}}$	(2.6)
fib Bulletin 14 [N5] (2001) fib Bulletin 65 [N7] (2010)	$l_{Eb} = \sqrt{\dfrac{E_f \cdot t_f}{2 \cdot f_{ctm}}}$	(2.7)
ACI 440.2R-08 [N1] (2008)	$l_{Eb} = \dfrac{23300}{\left(E_f t_f n_f\right)^{0.58}}$	(2.8)
CNR-DT 200 R1 [N9] (2013) fib Bulletin 90 (2019)	$l_{Eb} = \pi s_0 \sqrt{\dfrac{E_f \cdot t_f}{8 \cdot G_f}}$	(2.9)

where:

nf -   *number of applied CFRP strips*

Gf -   *fracture energy of the concrete-CFRP interface*

s_0 -   *ultimate slip of bond strength law (see Fig. 5.16).*

t_f -   *CFRP plate thickness*

In most cases, effective bond length depends proportionally on the square root of the part of the axial stiffness of EBR. For this reason, the use of CFRP with higher stiffness requires ensuring a higher value of effective bond length. If the provided anchorage zone is shorter than the effective length, there is a limitation of maximal stress value which the bond is capable to transfer (see *Fig. 2.13*) according to the formula below:

$$l_{Eb} \leq l_{Eb.max} \qquad\qquad \sigma_{fad} = \frac{l_{Eb.p}}{l_{Eb.max}} \left(2 - \frac{l_{Eb.p}}{l_{Eb.max}} \right) \cdot \sigma_{fad.max} \qquad (2.10)$$

where:

$l_{Eb.p}$ -   *provided bond length*

$l_{Eb.max}$ -   *effective bond length*

$\sigma_{fad.max}$ -   *maximal stress which a full bond length is capable to transfer*
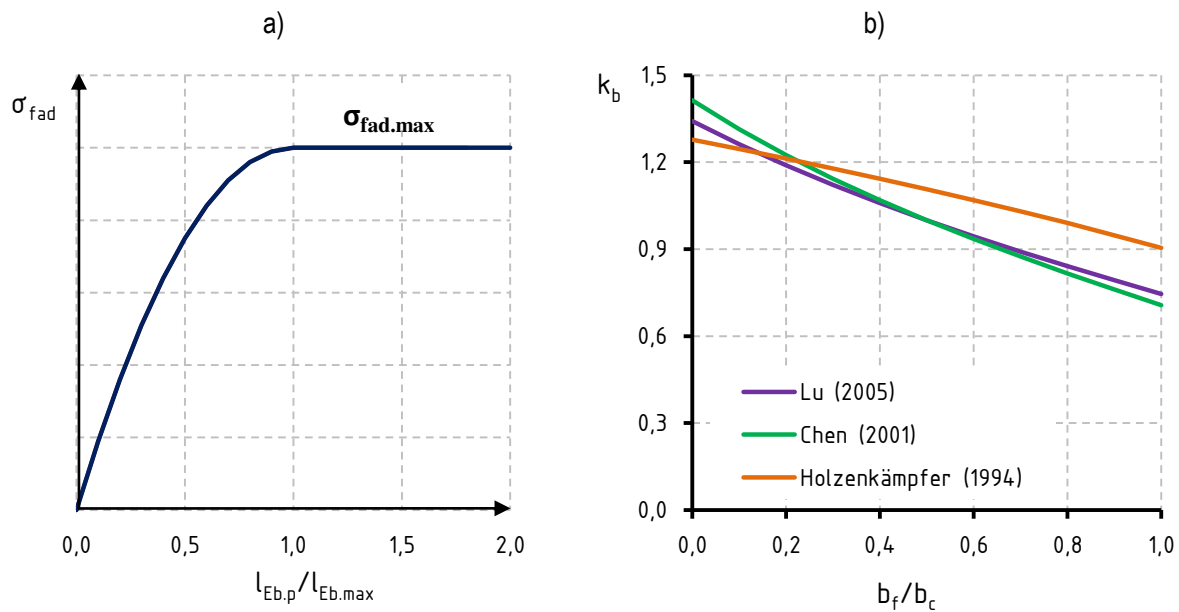
Fig. 2.13 a) Anchorable tensile stress in relation to anchoring length
b) width coefficients in a function of plate width to beam width ratio (described further in the text)

2.5.6. MEMBER WIDTH TO STRENGTHENING WIDTH RATIO

Based on numerous results from pull-off tests Chen and Teng using a regression method determined the linear relationship between ultimate bond strength and the coefficient relating member and laminate width [17]. If the width of the bonded plate is smaller than that of the concrete member, the force transfer from the plate to the concrete leads to a non-uniform stress distribution across the width of the concrete member. A smaller b_p compared to b_c may result in higher shear stress in the adhesive at failure, attributed to the contribution from the concrete outside the bond area. That expression was slightly modified by Lu et al. Various formulas for width coefficient calculation were presented in Table 2.4 and Fig. 2.13b.

Table 2.4. Selected width coefficients formulas.

HOLZENKÄMPFER [54] (1994)	$k_b = 1.06 \sqrt{\dfrac{2 - b_f/b_c}{1 + b_f/400}}$	(2.11)
CHEN & TENG [17] (2001)	$k_b = \sqrt{\dfrac{2 - b_f/b_c}{1 + b_f/b_c}}$	(2.12)
LU et. al. [98] (2005)	$k_b = \sqrt{\dfrac{2.25 - b_f/b_c}{1.25 + b_f/b_c}}$	(2.13)

where:

    b_f -   *CFRP width*

    b_c -   *Strengthened member width*

The coefficient appears usually as a multiplier in bond strength formulations influencing calculated limitation stress or strain [N1][N8][N9].

2.5.7. STIFFNESS OF STRENGTHENING (CFRP)

It has been mentioned before, that axial stiffness influences effective bond length. Nevertheless, from the experimental test made on CFRP as well as steel EBR, it has been noticed [39][114] that with lower EBR stiffness, a higher strain at failure can be achieved (*see Fig. 2.14a*)[79]. From the study made on different types of CFRP for strengthening [81], it has been noted that for CFRP strips with a higher value of axial stiffness (expressed by the modulus of elasticity and thickness of laminate E_f=220GPa, t_f=1.4mm) debond occurs at the lower value of strain ~5‰ in comparison to CFRP EBR with a lower value of stiffness (E_f=172GPa, t_f=1.2mm) with ultimate strain about 6‰.
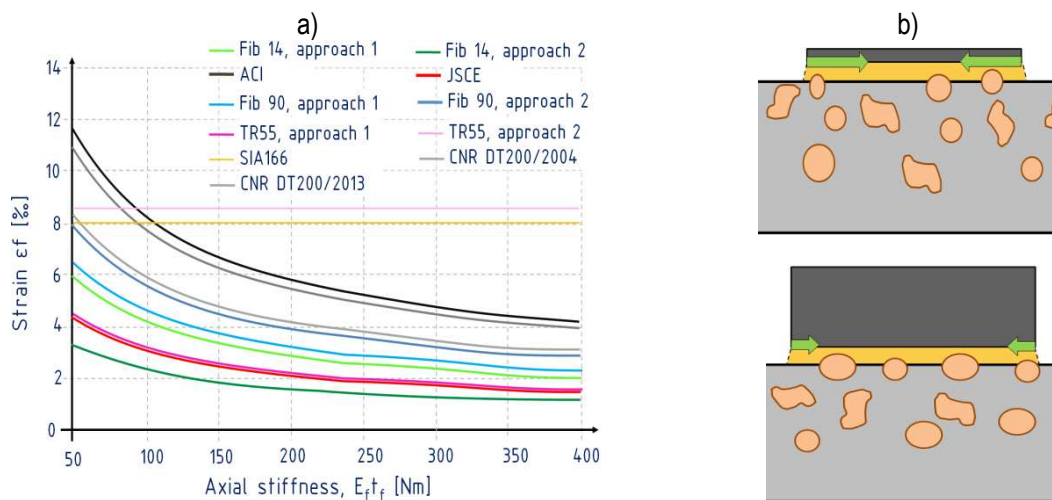

Fig. 2.14 a) strain – stiffness relationship according to different guidelines (based on [79])
b) transverse force concept in CFRP with different stiffness (based on [39])

With increasing CFRP strip stiffness, the maximum bond shear stress $\tau_{f.max}$ and the maximum fracture energy G_f decrease. According to Fickh [39], this is explained by greater transverse compressive forces acting along less stiff CFRP strips [39]. Those forces hinder the detachment of the aggregate at the bond interface (*see Fig. 2.14b*).

2.5.8. CONCRETE GRADE

Concrete grade affects minimal concrete strength properties and naturally increases beam bending capacity and as a consequence its strengthened equivalent [80]. According to Table 2.3, it can be noted that mechanical properties are related to a major number of formulas determining effective bond lengths. A general trend is as follows: CFRP – concrete bond interface with higher values of modulus of elasticity, tensile and compressive strength requires lower effective bond length (*see Fig. 2.15a*).
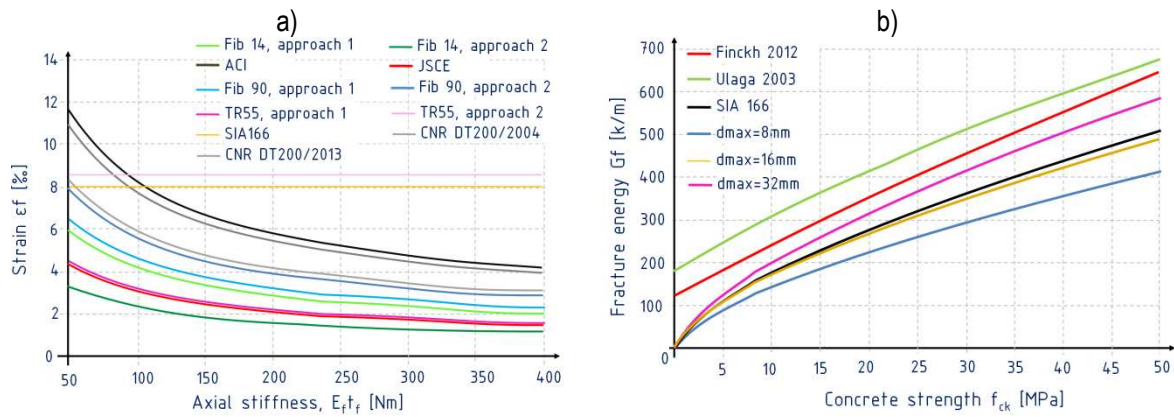
Fig. 2.15 a) Effective bond length – f_{ck} relationship (based on [79])
b) fracture energy in the function of f_{ck} (based on [25])

The concrete grade through its mechanical properties of concrete is correlated with the fracture energy of the interfacial CFRP – Concrete bond *(see Fig. 2.15b)*. Simplified equations to estimate the fracture energy Gf in the pull-off test depending on the concrete compressive strength and maximum aggregate size were presented in Table 2.5. As mentioned before G_f also is related to the stiffness of the CFRP strip.

Table 2.5. Selected formulas for fracture energy of the concrete-CFRP interface

ZEHETMAIER (2001)	$G_f = 0.046\sqrt{f_{ctm} \cdot f_{cm}}$	(2.14)
ZILCH [98] (2006)	$G_f = 0.25^2 k_b^2 \cdot f_{cm}^{\frac{2}{3}}$	(2.15)
CZADERSKI [25] (2012)	$G_f = 0.018 \cdot f_{ck}^{\frac{2}{3}} \cdot d_{max}^{\frac{1}{4}}$	(2.16)

where:

d_{max} -   *maximal aggregate size in concrete*

k_b -   *width coefficient (see 2.5.6)*

2.5.9. FATIGUE

The fatigue life is understood as the minimal number of cycles up to the failure of any component of the structural system. It was noted that strengthening RC beams using CFRP increases their fatigue life and the failure was always initiated by the brittle fatigue fracture of reinforcing steel [35]. The stress level of reinforcing steel due to applied load was indicated as the crucial factor in predicting the fatigue life of CFRP-strengthened RC beams [72]. According to [N8] as a design criterion, it is recommended to limit the stress range in steel rebar to that allowed in the member before strengthening. The utilisation of tensile strength in the passive CFRP strengthening of RC

beams is low which increases the fatigue life of the composite. Moreover, at a material level, carbon-based composites show significant fatigue resistance [74].

2.5.10. PRESTRESSING

The main allegation made against passive external CFRP strengthening is low utilization of potential fibre tensile strength as well as low contribution in dealing with deflection [75]. According to [34] [84] usage of tensile strength in such strengthening, the system is estimated in a range of 30-35%. Hence, more focus was put on improving the usage of tensile strength and aspects related to improving the serviceability of strengthened members. That is why more interest was dedicated to prestressing composites where many solutions of prestressing have been proposed and new ones are still being developed [120]. In contrast to passive strengthening, prestressed systems require special anchorage solutions to increase the transfer of shear stress resulting in a higher effectiveness of composite utilization and better limitation of deflection by introducing a prestressing load. More information can be found in related literature based on national research conducted in Poland mainly at the Silesian University of Technology [63], Łódź University of Technology [85] as well as Rzeszów University of Technology [121].

IN SITU APPLICATION AND EXPOSURE FACTORS

2.5.11. SURFACE PREPARATION

Iovinella et al. perform a vast study on the influence of several methods of surface preparation (sandblasting, bush hammering, grinding, brushing) on bond strength and fracture energy [56]. In the study, the relationship between bond strength and surface roughness was analysed. As a consequence, an additional multiplicator for the formula of fracture energy was proposed to include the effects of surface imperfections. Similarly, Soares et al. studied the influence of surface preparation on the bond behaviour of externally bonded CFRP reinforcement in single-lap shear tests where two different methods of concrete surface preparation: grinding and sandblasting [138]. In this study tests conducted with the use of a laser sensor revealed that sandblasting produced higher roughness of the surface than grinding. As a consequence higher ultimate shear force values were obtained in the case of sandblasting compared to grinding. Nevertheless, the initial stiffness of the strengthening system remained unchanged. Another study on surface preparation with the use of grooves with different shapes has been conducted by Mashrei et al [105]. The study revealed that prepared grooves filled with epoxy during CFRP had a positive impact on the bending capacity of the tested RC beams. By increasing the surface area in rectangular grooves significant increase in bending capacity can be achieved in comparison to triangular grooves with the same depth.

2.5.12.   ENVIRONMENTAL CONDITIONS

Temperature plays a crucial role in CFRP strengthening for each type of resin (*see Fig. 2.16a*). It is mainly because of relatively low values of the glass transition temperature characterised by commonly used epoxy adhesives.   There are several studies on the thermal influence on CFRP strengthening [157]. Krzywoń [88] tested CFRP strengthening of RC beams in different temperatures varying from 20 to 73°C (*see Fig. 2.16b*). A rapid decrease in bending moment capacity (>20%) was reached at 73°C when it was only a few per cent at 60°C. In higher temperatures debonding in the resin occurs.
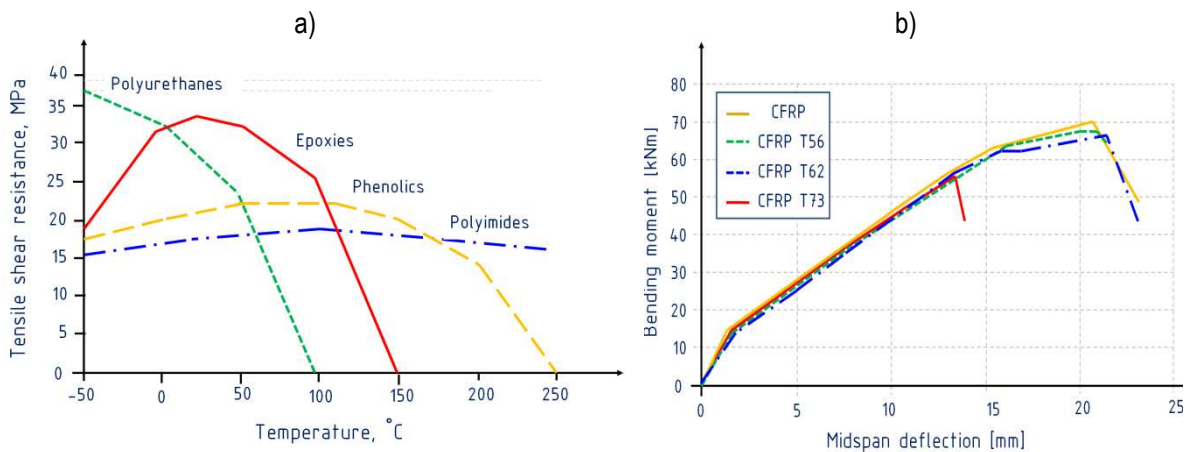
Fig. 2.16 Example of influence of temperature on a) adhesive performance (based on [61])
*b) load-deflection curves of CFRP-strengthened RC beams with epoxy resin (based on [88])*

A similar observation was made by Klamer [74]. For full-scale beams with low plate-support distance, the drop in ultimate load was relatively low up to 70°C. However, in specimens with a higher value of plate–end support distance about a 30% bending capacity drop was noted. On the other hand, research conducted by Trapko [145] shows a significant loss of strength even at a temperature range of 40°C ÷ 60°C in CFRP-confined compressed concrete cylinders. Experiments made by Ferrier et al. [3] imply that it is safe to use resins at ambient temperatures lower by at least 15°C than the glass transition temperature. For most epoxy resins, it is a limit of 30°C to 35°C. CFRP composite indicates no sensitivity and no tensile strength reduction due to moisture in wet-dry cycle tests. It is also less vulnerable to acid and alkaline media in comparison to other FRP composites [33], but it was found to be sensitive to exposure to seawater [69].

2.5.13.   LONGTERM-LOADING

There were several studies on long–term loading on the behaviour of CFRP-strengthened beams. Plevris and Triantafillou [123] revealed the relationship between the CFRP reinforcement ratio and time-dependent behaviour on strengthened RC beams. It was noted that creep strains can be limited with a higher composite reinforcement ratio under the same sustained load level. A

similar conclusion was derived by Kusa et al. [93]. Whereas Krzywoń et al. [90] found relatively good agreement in the use of the effective modulus method taken from Eurocode 2 to predict the long-term deflection of CFRP strengthening beams in one year period of laboratory tests timeline. It was noted that long-term deflection was about 43% of instantaneous deflection. Górski et al. [46] found possible delamination areas in the bond of strengthened RC beams subjected to long-term loads with the use of infrared thermography (*see Fig. 2.17*a and *b)* nevertheless, the defect growth rate in time has not been investigated.

a)   b)
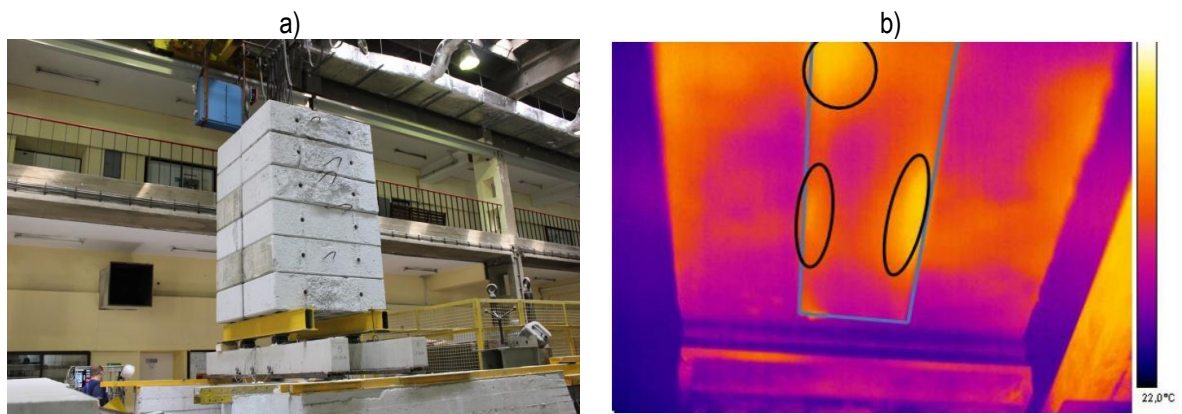
Fig. 2.17 a) Experimental setup of two RC free-supported beams under long-term loading [46]
b) IRT view at possible bond defects in one beam [46].

Mari et al. [106] pointed out the difference between the long-term deflection in RC beam strengthened before and after load application. When a beam is cracked before strengthening application, the CFRP plate hardly contributes to reducing instantaneous as well as time-dependent deflections under permanent loads. That is why the use of passive strengthening is not very effective in real design scenarios in the serviceability limit state. Except for the case that the beam is unloaded at a sufficient level before strengthening.

2.6. EFFECT OF DEFECTS

2.6.1. DAMAGE AND ITS TOLERANCE

Previously presented aspects of flexural strengthening are based on one fundamental assumption - a perfect bond between CFRP composite and the concrete surface. That is why the crucial aspect of the effectiveness of this kind of strengthening system lies in adhesive bonds. In other words, a perfect bond can be considered free from discontinuities and/or local defects (*see Fig. 2.18a* and *b*). Hence, a definition of defect can be understood as an accidental factor that affects directly the strengthening bond and as a consequence, its current state cannot be considered desirable.

a)   b)

Fig. 2.18 a) Examples of defects in CFRP strip [N18] b) poorly bonded CFRP mat [courtesy of Kałuża M.]

Generally, all the processes and products of human labour bear the risk of negligence or errors. The attempt to classify defects in FRP strengthening of RC structures was studied by Kaiser and Karbhari [61]. Defects can occur in all of the stages in the strengthening process: manufacturing, transportation, on-site installation and/or during the service life of the rehabilitated structural member (*see Fig. 2.19*).
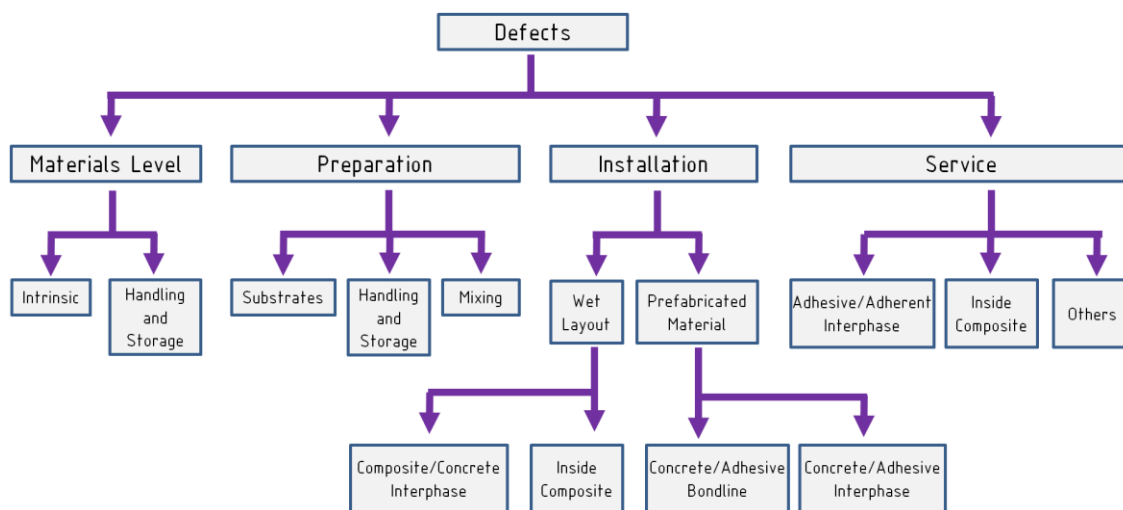

Fig. 2.19 Defect identification in different stages in the strengthening process (based on [61])

While the risk of inconsistencies in materials can be reduced via quality control of materials, defects that arose during installation or in-service interfacial bond defects are mostly hidden after FRP application (*see Fig. 2.20*). Many factors may increase the risk of human-induced bond defects at the application stage [5] [64]:

- Lack of selection and quality control of materials,
- No control of humidity and thermal conditions during application.
- Improper surface preparation before FRP application and lack of correct filling,
- No technology control in adhesive preparation resulting in cracks and porosity,
- Improper cleaning and degreasing of CFRP leads to improper adhesion between the adhesive and the adherents, low volume defects e.g kissing defects [151],
- Wrong application of adhesive on CFRP strips,
- Local pressure on CFRP results in local voids.

While encountering types of defects are mostly recognised [50], guidelines of the acceptable level of defects and their influence on structural performance, still remain rather unknown. FIB bulletins [N5] and its substitution [N8] concerning *Externally Bonded FRP Reinforcement for RC Structures* present remedial measures for bonding defects relying on replacement FRP material or compatible resin injection if considerable voids are present. However, no quantitive limits have been included.
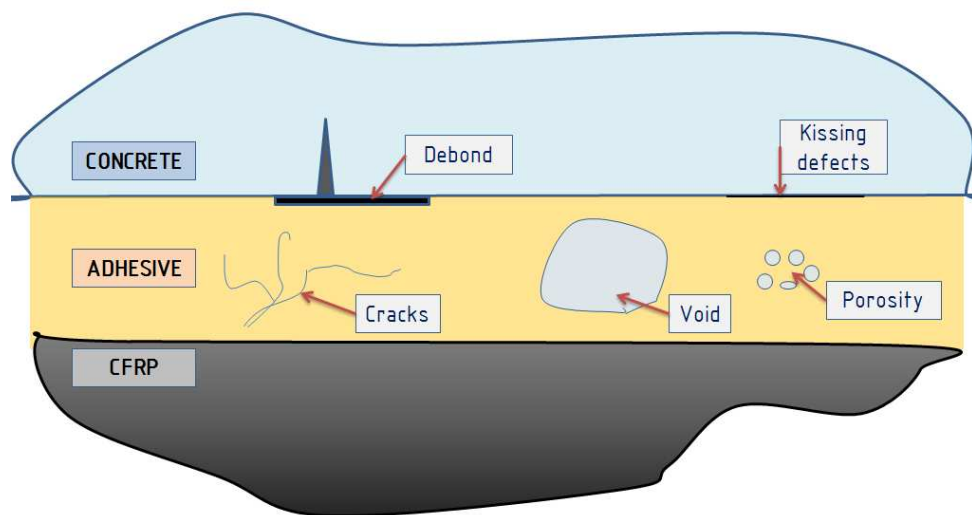
Fig. 2.20 Types of defects in the CFRP – concrete interface.

To some extent, those are included in ACI *Guide for the Design and Construction of Externally Bonded FRP Systems for Strengthening Concrete Structures* [N1] For wet layup systems, three levels of the delaminated area were distinguished: small – acceptable delaminations less than $1300mm^2$ and 5% of the total laminated area, simultaneously no more than $13000~mm^2$

per m^2; large - unacceptable delaminations greater than 16000 mm^2 require FRP replacement and intermediate values that require repair in form of resin injection. Nevertheless, precured FRP systems are treated independently and have to be repaired and evaluated via professional authority. This document indicates also the need for the determination of the threshold for critical defects and their identification using non-destructive techniques. A measure of the impact of the defects on strengthening performance in related literature is defined via the term: *defect criticality* [150]. This term is widely exploited in the case of composites control in aircraft design procedures where a damage tolerance approach was introduced [71][149]. Such an approach is related to the ability of the structural system to endure some level of existing damage without catastrophic failure.
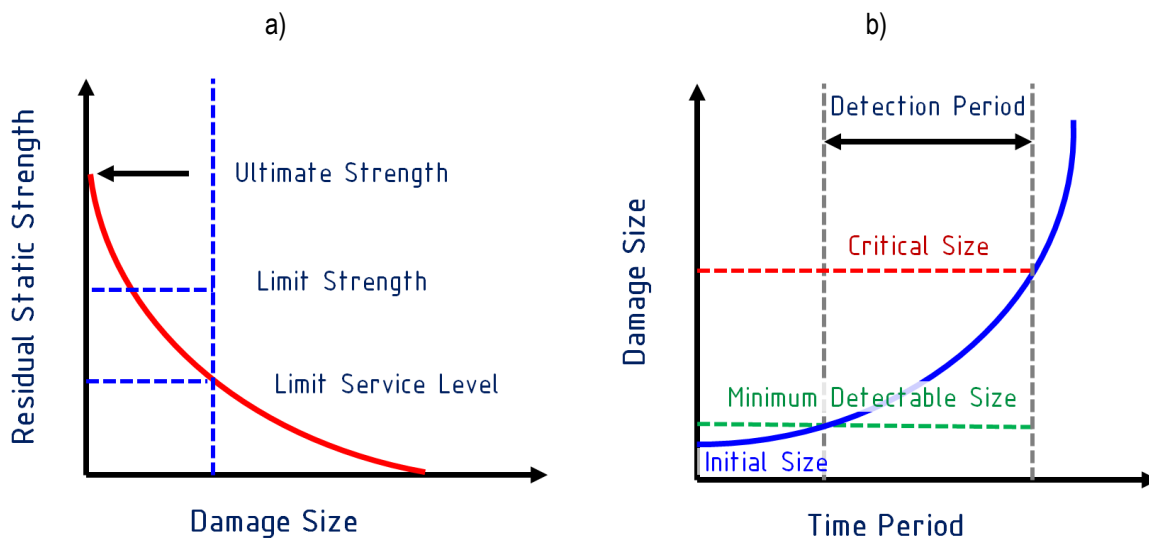

Fig. 2.21 a) Gradual loss of initial static strength due to damage size
b) the timeline of damage size in the damage tolerance approach in aircraft design (based on [71])

Until the defect is detected and repaired, it may reduce the residual strength of the structural component below the level of ultimate load [119], but is not allowed to drop below the design service load (*see Fig. 2.21a*). The main aim of damage tolerance analysis is to prevent defect growth under any service loads that could drive a defect to a critical dangerous size (*see* Fig. 2.21*b*). This objective can be achieved in a few co-related steps [48]: determination of initial damage, recognition of damage growth, determination of critical damage state (defect criticality) and proper inspection frequency.

Adopting such an approach to assessing existing CFRP-strengthened RC beams generates some questions that need to be answered. It is also creating scientific opportunities to fulfil some sort of research gap existing in this field. It is required to know how structural members behave when the defect is recognised under different load scenarios either in the short and long term, how to choose proper inspection intervals or what is the speed rate of defect growth.

## 2.6.2.   DISCUSSION OVER DEFECTS IN FLEXURAL STRENGTHENING OF RC BEAMS

By limiting considerations to simply supported strengthened RC beams there are a few potential defect locations that can be distinguished given expecting failure mode: in the mid-span, anchorage zone and also between them (*see Fig. 2.22*).
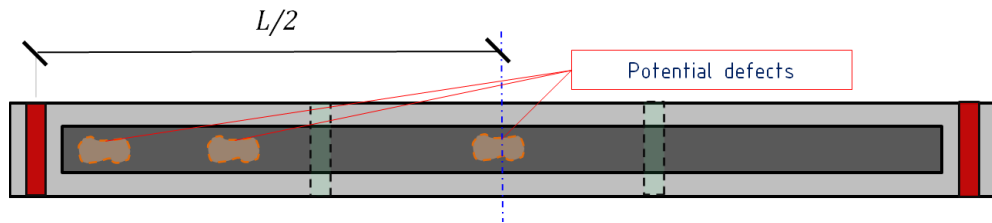
Fig. 2.22 Potential defects locations – bottom view on strengthened RC beam

In simply supported beams with uniformly distributed load, the mid-span zone is usually exposed to the highest values of bending moment, curvature, normal stress and strain. As a consequence, it is also the location of the earliest appearance of bending cracks. Brena et.al [14], suggest that formulating cracks causes a local increase of composite strain in crack proximity which ultimately may lead to the initialization of IC debonding (*see Fig. 2.23*).

Such a concept indicates that cracks formulated in defect areas may accelerate defect growth and decrease of bending capacity of the strengthened system when IC debonding is the leading failure mode. However, from the engineering point of view, it is hard to predict defect criticality quantitatively in this case. A similar situation occurs when defects exist between the mid-span and anchorage zone where the influence of shear is more significant. Shear or shear–flexural crack can occur right above the defect causing premature failure. According to a study conducted by Zhou et al. [156], bending moment capacity is more sensitive for such defect location.
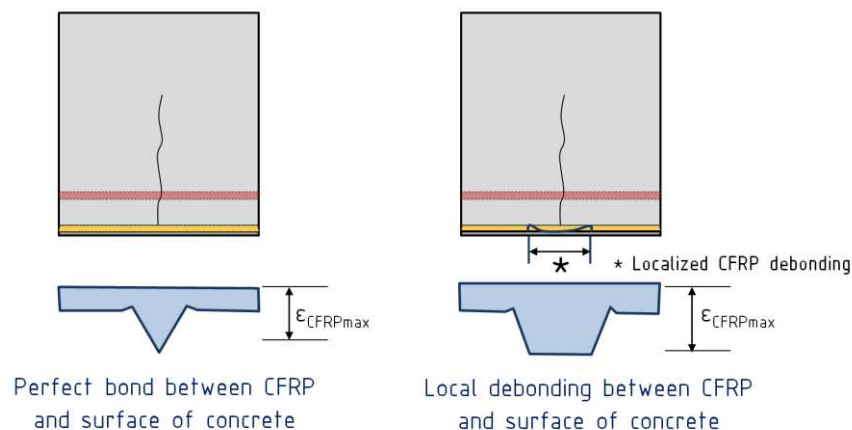
Fig. 2.23 Proposed distribution of strain on the surface of the CFRP composite (based on [14])

Considering the defect close to the plate-end it needs to be remembered that the interfacial bond between CFRP and concrete in the anchorage zone is subjected to complex normal and shear

stress states (see *Fig. 2.8*). However, in this case, defect influence on strengthened beam behaviour can be estimated. This can be done using the concept of treating the area affected by the defect as unbounded (*see Fig. 2.24*).
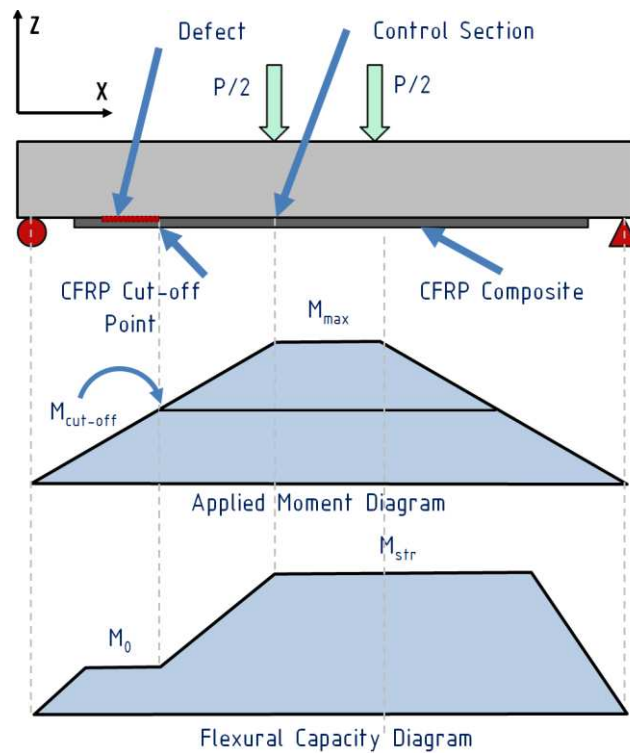

Fig. 2.24 Limitation of flexural capacity due to existing bond defect by considering shorter CFRP length (based on [14])

In such a scenario to maintain anchorage length, a predicted flexural capacity needs to be limited according to the rule of limiting stress and effective bond length based on the cracking moment.

LABORATORY TESTS OVERVIEW ON DAMAGE CRITICALITY

There are a few studies where the effect of defects was analysed, nevertheless, defects were understood in a few different ways. Wan et al. [150] conducted research where defects were considered as initial cracks in concrete before the CFRP application. The study was performed in the single shear-lap test as well as in the three-point bending test. Existing cracks were simulated by cutting the surface of the concrete perpendicularly to the main CFRP direction (*see Fig. 2.25*). A study showed that existing cracks in RC beams have little influence on the performance of CFRP strengthening. Similar outcomes over two decades earlier were achieved by Arduini and Nanni (1997) [4] in the study, where the behaviour of pre-cracked and strengthened RC beams was analysed. Test results have shown that pre-cracking slightly reduces the initial stiffness and ultimate strength of the beams, but the overall performance is quite comparable to that of uncracked beams.
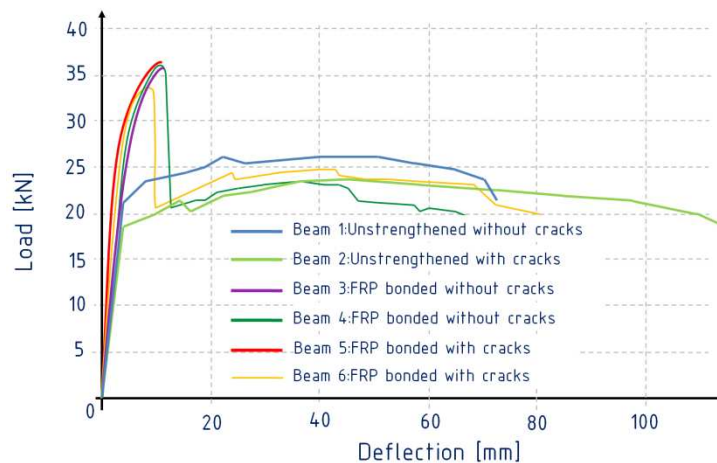
Fig. 2.25 Results obtained by Wan et al. (based on [150])

A wider look at defects has been taken by Kalayci et al. [62]. Besides the study on the effect of surface cuts, They presented the results of the effect of surface voids on the structural performance of RC beams with CFRP precured and wet layup systems. The main studied parameters were void diameters (*see Fig. 2.26*)   and surface cutting spacing on 2m long beams in a three-point bending test
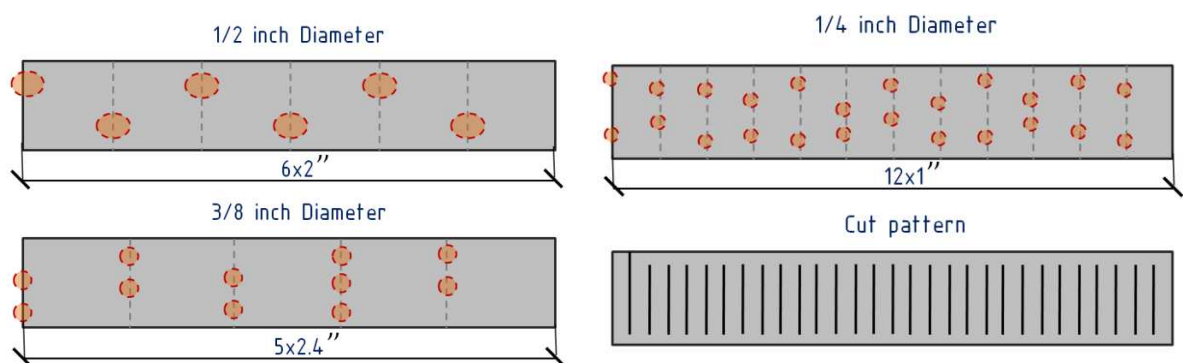
Fig. 2.26 Concrete specimens with defects used by Kalayci et al. (based on [62])

In the first case, voids were uniformly distributed along the beam and three different void diameters were studied remaining with the same total void area as 5% of the total bonded area. It was noted that with the increasing void diameter, the value of the ultimate load decreased (*see Fig. 2.27a*). Nevertheless, general stiffness remained the same. In all of the specimens, debonding failure initiated at mid-span (IC) was observed. The ultimate load decreased from the value of ~143 kN (6.4mm void) to ~130 kN (12.7mm void). A negligible effect of different surface cutting spacing has been observed (*see Fig. 2.27b*).
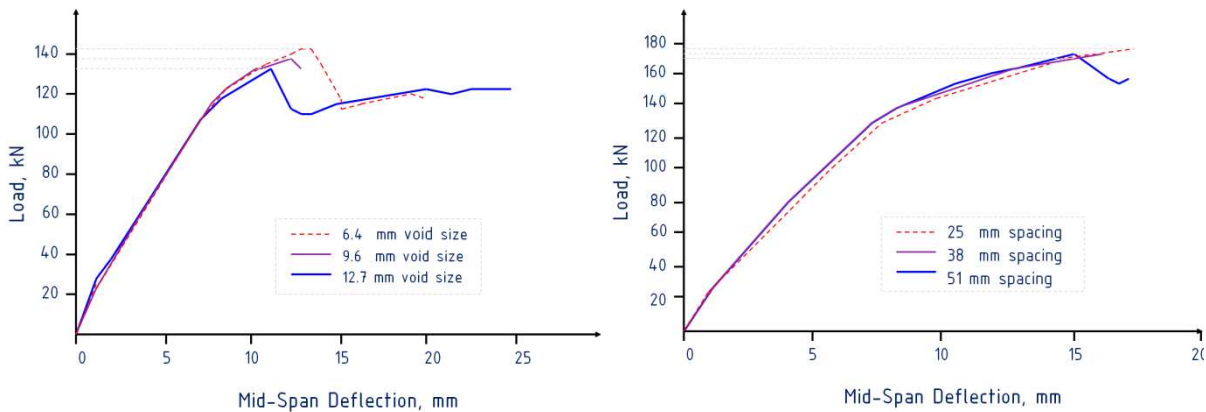

Fig. 2.27 Results obtained by Kalayci et al. in case of air voids a) and pre-cracking b) (based on [62])

Qin et.al [124] focused on interfacial defect criticality of CFRP-Confined concrete columns. The experimental investigation was conducted on typical cylindrical concrete samples in a compressive test. It was observed that the ultimate strength of FRP-confined concrete specimens was slightly reduced up to 5% when the area of interfacial defects was smaller than 50% of the total confinement area. A larger reduction was noted when the size of the interfacial defect was more than 50% of the total confinement area.

Zhou et. al [156] shed new light on the approach to defects in the strengthened RC beams. The research presents an experimental investigation of defect criticality in CFRP-strengthened beams in a four-point bending test. In this study, initial defects were considered locally in two major locations - in mid-span and shear-span as local unbounded areas. The experimental investigation consisted of small-scale concrete beams with a length of 0.5m where defects measured in various areas were artificially prepared. As a result relationship between the defect area and ultimate load has been analysed. According to the study, more vulnerable to defects were beams in a scenario when the defect was localized in the shear span rather than in the middle of the span (*see Fig. 2.28a* and *b*). The reduction of ultimate load for the beam with a defect located in the middle of the span does not exceed 5% when defects in the shear-span cause reduction of up to 46% of the ultimate load in the case of the defect with an area of 6000mm^2. Besides, extensive complimentary FE analysis was carried out for beams with a length of 3 and 6 meters where It was

noted that the beams with a low l/d ratio (deep beams) are more sensitive to the interfacial defect in comparison to the typical beam.
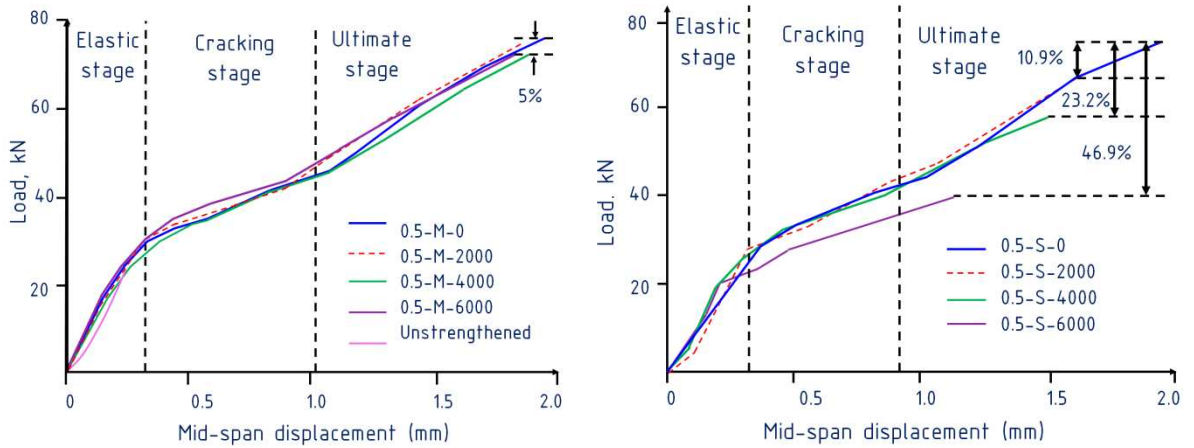

*Fig. 2.28 Results obtained by Zhou et al. in case of a defect in
a) mid-span and b shear-span) (based on [156])*

Based on results obtained in the numerical study authors proposed a procedure in form of a flowchart (*see Fig. 2.29)* for determining the impact of the defect relating to its size, location and l/d ratio of the RC beam. A small, medium and large impact has been distinguished where reduction of peak load respectively less than 10%, 20% and larger than 20%.
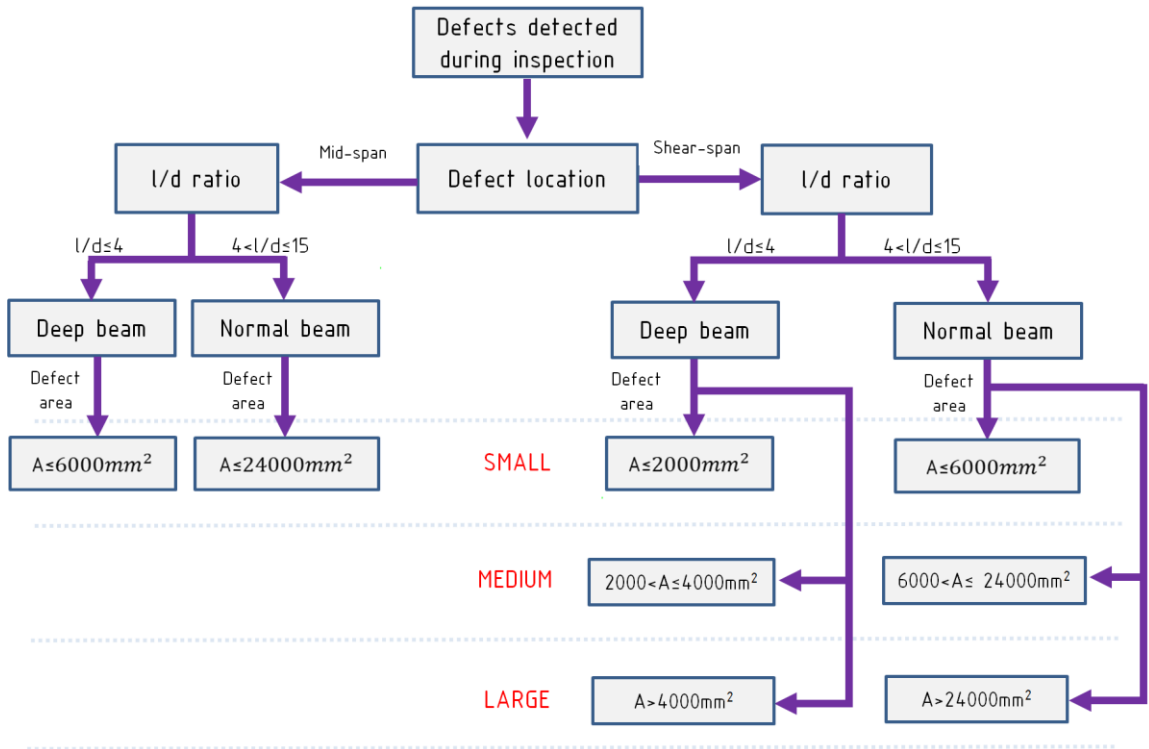

Fig. 2.29 Flowchart for defect assessment by Zhou et al.(based on [156])

2.6.4.   SUMMARY AND DISCUSSION

All strengthened beam specimens analyzed experimentally and described previously were summarized in *Table 2.6*.

Table 2.6. Summarized beam specimens

Author	Type	b [mm]	h [mm]	L [mm]	b_f [mm]	t_f [mm]	A_def [mm²]	P_u [kN]	Loc. [-]	Cap. red. [%]	f_c [MPa]	f_t [MPa]	E_c [MPa]	E_f [GPa]	Reinforcement top	Reinforcement bottom	Stirrups
Kalayci et al. [62]	EXP	152	305	2134	50	1.4	5%	140	U-V		36	N/A	N/A	227	2 Φ 10	2 Φ 16	Φ 10 @127
	EXP	152	305	2134	50	1.4	5%	135	U-V		36	N/A	N/A	227	2Φ10	2Φ16	Φ 10 @127
	EXP	152	305	2134	50	1.4	5%	125	U-V		36	N/A	N/A	227	2Φ10	2Φ16	Φ 10 @127
	EXP	152	305	2134	50	1.4	-	170	U-C		25	N/A	N/A	227	2Φ10	2Φ16	Φ 10 @127
	EXP	152	305	2134	50	1.4	-	170	U-C		25	N/A	N/A	227	2Φ10	2Φ16	Φ 10 @127
	EXP	152	305	2134	50	1.4	-	170	U-C		25	N/A	N/A	227	2Φ10	2Φ16	Φ 10 @127
Zhou et al. [156]	EXP	100	100	300	100	1.19	0	75,4	0	0	37,2	2,86	28850	155	-	-	-
	EXP	100	100	300	100	1.19	2000 (6,7%)	74,3	M	1,2	37,2	2,86	28850	155	-	-	-
	EXP	100	100	300	100	1.19	4000 (13%)	71,9	M	5	37,2	2,86	28850	155	-	-	-
	EXP	100	100	300	100	1.19	6000 (20%)	71,6	M	5	37,2	2,86	28850	155	-	-	-
	EXP	100	100	300	100	1.19	2000 (6,7%)	67,2	S	10,9	37,2	2,86	28850	155	-	-	-
	EXP	100	100	300	100	1.19	4000 (13%)	57,9	S	25,2	37,2	2,86	28850	155	-	-	-
	EXP	100	100	300	100	1.19	6000 (20%)	40	S	46,9	37,2	2,86	28850	155	-	-	-
	EXP	203	406	3000	50	1.19	0	70,3	0	0	37,2	2,86	28850	155	2Φ9.5	2Φ16	Φ 7 @ 102-596
Wan et al. [150]	EXP	100	125	1200	50	0.17	-	26.4	0		48.0	N/A	N/A	231	-	2Φ10	Φ 6 @ 50
	EXP	100	125	1200	50	0.17	-	23.9	U-C		47.3	N/A	N/A	231	-	2Φ10	Φ 6 @ 50
	EXP	100	125	1200	50	0.17	-	36.2	0		48.0	N/A	N/A	231	-	2Φ10	Φ 6 @ 50
	EXP	100	125	1200	50	0.17	-	36.7	0		47.3	N/A	N/A	231	-	2Φ10	Φ 6 @ 50
	EXP	100	125	1200	50	0.17	-	33.3	U-C		48.0	N/A	N/A	231	-	2Φ10	Φ 6 @ 50
	EXP	100	125	1200	50	0.17	-	36.4	U-C		47.3	N/A	N/A	231	-	2Φ10	Φ 6 @ 50

EXP - experimental investigation, FEA - Finite element analysis, N/A – Data not available, X% - Autor's estimation
U-C - uniformly distributed cracks, U-V - uniformly distributed voids, 0 - no defect, M - mid-span defect, S - shear-span defect,

It can be noted that the great majority of samples can be characterised by small dimensions where samples were up to 2m long and relatively narrow CFRP plates. Defects were considered artificial voids as well as initial cracking. In all specimens, the failure mode was described as intermediate crack debonding initiated in the middle of the span. Studies were focused mainly on comprising load-deflection plots of beams with and without defects. On the one hand, the defect area-based flowchart created by Zhou [156] gives some qualitative indication of debonding risk. On the other hand, such an indicator as defect area is affected by the scale of the total bonded area of the CFRP. Hypothetically, there can be a strengthened beam where the given area of the defect

may be a small percentage of the total bonded area as well as the beam where the same defect area to total area ratio will be relatively high. That is why the defect area cannot be the only valid parameter in the defect criticality of the CFRP strengthening.

Given the above, there is a great number of material and environmental factors that affect CFRP strengthening beams. Considering a beam with defects in the bond it is required to be aware of all presented in this chapter accompanying effects and conditions that can modify the behaviour of a perfectly strengthened beam. It can be seen that even without analysing the defects, the behaviour of the CFRP strengthening beam is not trivial. Defects introduce to the whole consideration an additional variable which needs to be analysed together and makes the analysis even more complicated.

In conclusion, the existing studies give some hints, however, do not exhaust a subject on the behaviour of CFRP-strengthened RC beams with defects. Karbhari and Kaiser [70] made a valid point that a sufficient level of knowledge about lifetime durability and the effects of accidental defects in strengthening techniques limits the hesitation of its usage when fundamentals for inspection and field acceptance of rehabilitated systems are developed. It can be noted that despite almost three decades of the history of CFRP strengthening, research interest in the effects of interfacial bond defects on structural member capacity increased only in recent years. There is still no full answer to how strengthened beams with defects behave under various circumstances, with different initial parameters or when other failure modes than IC are expected. Hence, further study on this topic needs to be investigated.

3. EXPERIMENTAL PROGRAMME, RANGE AND METHODOLOGY

3.1. AIM AND SCOPE OF LABORATORY TESTS

The main goal of this study was to investigate the behaviour of RC beams strengthened with CFRP with interfacial bond defects. To get closer to the determination of defect criticality of strengthened RC beams, laboratory tests described in this chapter were prepared and conducted. In this study main interest was put into determining the influence of defect location in strengthening bonds under statically realized monotonic load. As far as it is known failure modes of strengthened beams can be initialised by flexural or/and shear cracks, therefore beam models were divided into two series in terms of predicted failure mode: in bending - Serie A, and in shear - Serie B. As a consequence, it was planned to examine the response in the case of both: shear and bending moment-sensitive beams. The only difference between RC beams in both series (before strengthening application) was the number of used shear reinforcement.

In addition to the main goal, it was searched for any symptoms indicating in advance hidden voids during loading that inform about incoming failure or can potentially affect the capacity of CFRP-strengthened RC members. Results obtained in experimental tests were planned to be used for the validation of numerical analyses simulating the nonlinear response of strengthened structural members.

At this point, a valid objection can be made against the test where strengthening is applied on newly produced RC beams. In the real case scenario, structures usually have undergone some load history before the application of CFRP strengthening which decreases its initial stiffness due to cracking and long-term effects. It needs to be emphasised that this study concentrates on revealing the effects of the defects in general which are still not well known. It was decided to not introduce additional parameters, which could make results unclear and correlated. One of the specimens was planned to be initially preloaded and unloaded prior to strengthening. Nevertheless, the preparation of this beam specimen (poorly prepared adhesive thickness) was judged unsatisfactory and was excluded from this study.

Two main stages of experimental study can be distinguished: Investigations of full-scale RC beams and initial investigation of materials. The aim of the initial investigation of materials was to determine the mechanical properties of materials where concrete, CFRP laminate, and reinforcing steel were tested. The following properties have been determined during the investigation of materials:

- Concrete compressive strength
- Concrete modulus of elasticity and Poisson's ratio
- Concrete tensile strength

- Steel modulus of elasticity and yield strength
- CFRP modulus of elasticity and tensile strength

All of the tests were conducted on beams with a length of 3m. The beams had a rectangular cross-section, 200±2 mm in width and 300±5 mm in depth. Two 8mm diameter steel bars were used as a top reinforcement and the bottom reinforcement consisted of four 12 mm steel bars. The 6 mm diameter steel bars were used for shear reinforcement. The concrete cover was set as 25 mm. The geometry and the reinforcement of the beams are presented in Table 3.1.

Table 3.1. Type of series of beam models

SERIES	SECTION VIEW	SIDE VIEW
A		
B		

Characteristic bending and shear beam capacities were determined based on estimations according to simplified methods given in Eurocode 2. Characteristic capacity values calculated for concrete class C30/37 with assumed material safety factors equal to 1, were summarized in the table below.

Table 3.2. Estimated characteristic capacities according to EC2

No	Quantity	Concrete Class	EC2
1	Bending Capacity	C30/37	$M_{Rk} = 57.49 \ kNm$
2	Shear resistance without stirrups	C30/37	$V_{Rk.c} = 44.10 \ kNm$
3	Shear Resistance with stirrups (spacing)	C30/37	$V_{Rk.s}^{(10cm)} = 138,13 \ kN$ $V_{Rk.s}^{(30cm)} = 46,04 \ kN$
4	Capacity in terms of CFRP delamination of strengthened beam	C30/37	$M_{Rd} = 105.94 \ kNm,$ $\varepsilon_{min/max} = -1.75 \ ‰ \ / \ 6{,}51‰$

All beam specimens were prepared with the use of ready-mixed concrete from the same supply at one time and were stored next to each other in the same thermal-humidity indoor conditions: about 19˚C and 45% relative humidity. Strengthening was performed with the use of wide 120mm x 1.2mm CFRP strips, bonded to the bottom side of each beam. The location of the defect along the span of the beam was set as a main parameter in the experimental study. Three defect position has been chosen: in the mid-span under point load and just behind the anchorage zone. For the methodology of application of defects see section 3.3. After Serie A had been conducted, It was decided to increase the defect area in Serie B in order to increase the influence of the defects. For a comparative study, a reference RC beam (A1) and CFRP-strengthened beam with no defects (A2) were provided. All data of beam models were summarised in Table 3.3.

Table 3.3. Summarized data of beam models

No	Description	CFRP Strengthening	Reinforcement type	Defect Type	Abb.	Area of the defect	A_{def}/A_{tot}
1	Reference RC beam	-	A	-	**A-1**	-	-
2	Reference CFRP strengthened beam - no defects	Strip	A	-	**A-2**	-	-
3	CFRP strengthened Defect #a	Strip	A	a	**A-3a**	12 000 mm^2	5%
4	CFRP strengthened Defect #b	Strip	A	b	**A-3b**	12 000 mm^2	5%
5	CFRP strengthened Defect #c	Strip	A	c	**A-3c**	12 000 mm^2	5%
6	CFRP strengthened Defect #a	Strip	B	a	**B-3a**	24 000 mm^2	10%
7	CFRP strengthened Defect #b	Strip	B	b	**B-3b**	24 000 mm^2	10%
8	CFRP strengthened Defect #c	Strip	B	c	**B-3c**	24 000 mm^2	10%
9	Large defect	Strip	A	d	**A-6**	203 520 mm^2	61%

3.2. EXPERIMENTAL SETUP AND MEASUREMENTS

The whole study was conducted in a four-point bending test. The load points were located 1m away from the support on both sides of the beam. The load was applied in force control mode in a static-incremental scheme with 20 kN monotonic load increment up to 100 kN and 10 kN over this value in case of strengthened beams and 10 kN increment in the whole range in case of beam reference RC beam. The load was applied with the use of a hydraulic actuator with a range of 1000 kN equipped with a strain gauge sensor.
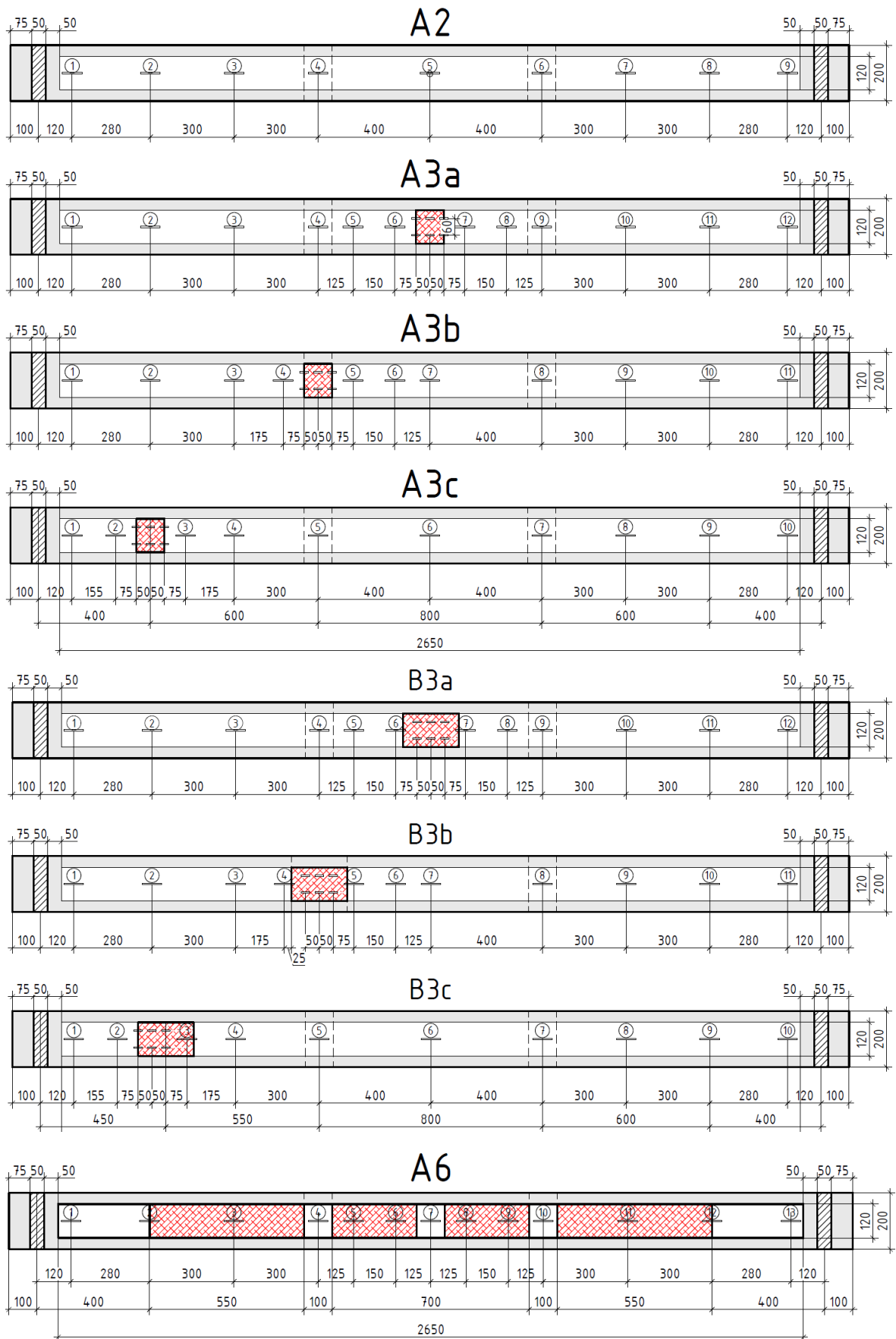
Fig. 3.1.: Types of tested specimens with applied defects - bottom view (defects area in red)
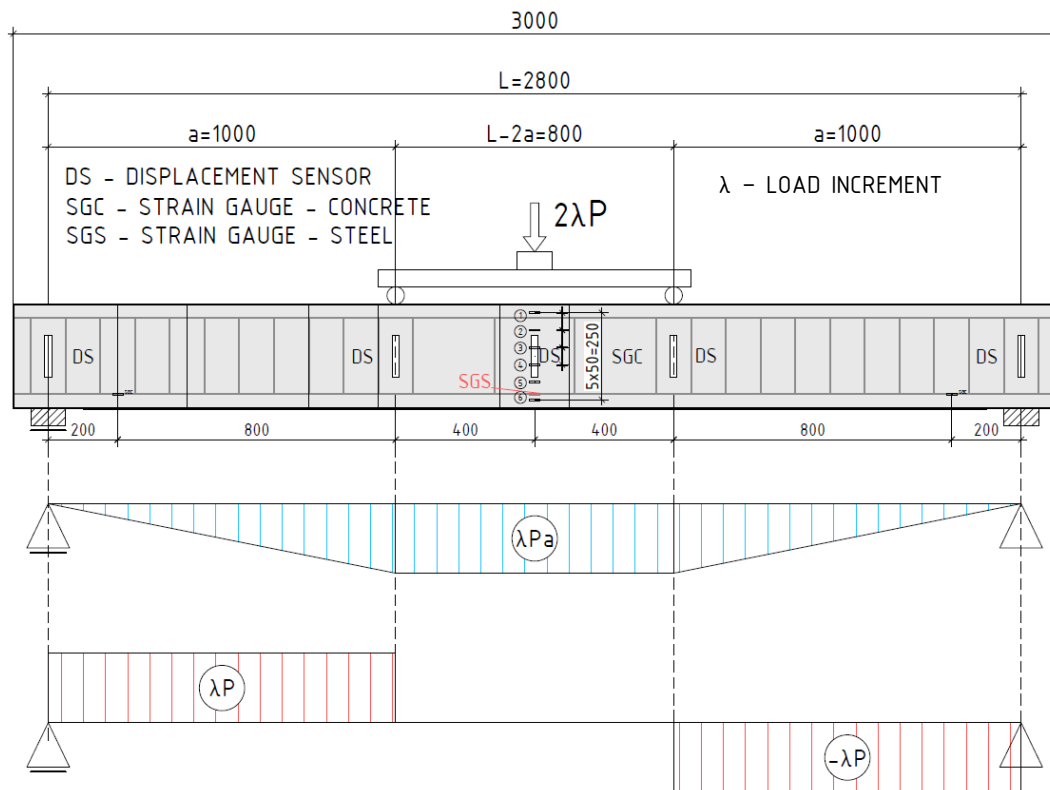
Fig. 3.2.: Expected internal forces during the test under external incremental load (excluding self-weight)

It was decided to measure strains at the concrete surface in the middle of the span with the use of a set of six foil strain gauges (*see Fig. 3.2*) with a base length of 70mm, uniformly distributed along the beam deep. For measuring vertical displacements inductive LVDT sensors in five points along one side of the beam were used. CFRP strain was measured with a set of paper strain gauges with a 50mm base length distributed along the beam (*see Fig. 3.1*). Additionally, strain gauges were located each time at the defect outline. The strain of bottom reinforcement was measured at the mid-span with the use of the strain gauge with a base length of 2 mm. A constant collecting data system with the use of a 64-channel analogue-to-digital converter (ADC) was used. The following quantities were measured during tests:

- load value,

- beam deflection,

- width, distribution and development of cracks,

- concrete, steel and CFRP strains.

Measurement check was performed each time at the beginning of the test by loading and unloading process in the load range of $0 \div 10$ kN for strengthened members and $0 \div 5$ kN for reference RC beam for initial records verification. After that, during the target tests, the distribution of cracks and their development were marked manually on one side of the beam at each load increment up to the value of 160 kN which was specified as a limit for safety reasons (*see Fig. 3.3*).
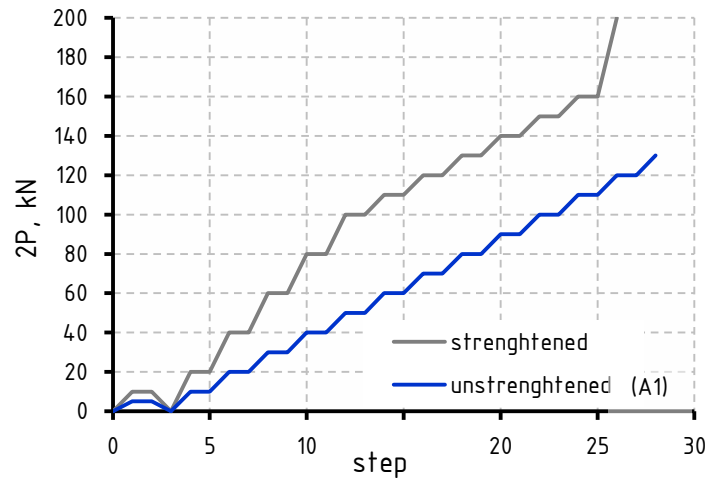
Fig. 3.3.: Loading protocol during tests

Crack width was measured with the accuracy of 0.1mm with the use of Brinnel's reading glass on the painted side of the beam (see *Fig. 3.4a*). Auxillary strain and displacement measurements were conducted on the opposite side of the beam using the digital image correlation (DIC) method by the Aramis GOM system (see *Fig. 3.4b*). For this reason, one side of each beam was covered with quasi-uniformly distributed dots of black paint in 50% of the side area.

Fig. 3.4 *a) Experimental setup of beam specimen on one side*
b) Measurement of the DIC system on the opposite side of the beam specimen

In Fig. 3.5 the whole research timeline has been shown. It can be noticed that 12 months passed after beam specimens have been prepared up to the test for reasons beyond the control. Before demolding, beams were stored on four wooden supports. After six months four beams have been strengthened. After the next six months, the CFRP on the rest of the beams were applied. Then, beams were stored as simply supported with supports in target positions. All beams and concrete specimens were tested within one week.
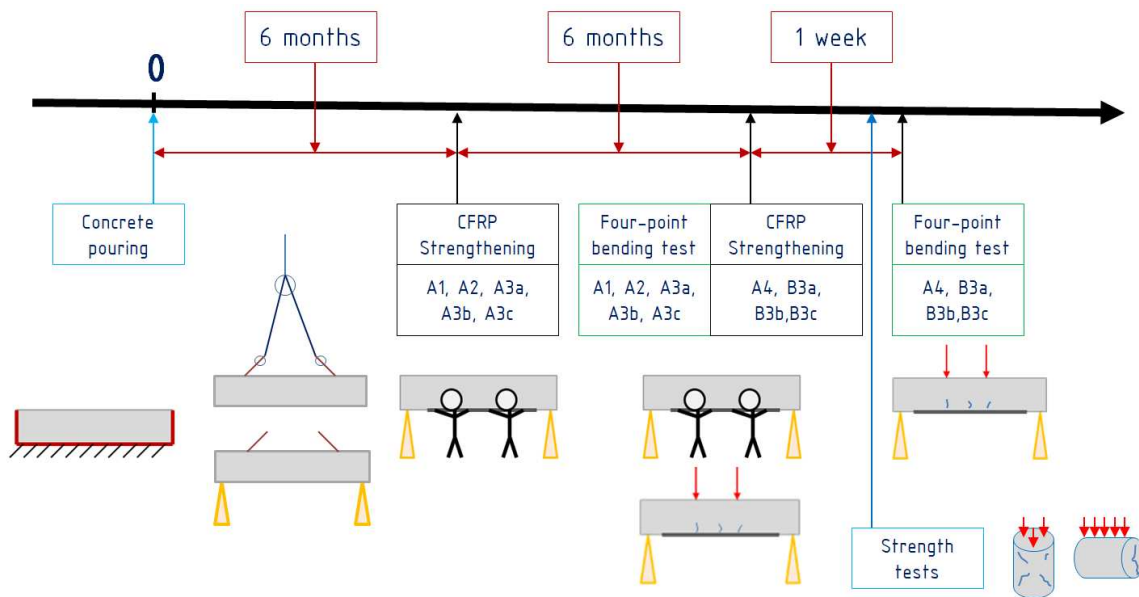
Fig. 3.5 Research timeline

3.3. TECHNOLOGICAL ASPECTS OF CFRP STRIPS APPLICATION

CFRP strips were applied to the bottom surface of the beam, after demolding (*see Fig. 3.6b*). The surface of the beams was prepared gently given that surface preparation has a significant impact on strengthening capacity. The manufacturer of the strengthening system recommends using sandblasting, shot-blasting, or grinding to remove the weak concrete cover. In this study grinding with a grinder and silicon carbide grinding disk was used. The process was prepared with great care in order to remove the outer layer of the release agent from the moulding stage and also to ensure proper roughness of the surface (*see Fig. 3.6a*). Afterwards, an industrial vacuum cleaner was used to clean the bottom surface of the beam from the dust. According to the manufacturer's technical guidelines, no surface priming was provided.
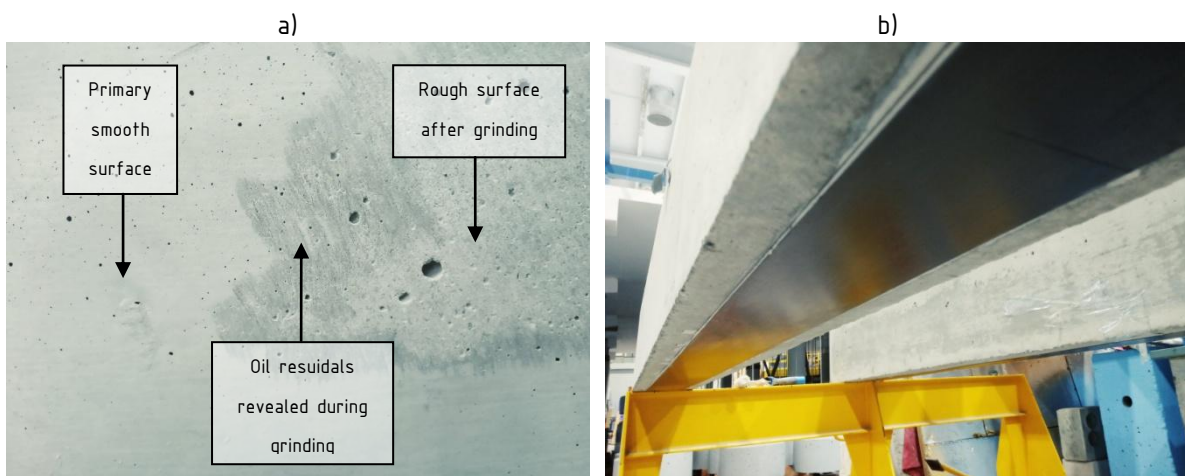
Fig. 3.6 a) Preparation of concrete surface b) Applied CFRP strip on the bottom side of the beam

Artificially created defects were prepared with the use of polyester foil installed in a desirable position along the RC beam (*see Fig. 3.7a*). Before application, the surface of CFRP strips had been cleaned and treated gently with solvent in the form of petroleum ether. A degreasing agent was applied directly to the CFRP surface by wiping to remove grease, dust, and any other contaminants that existed on the material. Target adhesive was prepared based on the two-component epoxy resin (component A: light grey epoxy resin solution, B: black hardener) mixed slowly in a weight proportion of 4(A):1(B). CFRP strips were covered uniformly with the adhesive mixture in the form of a roof-shaped layer with an average thickness of 5mm in the middle.

a)   b)
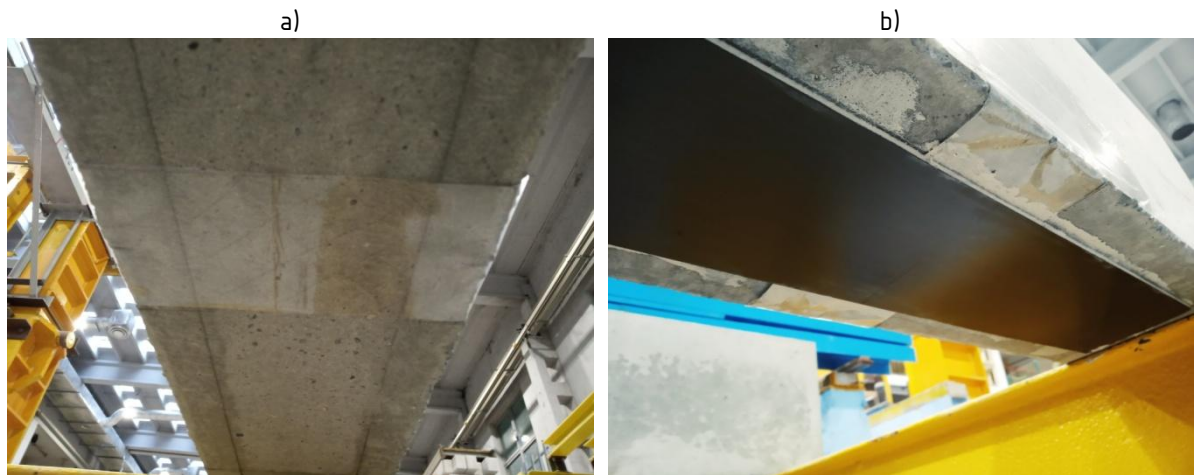
Fig. 3.7 a) Defect before and after b) application of CFRP strip

Prepared strips were set up in a desirable position from the bottom of the beam (under self-weight, with target support conditions) and gently pressed to its surface with the removal of excess adhesive on the sides (*see Fig. 3.7b*). Ultimately, the average measured thickness of the adhesive was 2÷3mm. In the case of specimen A6 with a large applied defect, an additional wooden beam and set of clamps have been used to keep the composite in the right position after application (*Fig. 3.8*).

Fig. 3.8 Prepared specimen A6 right after CFRP application

Without additional equipment, the composite was detaching during curing under the self-weight of adhesive due to the small bonding area.

4. EXPERIMENTAL INVESTIGATION

4.1. EXPERIMENTAL INVESTIGATION OF MATERIALS.

4.1.1. REINFORCING STEEL

For the main reinforcement of RC beams steel grade B500SP with nominal diameters of 8mm for top reinforcement and 12mm for bottom reinforcement were used. Stirrups were prepared with a diameter of 6mm and steel grade S500B. Six 400mm long specimens for each type of reinforcing bar were prepared for investigating material properties in the axial tensile test (*see Fig. 4.1b*).

a)   b)
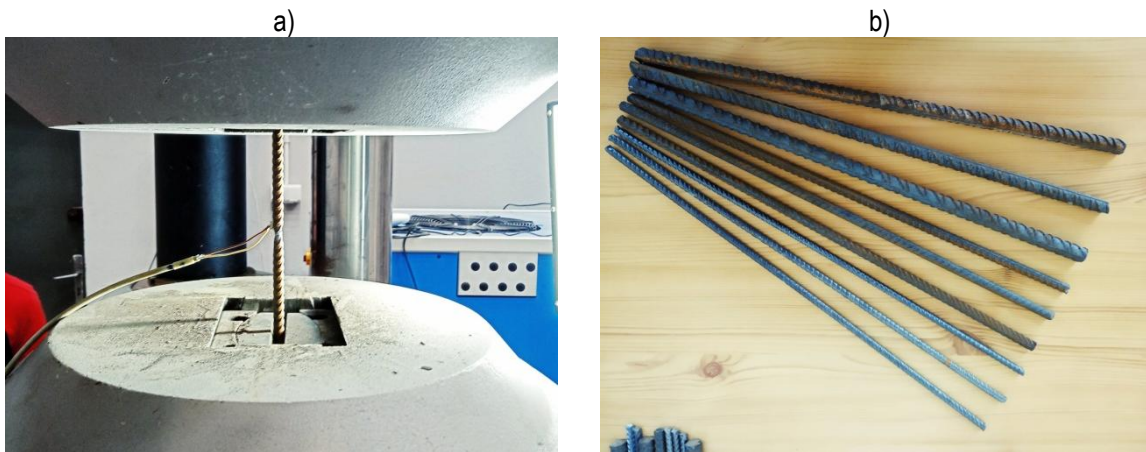
Fig. 4.1 a) Steel specimen in testing machine b) Example of reinforcing steel samples

The increasing displacement rate was set as 2 mm/min. Specimen strain was measured with foil strain gauges with a length of 2mm as well as a video extensometer (*see Fig. 4.1a*). The average values from recorded data for each diameter of reinforcement were summarized in the table below.

Table 4.1. Geometry and mechanical properties of specimens obtained in the test

No.	Nominal / Measured Diameter [mm]	Cross-section area [mm^2]	Elasticity modulus [GPa]	Yield strength [MPa]	Yield strain [‰]	Tensile strength [MPa]	Max Strain ε_{uk} [%]	Eurocode 2 Class
1	φ12 / 11.8 ± 0.2	113	201	575	2,8	700	12	C
2	φ 8 / 7.8 ± 0.4	50.3	199	575	2,8	670	8	C
3	φ 6 / 5.8 ± 0.2	28.3	201	500	2.5	550	6	B

A good agreement between the samples in the stress-strain plot can be observed. It can be noted that for diameters 12 and 8 the yield strength is in the range of 400-600, the tensile strength to yield strength ratio is higher than 1.15 and the ultimate strain is higher than 7.5 % which allows classifying as a C steel class standing for high-ductility class according to Eurocode 2 [N4] requirements. For stirrups lower value of ultimate strain was recorded.

It can be noted that for almost all samples of all diameters, the plastic plateau is almost horizontal for the strain value up to 10‰, which is mostly used value in static analysis and design.
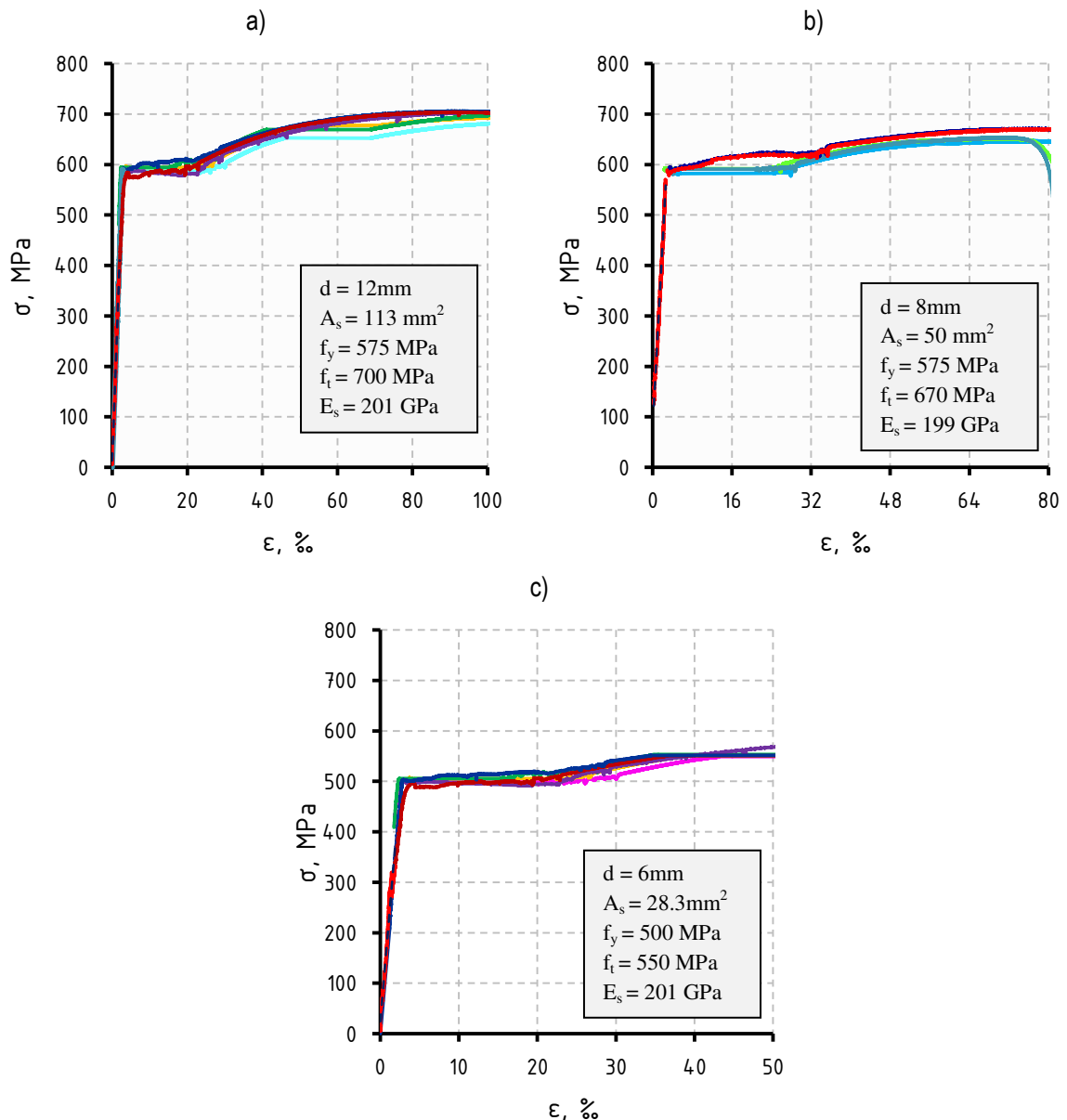
Fig. 4.2 Stress-strain relationship of prepared samples d=12mm a) d=8mm b) d=6mm c)

4.1.2. CARBON FIBER STRIPS

The tensile strength test of carbon fibre strip samples was prepared according to ASTM D3039 standard [N2]. Analyzed CFRP samples were signed as S&P Lamelle CFK 150/2000 (*see Table 4.2*). For the test, six specimens were prepared with an overall length of 500mm and width of about 20mm, trimmed from the primary strip with the use of a cutting knife. The width of each sample was measured with the use of a calliper with an accuracy of 0.1 mm. Steel tabs (S235) were bonded to the ends of the strips to get proper anchorage in a testing machine (*see Fig. 4.3a*).

Table 4.2. Manufacturer data of the used CFRP material

S&P Lamelle CFK 150/2000	
Elasticity modulus	>175 GPa
Tensile strength	2800 MPa
Width / Thickness mm/mm	120/1.2
Tensile force at strain 0,6 / 0,8 %	151.2 kN / 201.6 kN

A hydraulic machine signed as ZD-100 was used in the test. Each time, the CFRP specimen was placed vertically in the grips and then it was subjected to controlled, incremental, uniaxial displacement until failure. The displacement rate was set as 2 mm/min [N2]. Specimen strain was measured with strain gauges with a length of 2mm as well as a video extensometer (*see Fig. 4.3b*). Recorded data and geometry of specimens were summarized in the table Table 4.3.

a)	b)
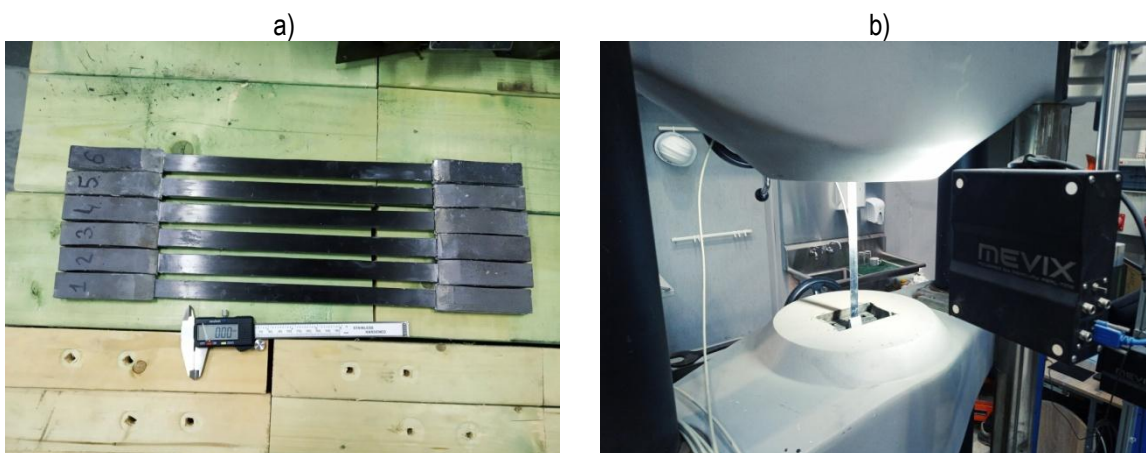
Fig. 4.3 a) Specimens prepared for tensile test b) Specimen in testing machine

Table 4.3. Geometry and mechanical properties of CFRP specimens obtained in the test

No.	Width [mm]	Thickness [mm]	Cross-section area [mm²]	Elasticity modulus [GPa]		Tensile strength [MPa]		Strain at rupture [‰]	
1	18.8 ± 0.2	1.2	22.5 ± 0.3	172,9		2147		12.3	
2	20.2 ± 0.2	1.2	24.2 ± 0.3	171,9		x		x	
3	19.9 ± 0.1	1.2	23.8 ± 0.1	172.9	170.9 ± 3.0	x	2027 ± 98	x	11.7 ± 0.4
4	19.8 ± 0.2	1.2	23.7 ± 0.3	163.4		1934		11.6	
5	20.0 ± 0.3	1.2	24.0 ± 0.4	170,7		1968		11.5	
6	20.0 ± 0.5	1.2	24.0 ± 0.5	172.5		1960		11.35	

Obtained results have shown the explosive type of failure mode (*Fig. 4.4a*) in four of six tested specimens. In the rest of them, premature failure was observed due to longitudinal fracture along its length. Nevertheless, in all samples highly linear behaviour was observed as expected (*Fig. 4.4b*). Relatively good matching with the data delivered by the manufacturer was obtained in the case of elasticity modulus and about a 25% lower value of tensile strength was recorded. However, this may be caused due to way of preparation of samples in the cutting process. Given that, CFRP tensile strength is hardly ever used in its full range in the case of RC strengthening, obtained results can be considered satisfactory.

a)   b)
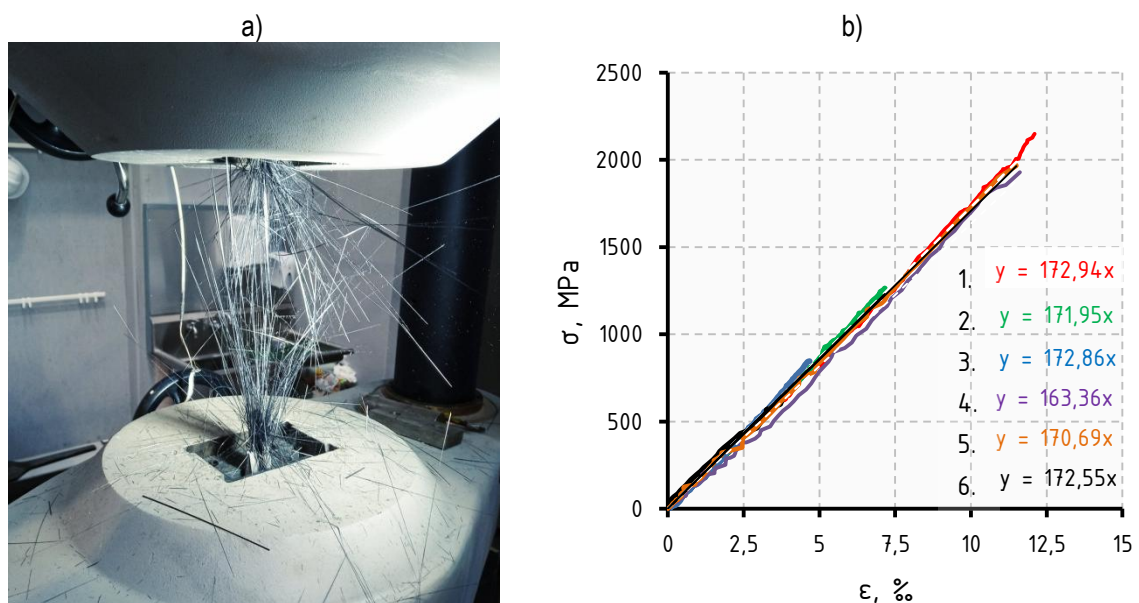
Fig. 4.4 Major failure mode obtained in the test. a) stress-strain relationship of CFRP samples b)

4.1.3. CONCRETE

In the study ready-mixed concrete from a local supplier was used. It was based on cement CEM III/A 42,5N - LH/HSR/NA with fly ash and the addition of a plasticizer described as MASTERPOLYHEED 220. The maximal aggregate grain was set as 16mm. A concrete mixture was cast at the lab temperature (19°C and about 45% humidity), during winter conditions outside (2°C). Detailed information about the concrete mixture composition was presented in Table 4.4.

Table 4.4. Concrete mixture composition

Component		Quantity [kg/m^3]
Sand (fraction 0/2)		814
Gravel	(fraction 2/8)	418
	(fraction 8/16)	525
Cement		285
Fly ash		90
Water		162
Water-cement ratio		0,58

Concrete was delivered via a concrete mixer truck and transported to the destination point using a concrete-mixer container and crane. Concrete in formwork was poured in layers and vibrated to reach the required compatibility (*Fig. 4.5a*). Beyond the main RC beams, three different kinds of specimens of concrete were cast: twelve concrete cylinders and ten concrete cubes (*Fig. 4.5b*). Small samples were prepared from the same delivery, poured and vibrated using a metal spatula.

a) b)

Fig. 4.5 a) Concrete pouring b) Concrete cubic and cylindrical specimens

The formwork of the beams was constructed from 22mm thick plywood and covered with a thin layer of release agent inside (*see Fig. 4.6a and b*). Beams were treated with the required technological care after forming in the first few days.

a)   b)

Fig. 4.6 a) Beams before pouring concrete b) Beams after pouring concrete

In contrast to beam specimens, concrete cylinders in the size of 300x150 mm and cubes 150x150 were treated in accordance with PN-EN-12390-2 [N16] after had been poured. After removing the formwork, irregular and relatively small surface air voids were observed in a diameter of less than 5mm. Concrete cylinders were used in the compressive strength test and splitting tensile strength test also known as the Brazilian test [N12]. Modulus of elasticity and Poisson's ratio were estimated based on measured average strain during tests in both vertical and horizontal directions (*see Fig. 4.8*). To reach this goal, six strain gauges (three for vertical and three for horizontal direction) were used in total at each sample in a compression test. The load speed rate was set as 10kN/s and plywood pads were used on the top and bottom surface of the specimen.

Concrete cubes were used in the compressive strength test only. Specimens were placed directly in the testing machine and tested for the ultimate load value without strain control.

a)   b)
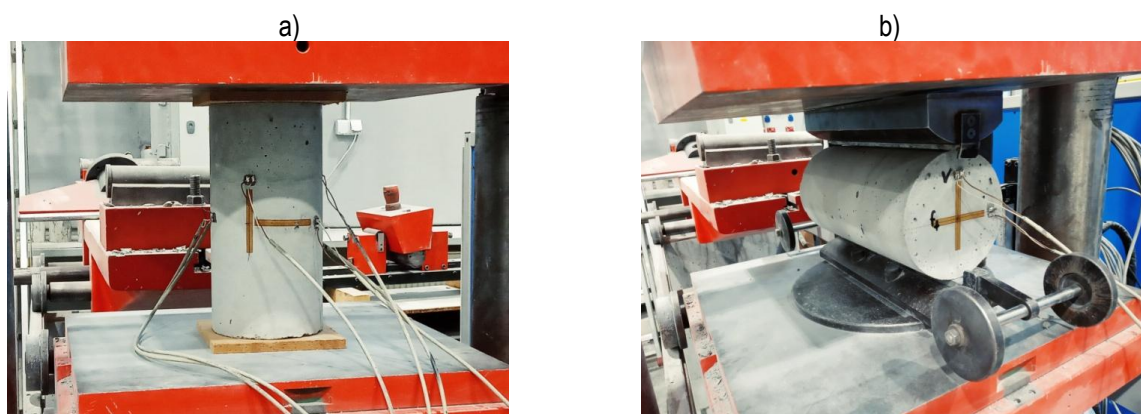
Fig. 4.7.: Cylindrical specimen during a) compression and b) splitting tension Brazilian method test

Tensile strength was estimated indirectly from the splitting tensile strength test. In this case, the load speed rate was set as about 2 kN/s.

A direct tensile strength of concrete was estimated according to [127], where it is expressed as a function of the split tensile strength of cylindrical specimens via the equation:

$$f_{ct} = f_{ctm.spl} \cdot (1 - \beta^2)^{\frac{3}{2}}$$

(4.1)

where:

$f_{ctm.spl}$ - *tensile strength from splitting tensile test*

$\beta = b/D$ - *load-bearing strip width to specimen diameter ratio.*
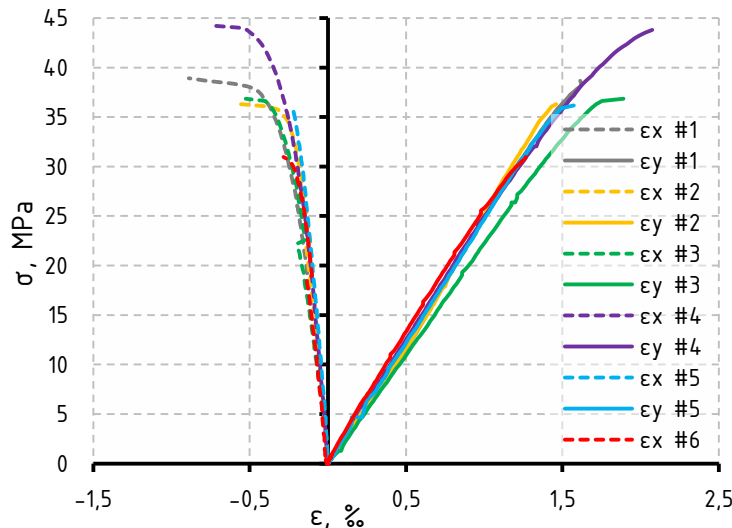
Fig. 4.8.: Avg. strain in vertical (y) and horizontal (x) directions from compressive tests of cubic specimens

In this case, the measured load-bearing strip width was 19mm. Obtained results on concrete samples were summarized in Table 4.5. On the one hand, a relatively good agreement among results in the compression test was obtained in the case of compressive strength as well as the estimated modulus of elasticity. All of the failure modes of samples in the compressive strength test were the same and can be considered satisfactory according to ISO 1920-4 [N12] for both cylindrical (*Fig. 4.9*a). and cubic specimens (*Fig. 4.9*b).

Fig. 4.9.: Typical failure mode of compressed samples: a) cylindrical b) cubic

On the other hand, a variety of tensile strength results obtained in the Brazilian test can be noticed. Furthermore, the average tensile strength values, are lower than those corresponding to the delivered concrete grade. The most possible reason for such an effect can be explained by insufficient concrete vibrating during the pouring of small cylindrical samples using hand tools.

For this reason, non-destructive strength estimation using a concrete rebound hammer was performed to exclude the influence of potential discrepancy of strength on results in target bending tests of beams, however, this additional test shows good agreement in results obtained from all of the prepared beams.

Table 4.5. Test results on cylindrical and cube concrete specimens

Sample Cylindrical 15x30cm No.	Age of concrete [days]	f_c [MPa]								
		Results		Mean value			Standard deviation		Coefficient of variation	
		f_c [MPa]	E_c [GPa]	f_c [MPa]	E_c [GPa]	ν [-]	s_{fc} [MPa]	s_{Ec} [GPa]	ν_{fc} [%]	ν_{Ec} [%]
1 2 3 4 5 6	374	39.6 36.1 36.2 43.6 35.9 31.0	24.0 23.7 22.0 25.0 24.4 25.6	38.2	24.1	0.15	2.6	1.1	6.88	4.7

Cylindrical 15x30cm No.	Age of concrete [days]	f_{ct} [MPa]					
		Results $f_{ctm.spl}$ [MPa]		Mean $f_{ctm.spl}$ [MPa]	Mean f_{ctm} [MPa]	Standard deviation s [MPa]	Coefficient of variation ν [%]
7 8 9 10 11 12	374	2.07 2.81 2.35 2.04 ~~3.78~~ 2.94		2.44	2.38	0.4	15.26

Cube Sample 15x15cm No.	Age of concrete [days]	$f_{c.cube}$ [MPa]			
		Results	Mean value	Standard deviation	Coefficient of variation
		f_c [MPa]	f_c [MPa]	s_{fc} [MPa]	ν_{fc} [%]
1 2 3 4 5 6	475	60,1 54,6 58,1 61,2 55,4 58,7	58,1	2,36	4,3

4.2. EXPERIMENTAL RESULTS OF FULL-SCALE TESTS

4.2.1. FAILURE MODES

In the case of reference non-strengthened beam A1 and strengthened beam A2, occurred failure modes were as expected. The test of beam A1 was stopped when a large deflection of 70mm due to exceeding yield strength in bottom reinforcement was obtained in the experiment. Simultaneously concrete was crushed in the top part of the beam in the mid-span zone after such deflection occurred. Buckling of top reinforcement in the compressive zone was noted (*see Fig. 4.10a-b*). In the case of strengthened specimen A2, a failure due to loss of composite action was observed (*see Fig. 4.10c-d*). A thin layer of concrete remains on the CFRP strip after the failure occurred.

Fig. 4.10.: Typical failure mode of reference beam specimens A1 a) and b) and A2 c) and d)

The failure happened rapidly when a critical crack occurred near the end of the anchorage zone after gradual degradation of the bond due to successively occurring cracks starting from the middle of the span. Total debonding occurred on the length of one-half of the span. Based on theory (*see chapter 2.4*) and expectations, this type of failure was described as IC debonding (IC).

A full compilation of failure modes of all strengthened beam specimens was presented in Appendix C. Similarly to the reference beam A2, an intermediate crack debonding was observed in all cases in specimens: A3a, A3b and A3c (*Fig. 4.11a-b*). In contrast to specimens A2 and A3a, in the case of A3b and A3c debonding occurred on the side of the non-sliding support. Simultaneously this was the side where defects were initiated. In series B, where less shear reinforcement has been used, failure modes were initiated due to diagonal cracks (Fig. 4.12*a-b*). Failure was initiated in the proximity of the end of CFRP and was propagating horizontally towards the middle of the span at the level of bottom reinforcement. Relatively large parts of concrete were attached to the composite after debonding. Occurred symptoms of failure allow classifying it as the concrete cover separation (CCS) failure mode. This type of failure was observed in all beams in series B.

In all specimens in both series A and B, the failure took place suddenly each time. A clear distinction in failure mode could be observed between series A and series B. From the quantitative point of view, it can be concluded that the location of the defect with a given size does not affect failure mode directly in both flexural controlled beams as well as shear controlled beams.

a)   b)
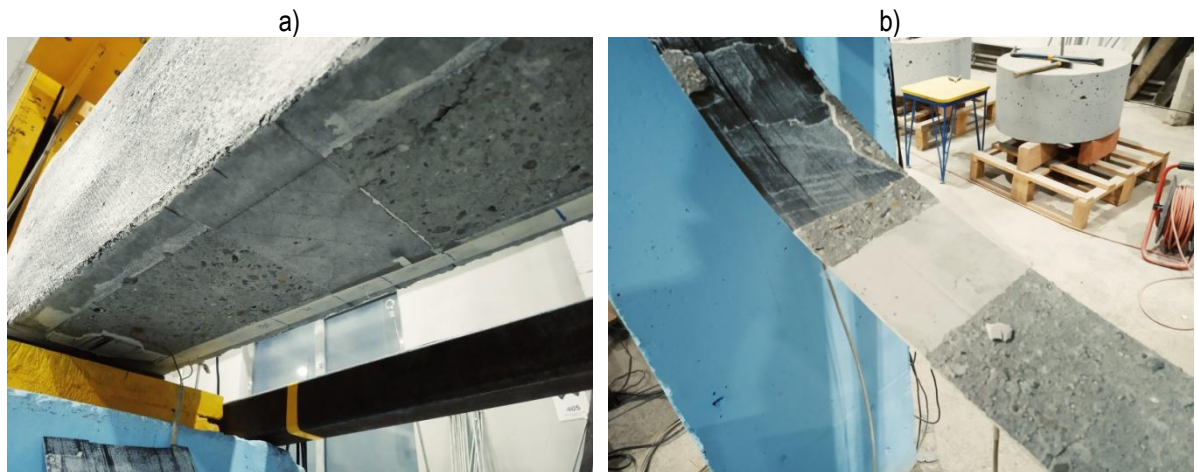
Fig. 4.11.: Typical failure mode (IC) of beam specimens in series A (here A3a)

a)   b)

Fig. 4.12.: Typical failure mode (CSS) of beam specimens in series B (here B3b)

In the case of specimen A6 with a large 60% defect failure occurs at the end of CFRP in the anchorage zone. During the tests, twice the loud sounds of breaking material had been heard before failure occurred. The result of the failure was the pulling of the strip from the anchorage zone.
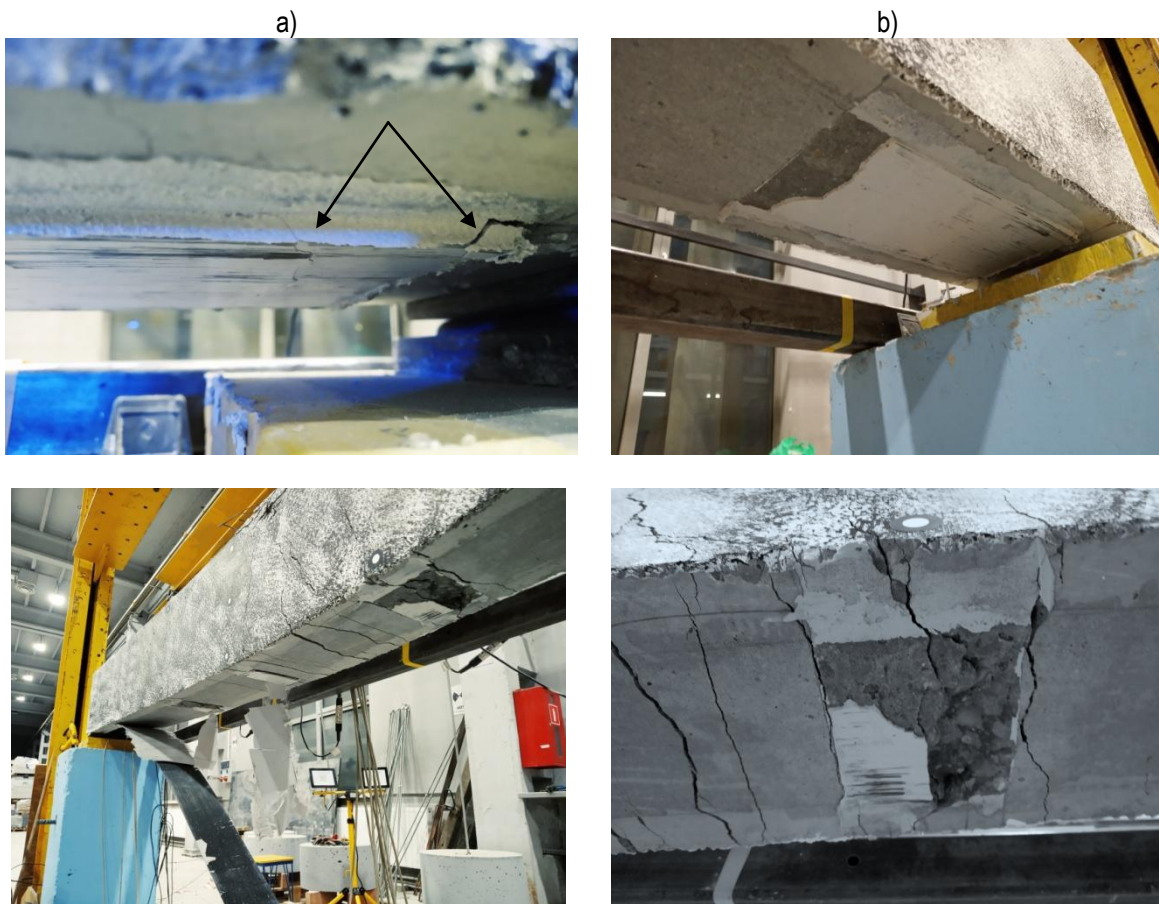
Fig. 4.13.: Failure mode of beam specimen – A6 a) cracks in the adhesive layer of anchorage zone, b) broken adhesive layer; c) general view of the beam; d) the debonding area under the point load

On the side where debonding occurs broken adhesive layer partially attached to the beam in the anchorage zone and partially to the composite has been observed. In close-up, small cracks in the adhesive have been visible and probably here failure was initiated (*see Fig. 4.13a and b*). In the midspan, the adhesive layer remained on the beam, when directly under the point load concrete has been pulled off from the side of supports (*see Fig. 4.13c and d*).

4.2.2. LOAD - DEFLECTION RESPONSE AND CRACK PATTERNS

In the figures (*Fig. 4.14a÷b*) load - mid-span deflection relationships in both the A and B series were presented. Specific slight drops of applied force values are related to the holding of the load in order to crack measurement (*see also   Fig. 3.3*). Analysis of load-deflection response can result in information on specific stages of beam behaviour (see 2.2). The clear difference between strengthened beams and RC can be seen. An increase of ca. 58% of the ultimate load of the strengthened beam was achieved in comparison to the reference A1 beam. No significant difference

can be observed among all of the strengthened beams in series A in behaviour under loading but also in ultimate load values. Although it was decided to increase the defect area in series B, the general behaviour of all three specimens with various defect locations was rather similar. No clear part of the diagram related to steel yield can be seen in the beams of series B. A good agreement between slopes of load-deflection response can indicate also coherent material properties obtained between them.
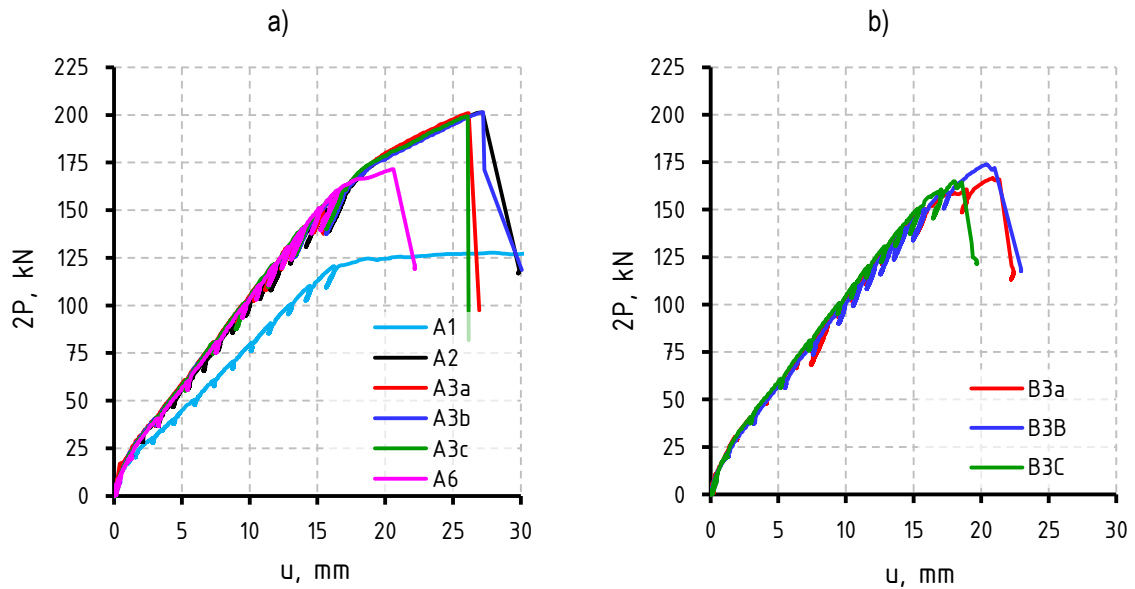
Fig. 4.14.: Load-deflection response of strengthened beams a) series A b) series B

A comparison of values of the ultimate load P_u was presented in Table 4.6. The differences between specimens in both series were calculated in relation to specimens with type 'b' of the defect – where the highest ultimate load value in each series was recorded. The difference in ultimate load value ΔP_u among specimens with initiated defects does not exceed 1% in the case of series A (A3a,A3b,A3c) and 5.1% in the case of results obtained in series B (B3a,B3b,B3c).

Table 4.6 Ultimate load and corresponding mid-span deflection values

ID	P_u, kN	ΔP_u	u, mm	Δu
A1(ref.)	127.1	-	-*	-
A2 (ref. strengthened)	201.3	-	27.2	-
A3a	200.9	0.2 %	26.1	4.0 %
A3b	201.4	0 %	27.2	0.0 %
A3c	199.3	0.99 %	26.1	4.0 %
A6	171.6	14.8 %	20.6	24.3 %
B3a	166.77	4.0%	20.8	-1.5 %
B3b	173.8	0.0 %	20.5	0.0 %
B3c	164.9	5.1 %	18.5	9.8 %

*deflection was increasing in the whole loading range (see Fig. 4.14)

It can be noted that the average value of the ultimate load of about 17% lower in beams of series B in comparison with series A. The defect of 60% of the total area causes only about a 15% reduction in ultimate load. Vertical displacements measured in five points along the beam for series A and series B were presented in Fig. 4.15a and b. Symmetrical deformation of the beams in relation to the midspan can be observed in the whole load range in both series. This indicates that the assumed defects in each selected location have a negligible effect on deflection shape.

a)

b)
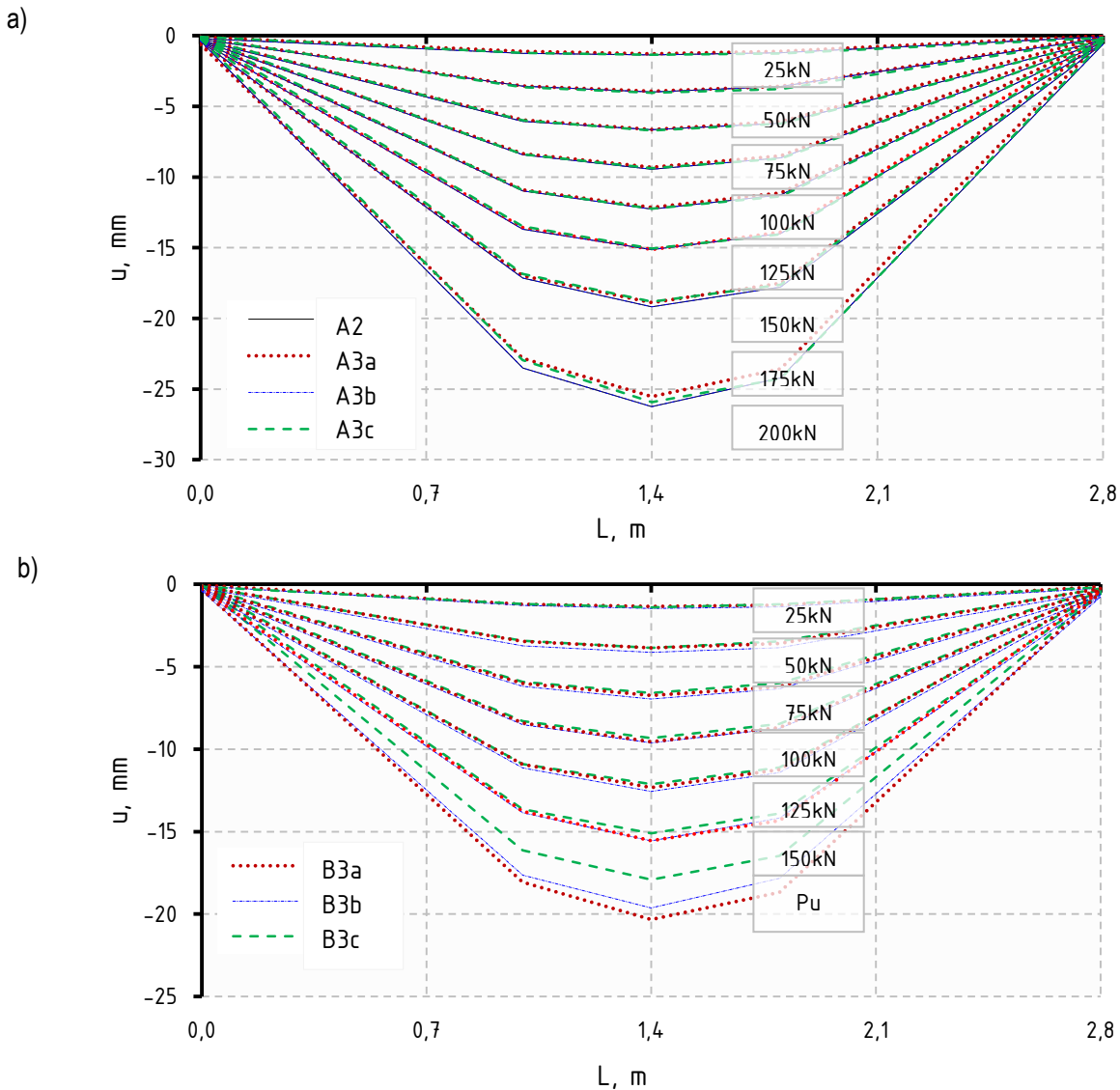
Fig. 4.15.: Vertical displacements along the beam at different load levels

Appearing cracks which were manually marked during the tests up to the load value of 160kN were presented in Fig 4.16. In general, a more vertical crack pattern can be seen in beams series A in comparison to series B where cracks occur in a more diagonal form. This was caused by a lower number of used stirrups. In both cases, the highest recorded crack width was 0.4mm, but in general, in series B higher average values of the width of cracks were observed. It can be seen that crack patterns in both series are not clearly affected by defects and their location on the beam.

A3a

A3b

A3c

B3a

B3b

B3c

Fig 4.16 Recorded crack patterns at beam specimens of series A and B

4.2.1.   CURVATURE AND STRAIN DISTRIBUTION

Bending moment-curvature relationships for both series A (*Fig. 4.17a*) and series B (*Fig. 4.17b*) were presented which is common when numerical cross-section analysis is performed. This relationship was derived from geometrical properties and circular approximation of deflection shape between load points for each beam corresponding to strain distribution in the mid-span cross-section (*see Fig. 4.18*).

a)   b)
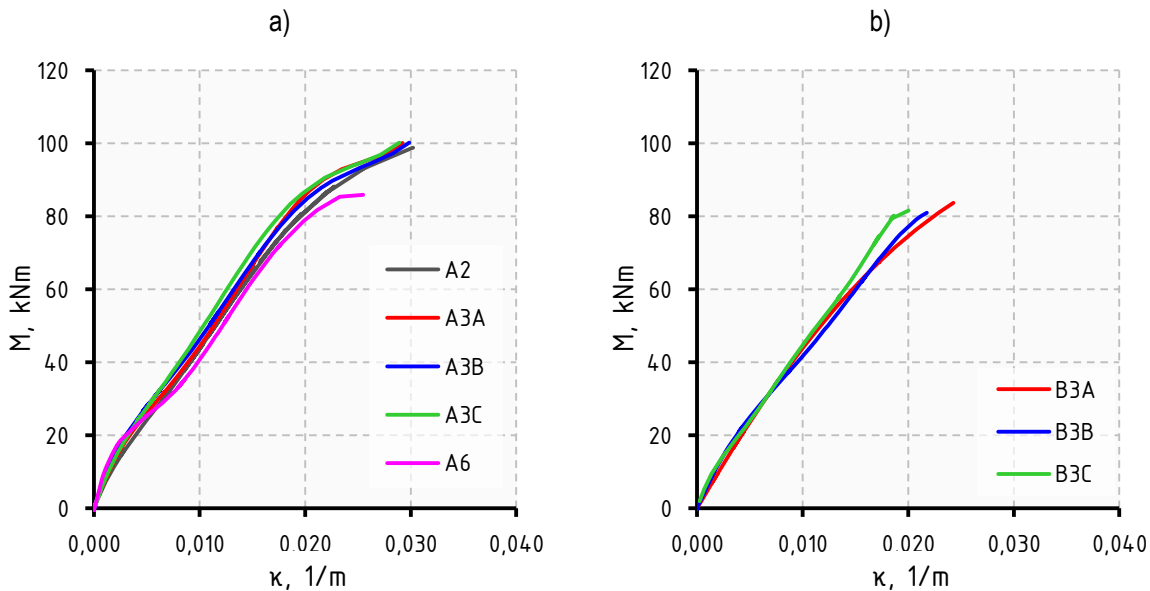
Fig. 4.17.: Bending moment-curvature response of tested beams in series A and B

Like in the case of load-mid-span deflection, there is no significant difference between the bending moment-curvature relationship among results obtained in series A. Moreover, similarly to the load-deflection curves, the part of the diagram related to steel yield can be seen in the beams of series A beyond the value of about 0.02 *1/m*. This is not clearly visible in diagrams in series B.

$$R^2=|BD|^2+|CD|^2$$
$$R^2=|BD|^2+(|CE|-|DE|)^2$$
$$R^2=|BD|^2+(R-|DE|)^2$$

$$\frac{1}{R}=\frac{8f}{f^2+4g^2}$$
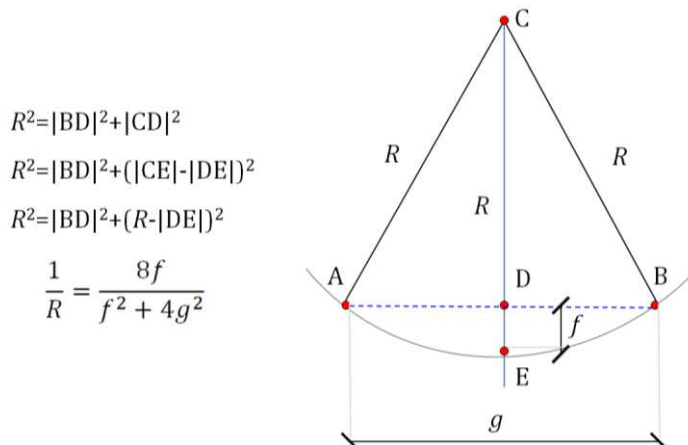
Fig. 4.18.: Determination of curvature in the study

A small distinction between the results of specimens in series B can be noticed, where 9% and 4% lower curvature values were obtained in specimen B3C and B3B respectively in reference to

specimen B3A. In series A all specimens achieved curvature of about 0.03 *1/m* just before failure when curvature values in series B were close to 0.02 *1/m*.

According to the Euler-Bernoulli beam theory [144], a natural consequence of existing curvature is strain distribution in each cross-section of the beam in flexure. In Fig. 4.20 strain measured at CFRP strip along the span at a different loading level of all specimens was presented where defect location was additionally marked at each figure. In series A as well as reference beam A2 maximal measured strain value of 5.8‰ was measured at failure which is close to the results obtained in the study [79] (see 2.5.7). In series B, maximal measured strain values at failure varied in the range of 3.26 ÷ 4.16‰. It can be noticed a slight variation of strain values measured in the proximity of the defects, especially for load values close to the ultimate load. It can be seen that up to a load level of 150kN strain value increased steadily. Over this value, the strain rate increased for specimens A3a-A3c with the same load increment due to exceeded yield strength in bottom reinforcement. For the specimen with a large defect (A6), delayed strain response was observed at the beginning of loading. Lower strain values at the same load level were measured in specimen A6 in comparison to the rest of the specimens. This can be explained by the existing clearance between CFRP and adhesive and local slip of composite in areas where defects were applied before full composite action occurs.

It is worth mentioning that accidentally, the behaviour of specimen A6 with a proposed pattern of the defects, some analogy can be found to the behaviour of reinforced RC beams with external ties/tendons (see *Fig. 4.19*). In such systems, the initial slip of the tendon usually occurs at the initial loading stage in the anchorage. Similar behaviour was observed in the case of sample A6. Adhesive placed locally under point loads performs the function of deviators and the adhesive located at the ends creates a clear anchorage zone. A large defect caused a visible slip of the CFRP strip which is close to the behaviour of typical systems with ties/tendons without adhesion. However, this small consideration will not be further investigated in this study.
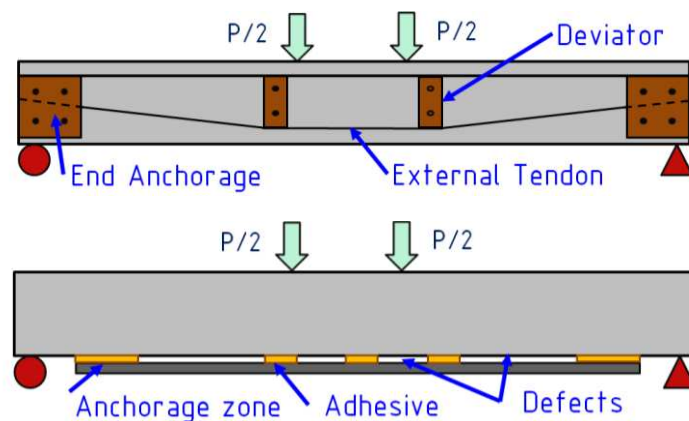
Fig. 4.19.: Analogy found for a) external tendon b) specimen with a large defect

Recorder distribution of cracks based on strain using the digital image correlation method, before and after failure was presented in Fig. 4.21, Fig. 4.22 and Appendix D.
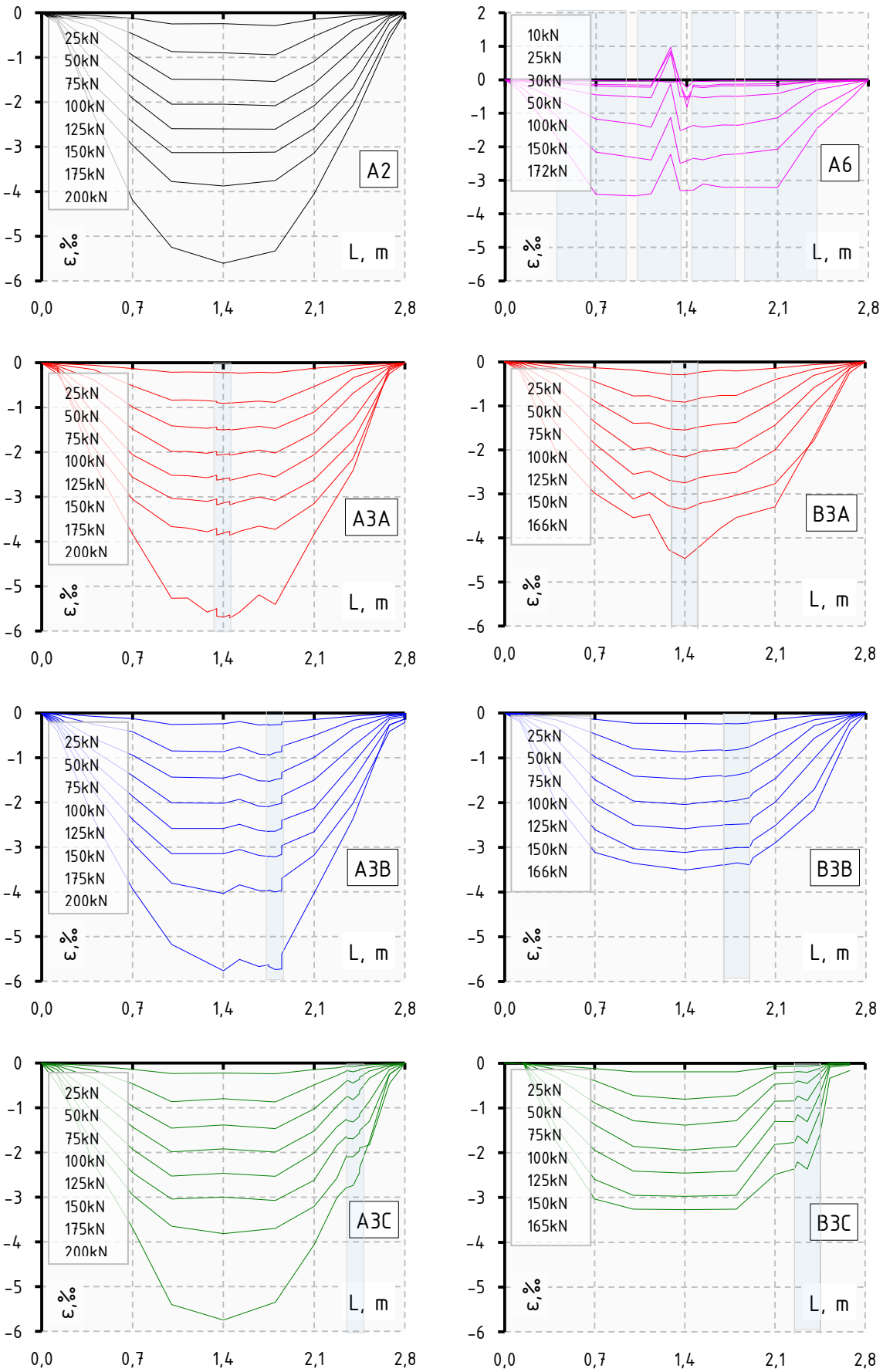
Fig. 4.20.: CFRP strain measured along the beam specimens in selected load steps
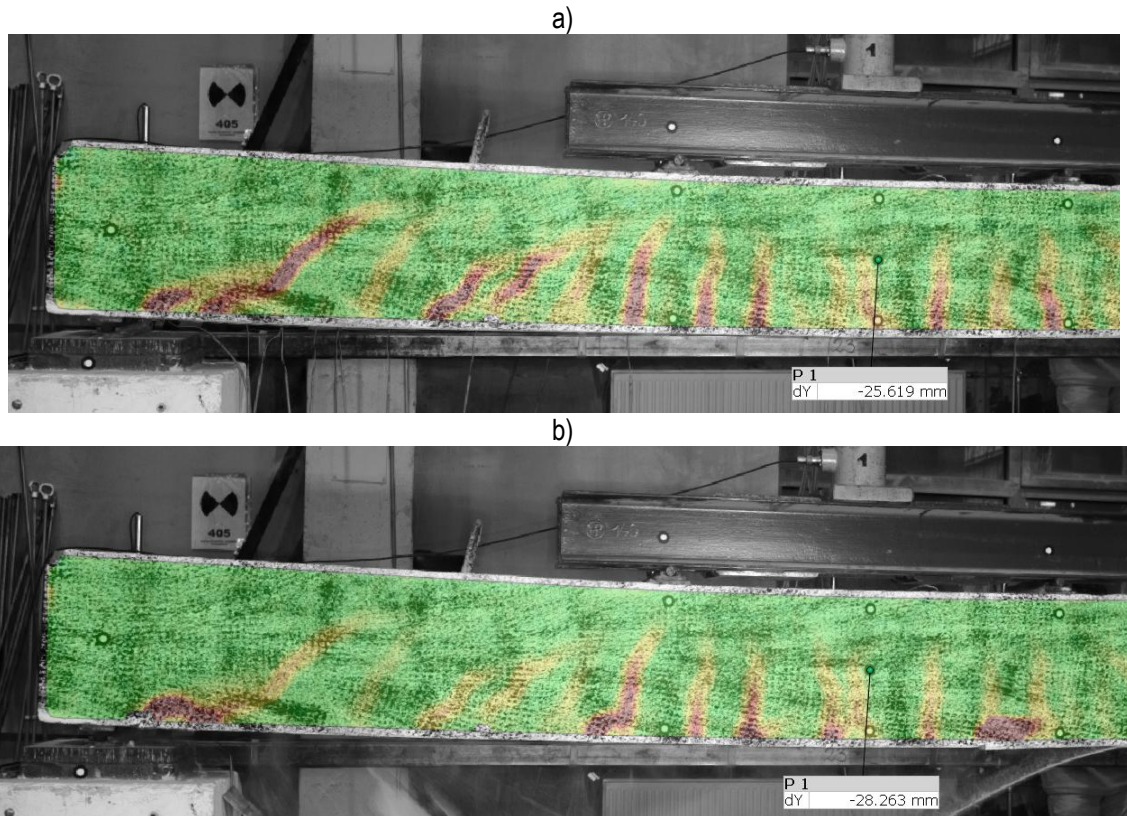
Fig. 4.21 Strain ε₁ distribution in specimen A3c a) before and b) after failure
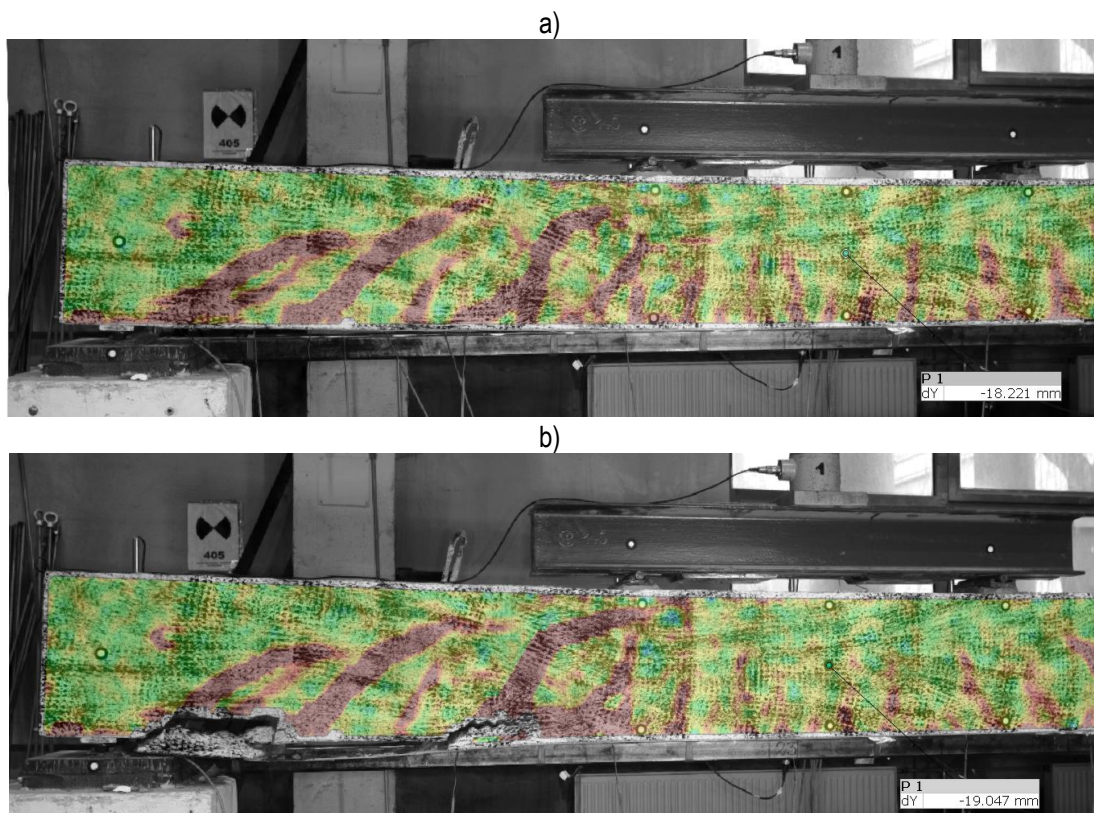
Fig. 4.22 Strain ε₁ distribution in specimen B3c a) before and b) after failure

4.2.2.   SUMMARY OF EXPERIMENTAL PART

The following summary and conclusions can be formulated based on the results obtained in the experimental study:

- The defects did not affect the type of expected failure mode in both series of beam specimens. In series A, IC debonding failure was obtained while in series B, CCS failure mode was observed.

- For series A, delamination occurred after and in series B, failure occurred before reinforcement reached its yield strength,

- Results obtained from series A show that applied defects up to the value of 5% of the total strengthening area almost do not affect the ultimate load of tested beams. In other words, all specimens in series A had almost the same ultimate load value. The difference in ultimate load between strengthened beams with defects and the strengthened reference beam does not exceed 1%.

- There is also no significant difference between the ultimate load values of beams in the B series where the defects of up to 10% of the total strengthening area were applied. The difference does not exceed 5.1%. It is worth noting that there was no tested beam with no defects in the B series. However, based on results obtained in series B, and results obtained in series A, it can be presumed that the ultimate load of the strengthened beam with type 'B' geometry with no defects (B2) could be similar to values obtained in conducted tests,

- In the case of both series, the highest ultimate load was obtained when the defect occurred directly under the point load and the lowest value occurred near the anchorage zone.

- Fig. 4.23 presents the distribution along half of the beam of the relative ultimate load values (P_u) related to the maximal ultimate value obtained in the series (P_{uimax}) based on Table 4.6. Distribution is correlated to the location of applied defects. Ultimate load values for given 5 and 10% defects levels are not significantly location-dependent. It means that the relationship between ultimate load values and defect location along the beam is almost a constant function for given defects and geometry of the beams (Fig. 4.23). Results confirm the numerical study presented by Zhou et al. [156] that mid-span defects less than 12000mm^2 have little effect on the ultimate load values of the beam with an *l/d* ratio higher than 4. In contrast to Zhou, results obtained in this test show that shear-span defects up to 24000mm^2 has also a little effect on strengthening performance in this case. Such behaviour may be a result of wider CFRP strips used in this study and the high longitudinal steel reinforcement ratio.
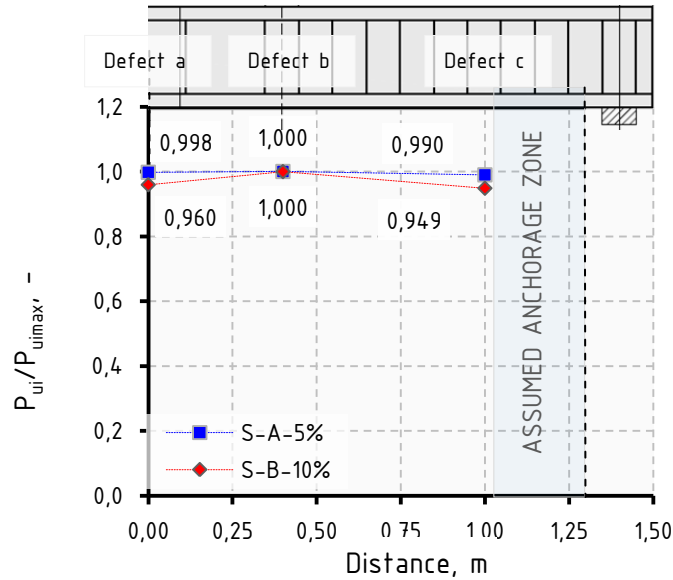
Fig. 4.23.: Relationship between relative ultimate load values and defect location for series A (blue), series B (red)

- Beams with initiated defects in all tested beams show the same stiffness and curvature up to the failure. This also indicates good agreement in material properties between specimens.

- The obtained crack patterns do not show any symptoms of hidden defects in the interfacial bond and that is why it cannot be treated as a bond defect indicator.

- The defect with 60% of the total area, reduced the ultimate load of the strengthened beam (A6), by 15% in comparison to the strengthened beam with no defects (reference specimen A2). It leads to a more or less obvious conclusion that the ultimate load value depends not only on the bond in anchorage zones but also there is the influence of the composite-concrete bond between anchorage zones in the passive strengthening systems.

- Referring to the absolute decrease of the ultimate load value does not inform about the change of the effective part of the capacity of the strengthened element. It is helpful to express the effective part of the bearing capacity of strengthening relative to the non-strengthened element and strengthened element with a perfect bond (*see Fig. 4.24a*). For this reason following quantities can be introduced:

$$\Delta_{i.eff} = \frac{\Delta_i}{\Delta_{u100}} = \frac{P_{ui} - P_{uRC}}{P_{u100} - P_{uRC}} \tag{4.2}$$

$$\Delta_{i.red} = 1 - \Delta_{i.eff} \tag{4.3}$$

where:

P_{uRC} -   *The ultimate load of the RC beam*

P_{u100} -   *The ultimate load of CFRP strengthened beam with no defects (reference specimen)*

P_{ui} -   *The ultimate load of CFRP strengthened beam with defect,* $P_{uRC} \leq P_{ui} \leq P_{u100}$

Quantity Δ_{eff} (called here *strengthening efficiency*) takes values from 0 to 1 and informs what is the increase of capacity of strengthening with interfacial bond defects in relation to the unstrengthened member. Nevertheless, from the point of view of diagnostics, it is more appropriate to operate on the loss of the strengthening capacity. Thus, Δ_{red} informs what is the bearing capacity drop of the strengthened member with defects relative to the strengthened member with no defects. The quantity Δ_{red} as a function of the defect percentage ratio for tested specimens was presented in Fig. 4.24b. A defect ratio of 0% can be considered as no defects, and 100% basically means that there is no CFRP- concrete bond and the beam behave as unstrengthened. It can be seen that for the ratio of the analysed defects (5%,10% and 64%) only one point between a range of 5% to 100% was obtained. That shows the significance of the specimen A6 test from the point of view of this study. It shows that strengthening efficiency is not a linear function of the defect ratio. Based on three points, a second-order polynomial approximation can be used. Confirmation for such function for given beam geometry and boundary conditions can be validated later using a numerical approach.
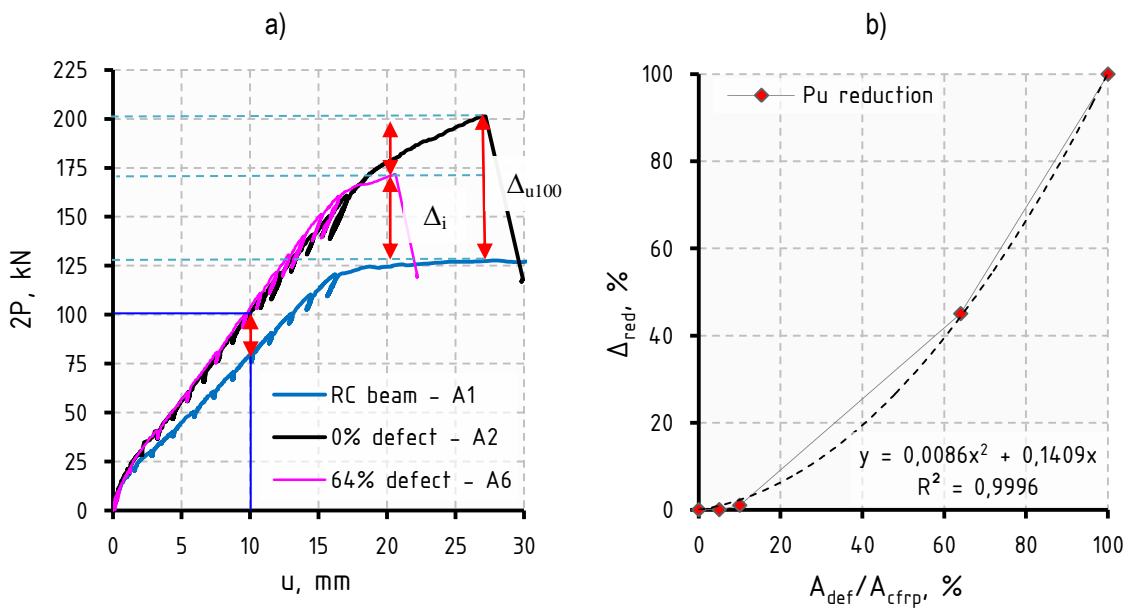
Fig. 4.24.: The logic behind the introduced capacity reduction factor a)
capacity reduction factor in a function of defect percentage ratio b)

It is worth mentioning that by changing Δ_{red} to Δ_{eff} a decreasing parabolic function can be obtained that corresponds to the general damage tolerance approach used in aircraft design (*compare Fig. 2.21*a).

5. NUMERICAL STUDY

5.1. A BRIEF OVERVIEW OF FE ANALYSIS OF CFRP STRENGTHENING

Numerical analysis of CFRP-strengthened RC beams was the subject of many studies over the years [21][78][97][116][132]. A wide range of research in this field was dictated by highly complex phenomena like nonlinear concrete behaviour or adhesive bond between FRP and concrete in different loading conditions were studied. There are limited studies where the defect in the bond in CFRP-strengthened RC beams is considered an initial parameter [156]. Nevertheless, various attempts for modelling CFRP strengthening of concrete were popular subjects of study in recent years. Calculations are performed with different levels of simplification. Different approaches to simulating bond behaviour can be distinguished depending on the aim of the research. The simplified method of perfect bond assumption was mostly adopted [52][110][147] but also used as a reference to more complex approaches [21][95][116]. Selected studies of numerical analysis of CFRP-strengthened beams based on FEA were briefly described below with an emphasise on the used bond-slip law parameters.

Kotynia, Baky et al. [78] presented a numerical study that consisted of a three-dimensional nonlinear finite element analysis of reinforced concrete beams strengthened with FRP laminates. A quarter of the beam was analysed with the use of symmetrical boundary conditions. The whole study was performed in ADINA software using FE element sizes of 50mm and 12.5mm in the tension zone. A bond-slip model according to [98] was adopted to characterize the behaviour of the CFRP/concrete interface. The nodes of the CFRP elements were connected to those of the concrete elements through additional interface finite elements. Good agreement was found with experimental results where the main focus was put to analyse shear stress distribution through the interface. Another study conducted by Obaidat et al. [117] focused on a numerical study of CFRP-strengthened beams in flexure with different anchorage lengths. 3D modelling was limited to one-quarter of the beam with the use of symmetry in boundary conditions. The whole study was performed in ABAQUS software. The concrete damage plasticity (CDP) model of concrete was used and the CFRP-concrete interface was modelled using a cohesive zone concept via cohesive elements. Initially, the bond-slip law was adopted according to Lu [98] and additionally, the perfect bond was analysed. Nevertheless obtained ultimate load was too high in comparison to experimental data in all specimens. Good agreement in all specimens was obtained when maximal shear stress was reduced from 3 MPa to 1.5MPa when concrete tensile strength was 1.81 MPa. A symbolic influence was observed for different bond fracture energy values of 500-900 N/m when the composite–beam width ratio parameter was 0.33.

Zhou et al. [156] presented one of the few FE studies concerning defects' influence on FRP-strengthened concrete beams. The influence of the geometry parameters of the beam and the location of defects were analyzed. The numerical part of this study was performed in a two-dimensional analysis. Steel and FRP reinforcement were considered as truss elements when the concrete part was modelled using plane stress finite elements with the use of the CDP model. For the concrete uniaxial behaviour, the stress-strain relationship according to the model code was adopted. The FRP-concrete interface was considered with the use of additional cohesive elements and damage evolution was assumed with the use of bilinear traction-separation law also according to [98]. The lack of cohesive elements was treated as a defect. The expressions for bond-slip models have been presented however, the used values in the analysis have not been shown explicitly.

The comprehensive work presented by Cohen [21], was focused on analysing different parameters of numerical models of RC beams strengthened with CFRP strips. The whole study was performed using the CDP concrete model and cohesive elements. Like in previous studies, a 3-dimensional analysis was limited to one-quarter of the beam model. Mesh sensitivity study, strain calibration and concrete model parameters were analysed. For cohesive bond-slip law, the maximal shear stress was estimated as 5.49 MPa when the tensile strength of concrete was 3.66 MPa. The exponential damage evolution of the bond has been adopted and expressed by an exponent value of 1.194 and a maximal displacement of 0.214mm.

Serega, Kotynia et al. [132] presented vast complex numerical research on prestressed CFRP strips for strengthening RC beams in their study based on experimental results. The two-dimensional analysis was performed and it was divided into a few steps including self-weight deformation, concrete shrinkage, application of prestressing and external preloading. A concrete constitutive model using the smeared cracks concept was adopted. The whole study was performed in DIANA commercial software for which a developed user subroutine of interface modelling was used. The traction-separation relationship in a tangential direction was expressed as an extended function including an exponential branch according to [98]. In contrast to other studies, the bond-slip relationship was described not only for monotonic load but also it was developed for the cyclic type of loading. Beyond the concrete - CFRP interface, a bond-slip relationship between steel and concrete as well as the bond-slip relationship in the mechanical anchorage region were distinguished and taken into account. Bond–slip parameters of CFRP – concrete interface were determined individually for each specimen.

5.2. FINITE ELEMENT ANALYSIS

5.2.1. NUMERICAL METHODOLOGY

Due to the use of a combination of nonlinear material models and bond behaviour of CFRP-concrete interface, a finite element analysis (FEA) was divided into a few steps (*see Fig. 5.1*). Firstly, material models were determined and described with required parameters based on laboratory tests and literature. Secondly, a trial run for the selected case found in the literature was performed. Initial analysis to validate assumed data was conducted for reference RC beam A1 and reference strengthened beam A2 with perfect bond assumption to avoid interference of bond-slip model on results. Additionally, to confirm obtained at this stage results, a numerical tool was developed by the author in Python programming language based on the fibre-beam approach. The theory behind the tool and validation process was described widely in Appendix A.

After confirmation of the results, calibration of the bond-slip relationship parameters was conducted based on the trial and error method for specimen A2. The final stage consisted of the validation of all taken assumptions on all tested experimentally beam models with defects. In the final step, analysis was extended to additional numerical beam models to obtain the ultimate load–defect ratio relationship.
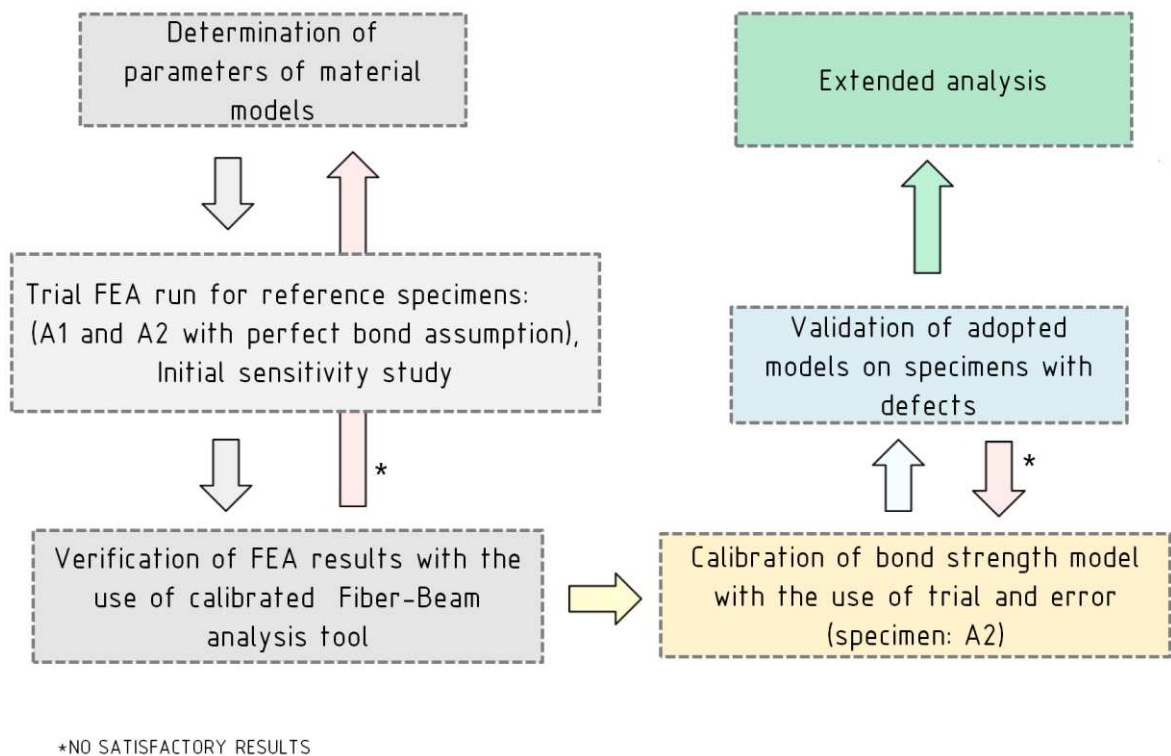
Fig. 5.1. Adopted methodology in numerical FE analysis

5.2.2.   INITIAL CONDITIONS

Numerical calculations were performed in ABAQUS Standard software [1]. In the case of 3D models, 8-node hexahedral (C3D8R) solid finite elements were used for modelling the concrete of the beam (*see Fig. 5.2*). For steel reinforcement, 2-node beam elements (B31) were used for both longitudinal bars and stirrups. Reinforcement was embedded in solid elements of concrete and the bond-slip relationship between steel reinforcement and concrete was neglected. CFRP strips were modelled as 4-node shell (S4R) finite elements. Steel rectangular plates were used for supports as well as for intermediate elements transferring load directly to the beam.

Newton's numeric technique has been used for solving the nonlinear equilibrium equations in the analysis. A few finite-element mesh sizes were used for the mesh sensitivity study: 15mm, 25mm and 50mm, from which 25mm was finally selected for further calculations. Analysis was conducted in two steps. In the first step, the self-weight of the beam was taken into account. In the second, a monotonic external load was applied using the displacement control technique. The maximum range of displacement was set as 30mm and displacement increments vary between 10^{-15} mm and 0.01mm. The load was applied to the beam through steel plates on the top surface. Beam was supported on steel plates where simpe boundary conditions were used. On the centre line of the bottom surface of steel plates, translations in all directions were restrained ($u_x = u_y = u_z = 0$), while on the other side only vertical and transverse translations ($u_y = u_z = 0$) were restrained. Symmetry boundary conditions in relation to the YZ plane were used at nodes in the midsection plane.
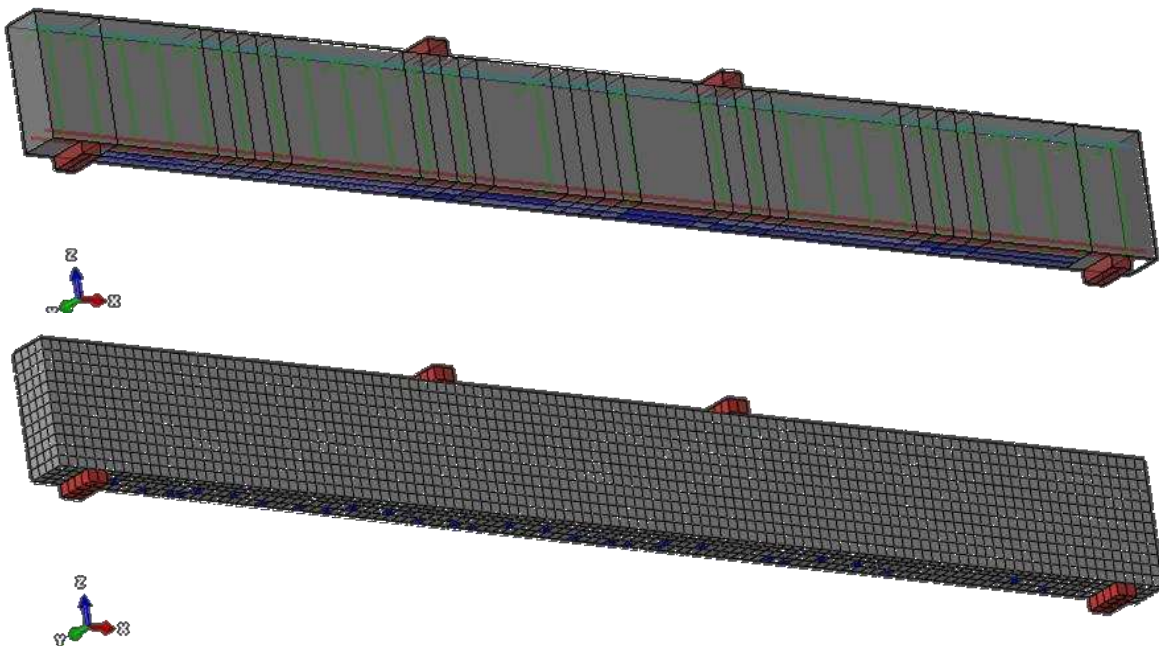
Fig. 5.2.: Visualisation of the 3D RC beam model and main mesh size (25x25mm)

5.3. MATERIAL MODELS

5.3.1. REINFORCING STEEL

The stress-strain relationship for reinforcing steel was adjusted to the results obtained in the material investigation. An elastic-plastic material model with kinematic hardening was assumed, thus the stress-strain curve was approximated using a bi-linear relationship as shown in Fig. 5.3a. The slope of the elastic segment is represented by Young's modulus based on laboratory tests and was set as 200GPa for associated yield strength of 575MPa. Poisson's ratio was assumed based on similar studies found in the literature. All parameters taken in the numerical analysis were summarised in Table 5.1.

Table 5.1. Reinforcing steel material parameters used in the model

Parameter	Symbol	Value	Unit
Yield strength	f_y	575	*MPa*
Yield strain	ε_y	0.0028	-
Young's modulus	E_s	200	*GPa*
Poisson's ratio	ν	0.3	-
Strength	f_t	665	*MPa*
	ε_{sh}	0.028	-
	E_{sh}	2.0	*GPa*

To avoid convergence issues, a plastic plateau beyond yield strain was assumed with a slight slope described by hardening modulus with the value of 2GPa.
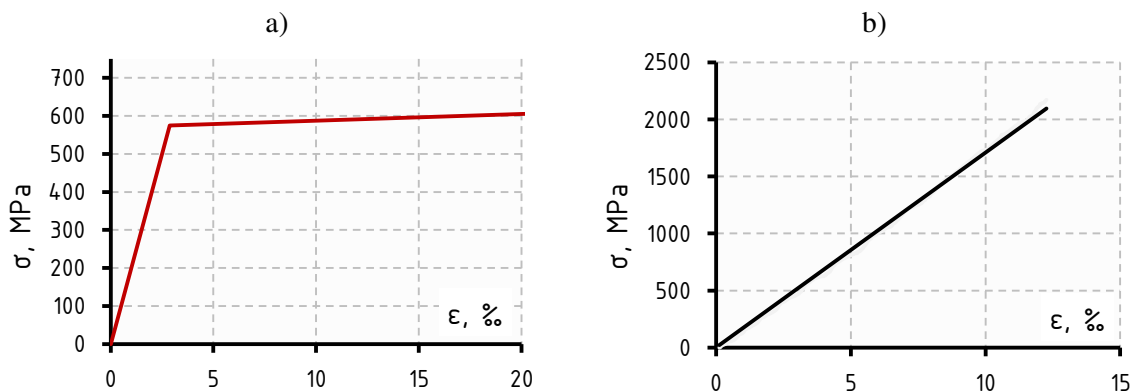
Fig. 5.3.: Bi-linear material model for reinforcing steel a) linear elastic material model for CFRP strip b)

5.3.2.   CFRP STRIPS

The stress-strain curve of the CFRP strip was assumed to be perfectly elastic up to the failure as shown in Fig. 5.3b based on average values obtained in laboratory tests. The parameters needed to specify this behaviour in the numerical model were summarised in Table 5.2.

Table 5.2. CFRP material parameters used in the model

Parameter	Symbol	Value	Unit
Ultimate strength	f_{pu}	2179	*MPa*
Rupture strain	ε_{pu}	0,012	-
Young's modulus	E_{CFRP}	171,9	*GPa*
Poisson's ratio	v	0,3	-
Thickness	t	1,2	mm

5.3.3.   CONCRETE

Over the years modelling of complex nonlinear behaviour of concrete has been developing and nowadays it can be considered an independent branch of engineering [104]. Nevertheless, numerical analyses (based on the finite element method [7][24] [158]) mentioned in the previous chapter were performed mostly using available material models in FEA commercial packages [60][73] and adjusted to results obtained in the experimental investigation. In this study, for the nonlinear response of concrete, the concrete-damage plasticity (CDP) model was adopted. This model was firstly proposed by the team Lubliner, Oller, Oliver, and Oñate in 1989 [99], in collaboration between the University of California (Berkeley, USA) and Universitat Politecnica de Catalunya, (Barcelona, Spain). The main effort of the authors has been focused on the determination of a mathematical model describing more precisely, the nonlinear response of reinforced concrete structures. It has been developed over the years by Fenves and Lee [94], and implemented in commercial software ABAQUS in 2002. In 2017 validated modification of this model was proposed by the research team including one of the authors of the model [2], where a new method of calculating concrete damage variables depending on mesh size was introduced.

CDP is a combination of elastoplastic material stress-strain relationships where isotropic degradation is considered. The degradation process of material starts after the ultimate level of stress on the damaged surface is reached. The CDP model assumes two major damage mechanisms - cracking in tension, as well as concrete crushing in compression. The degradation process of material is a result of the development of micro-cracks under the monotonic as well as cycling load, which is why the concept of effective stress was introduced (see Fig. 5.4) The general

relationship between the stress state of undamaged material and the effective stress state is determined by damage variables that can be defined as a scalar or tensor quantity.
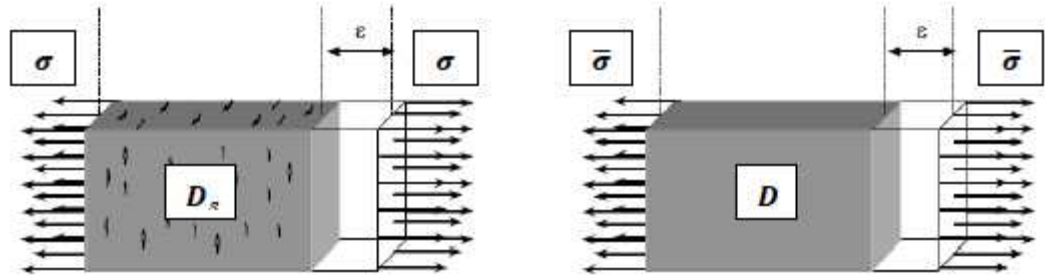
Fig. 5.4 The concept of effective stress

In the case of the isotropic damage model, such a relationship is formulated as follows:

$$\overline{\sigma} = \left(\frac{1}{1-d}\right) \cdot \sigma \tag{5.1}$$

where:

$\overline{\sigma}$ *effective stress tensor*

d *scalar damage parameter* ($0 \leq d \leq 1$)

Formulation of effective stress by the Cauchy stress tensor can be related to the constitutive relationship which in iterative plasticity theory can be expressed as follows [11]:

$$\boldsymbol{\sigma} = (1-d)\boldsymbol{D} : (\boldsymbol{\varepsilon} - \boldsymbol{\varepsilon^p}) \tag{5.2}$$

During the unloading process, the elastic behaviour of the material is maintained with lower stiffness in both cases - tension and compression. Damage is progressing by reduction of initial stiffness which is dependent on two damage parameters: d_c (*DAMAGAC*) in case of compression and d_t (*DAMAGET*) in case of tension. Parameters take values in the range of 0 (perfect elastic behaviour) to 1 (total stiffness loss). During uniaxial tension (*Fig. 5.5a*) material works fully elastic up to stress reaches a value of σ_{t0}.
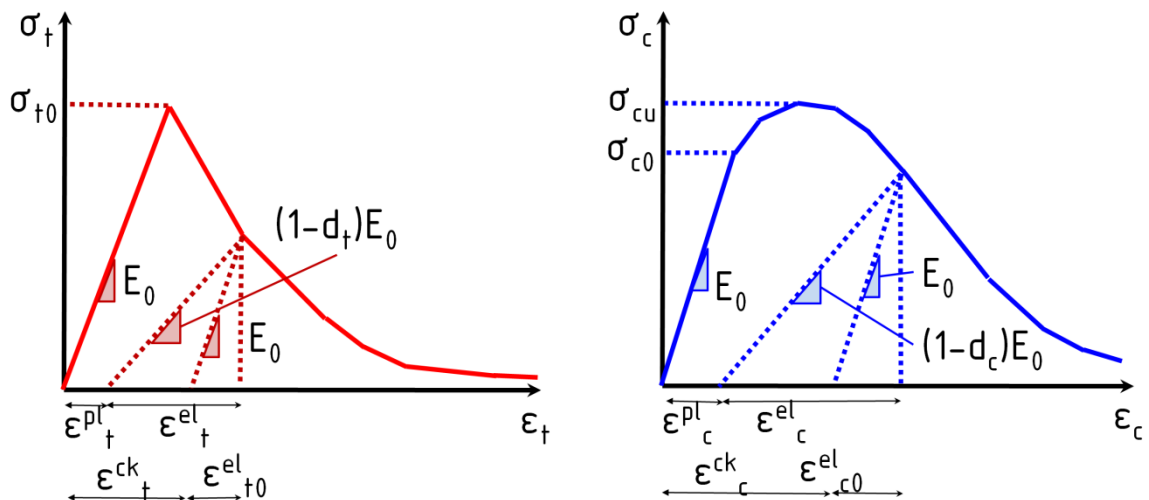
Fig. 5.5.: Uniaxial concrete response due to (a) tension (b) compression

After σ$_{t0}$ value is exceeded, material degradation in form of tension softening starts which is related to appearing of micro-cracks in concrete. In the case of uniaxial compression (*Fig. 5.5b*), the concrete response starts to be nonlinear after the stress value exceeds σ$_{t0}$ up to the ultimate stress value σ$_{cu}$ when the softening behaviour of concrete has begun. In case of a change of stress sign, the effects of closing and opening micro-cracks in the material structure are provided in the model.

It was achieved by connection tension and compression damage parameters with the use of the following relationship:

$$(1 - d) = (1 - s_t d_c)(1 - s_c d_t) \tag{5.3}$$

where:

s_t, s_c -   *functions related to sign changing of stress*

d -   *general damage parameter (SDEG)*

Functions s_t and s_c are defined as follows:

$$s_t = 1 - w_t \cdot r^*(\sigma_{11}) \qquad 0 \leq {}_\_w_t \leq 1$$
$$s_c = 1 - w_c\big(1 - r^*(\sigma_{11})\big) \qquad 0 \leq {}_\_w_c \leq 1 \tag{5.4}$$

where:

w_t, w_c -   *coefficients that control the stiffness in the transition between compression and tension, which are a property of the material.*

$r^*(\sigma_{11})$ *- the function of the state is expressed as follows:*

$$r^*(\sigma_{11}) = H(\sigma_{11}) = \begin{cases} 1 \ for \ \sigma_{11} > 0 \\ 0 \ for \ \sigma_{11} < 0 \end{cases} \tag{5.5}$$

As far as concrete in real conditions is subjected to a complex stress state, damage to concrete is described as a yield surface which is considered in 3D principal stress space. The yield function in the CDP model is based on a modified Drucker-Prager function in the form as follows [59]:

$$F(\bar{\sigma}, \dot{\varepsilon}^{pl}) = \frac{1}{1 - \alpha}(\bar{q} - 3\alpha \cdot \bar{p} + \beta(\kappa)\langle\bar{\sigma}_{max}\rangle - \gamma\langle-\bar{\sigma}_{max}\rangle) - \bar{\sigma}_c(\dot{\varepsilon}^{pl}) = 0 \tag{5.6}$$

where:

α, β, γ -   *dimensionless model parameters*

$\bar{p}, \bar{q}$ -   *effective values of invariants p and q*

$\bar{\sigma}_{max}$ -   *maximal value of effective principal stress*

$\dot{\varepsilon}^{pl}$ -   *stiffening variable, defined by two independent parameters $\dot{\varepsilon}_t^{pl}$ for tension and $\dot{\varepsilon}_c^{pl}$ for compression.*

The effective values presented above, marked with the accent "$^-$" depend on the degree of material degradation, while the designation "$\langle\ \rangle$" is defined as Macauley brackets, where $\langle x \rangle = \frac{1}{2}(|x| + x)$. The parameters of the plasticity function are described as follows:

$$\alpha = \frac{(\sigma_{b0}/\sigma_{c0}) - 1}{2(\sigma_{b0}/\sigma_{c0}) - 1} \qquad (5.7)$$

$$\beta = \frac{\overline{\sigma_c}(\dot{\bar{\varepsilon}}_c^{pl})}{\overline{\sigma_t}(\dot{\bar{\varepsilon}}_t^{pl})}(1 - \alpha) - (1 + \alpha) \qquad (5.8)$$

$$\gamma = \frac{3(1 - K_c)}{2K_c - 1} \qquad (5.9)$$

where:

σ_{c0}, σ_{b0} -   *concrete strength value in uniaxial and biaxial compression*

$\dfrac{\overline{\sigma_c}(\dot{\bar{\varepsilon}}_c^{pl})}{\overline{\sigma_t}(\dot{\bar{\varepsilon}}_t^{pl})}$ -   *concrete strength in compression to concrete strength in tension ratio*

K_c -   *The ratio of Inclination of tension to compression meridian $0 \leq K_c \leq 1$.*

The shape of the yield surface in plain stress space and meridian and deviatoric sections were presented in Fig. 5.6.
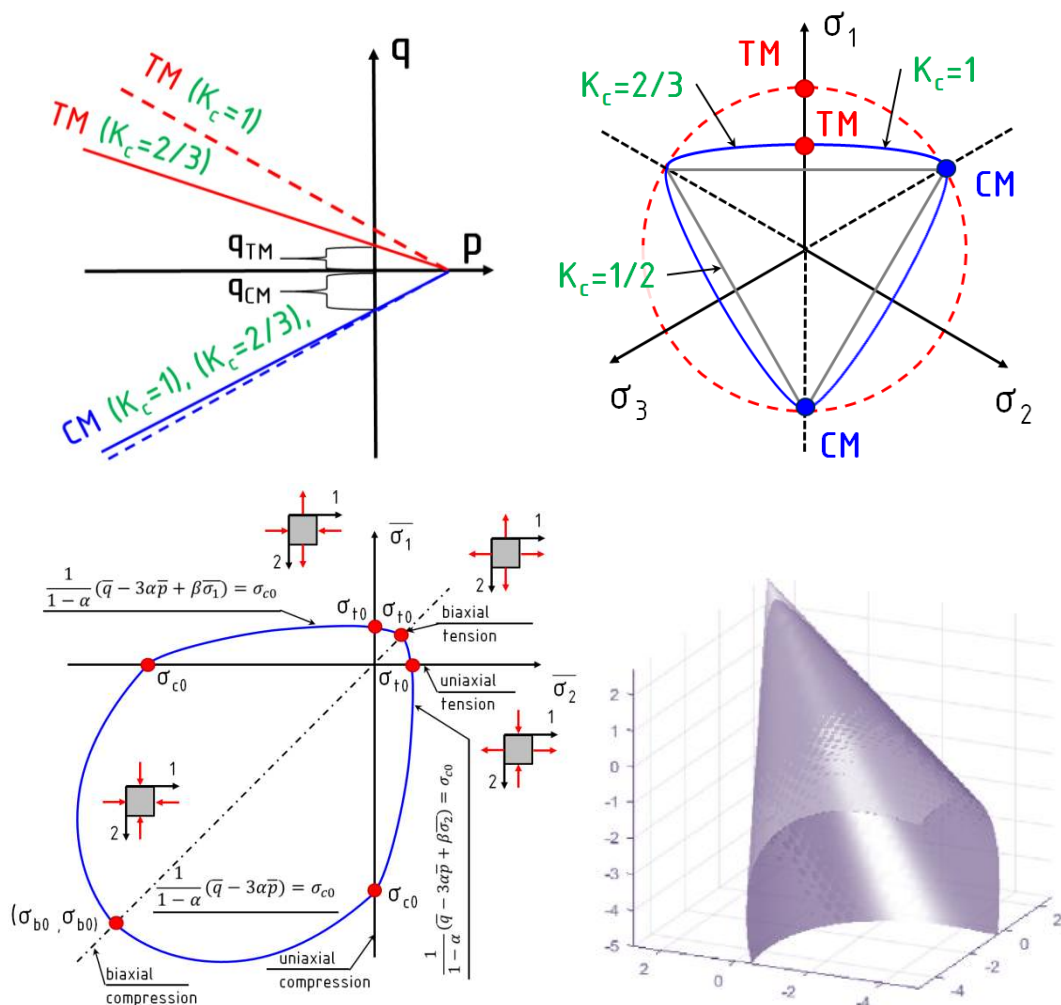
Fig. 5.6.: Shape of failure surface a) meridian section
b) deviatoric section   c) plain stress projection d) 3D view [6]

CDP model of concrete assuming non-associated flow rule, where the plastic potential is based on hyperbolic Drucker-Prager potential function (*see Fig. 5.7*), which is expressed as:

$$G_{CDP} = \sqrt{(e\sigma_{t0}\tan\psi)^2 + \bar{q}^2} - \bar{p}\tan\psi \qquad (5.10)$$

where:

   e   -   *Eccentricity parameter*

   ψ   -   *Dilation angle.*
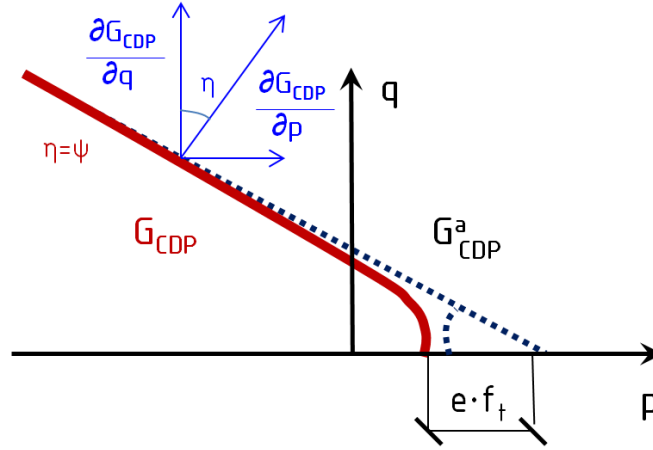
Fig. 5.7.: Yield function, its asymptote, and gradient in P point
where the graphical representation of parameters e and ψ were included

For concrete, experimental data of uniaxial compression and tensile stress-strain relationship was calibrated with the FIB model [N7]. In the case of uniaxial compressive behaviour, the stress-strain curve was prepared according to equations describing the linear elastic phase and softening parts related to concrete crushing [2].

$$\sigma_{c(1)} = E_0\varepsilon_c \qquad (5.11)$$

$$\sigma_{c(2)} = \frac{E_{ci}\cdot\dfrac{\varepsilon_c}{f_{cm}} - \left(\dfrac{\varepsilon_c}{\varepsilon_{cm}}\right)^2}{1 + \left(E_{ci}\cdot\dfrac{\varepsilon_c}{f_{cm}} - 2\right)\dfrac{\varepsilon_c}{\varepsilon_{cm}}} \qquad (5.12)$$

$$\sigma_{c(3)} = \left(\frac{2 + \gamma_c f_{cm}\varepsilon_{cm}}{2} - \gamma_c\varepsilon_c + \frac{\varepsilon_c^2\gamma_c}{2\varepsilon_{cm}}\right)^{-1} \qquad (5.13)$$

$$\gamma_c = \frac{\pi^2 f_{cm}\varepsilon_{cm}}{2\left[\dfrac{G_{ch}}{l_{eq}} - 0.5f_{cm}\left(\varepsilon_{cm}(1-b) + b\dfrac{f_{cm}}{E_0}\right)\right]^2} \qquad (5.14)$$

where:

$$b = \frac{\varepsilon_c^{pl}}{\varepsilon_c^{ch}} \qquad (5.15)$$

In the case of uniaxial tensile behaviour, the stress-strain curve was prepared according to two parts describing the linear elastic phase and softening part expressed as an exponential function related to concrete cracking according to [2][55]:

$$\sigma_{t(1)} = E_0 \varepsilon_t \qquad (5.16)$$

$$\frac{\sigma_t(w)}{f_{tm}} = \left[1 + \left(c_1 \frac{w}{w_c}\right)^3\right] - \frac{w}{w_c}(1 + c_1^3)e^{-c_2} \qquad (5.17)$$

where:

$$c_1 = 3; \qquad c_2 = 6.93 \qquad (5.18)$$

Concrete response in relation to finite element size was correlated with the tensile strain through kinematic relation based on crack band theory [8] relating strain with the crack opening:

$$\varepsilon_t = \varepsilon_{tm} + w/l_{eq} \qquad (5.19)$$

where:

w - *crack opening*

l_{eq} - *finite element size*

Tensile and compressive damage variables were determined according to the iterative approach [2] by adjusting the *b* parameter as follows:

$$d_t = 1 - \frac{1}{2 + a_t}\left[2(1 + a_t)\exp\left(-b_t \varepsilon_t^{ck}\right) - a_t \exp\left(-2b_t \varepsilon_t^{ck}\right)\right] \qquad (5.20)$$

$$d_c = 1 - \frac{1}{2 + a_c}\left[2(1 + a_c)\exp\left(-b_c \varepsilon_c^{ch}\right) - a_c \exp\left(-2b_c \varepsilon_c^{ch}\right)\right] \qquad (5.21)$$

where auxiliary parameters according to [2]:

$$a_i = 1 \qquad a_t = 7.873 \qquad b_{t_i} = \frac{0.453 f_{ck}^{\frac{2}{3}}}{G_F} \cdot l_{eq} \qquad b_{c_i} = \frac{1.97 \cdot (f_{ck} + 8)}{G_{ch}} \cdot l_{eq}$$

Table 5.3. Parameters used in for determining stress-strain relationship and damage variables

Parameter	Symbol	Value	Unit
Compressive strength	f_{cm}	38.1	*MPa*
Tensile strength	f_{ctm}	2.37	*MPa*
Peak strain	ε_{c0}	0.0019	-
Ultimate strain	ε_u	0.0035	-
Shear modulus	G	11435.96	*GPa*
Fracture energy	G_F	0.141	*N/mm*
Crushing energy	G_{ch}	33.80	*N/mm*
Regular mesh size	l_{eq}	25	*mm*
Auxillary Parameter 1	b	0.9	-
Auxillary Parameter 2	a_c	7.873	-
Auxillary Parameter 3	a_t	1.00	-
Auxillary Parameter 4	b_c	55.369	-
Auxillary Parameter 5	b_t	778.219	-

Table 5.3 summarise the required values for determining post-elastic response and damage variables in the function of strain. It can be noted that those functions in this approach are related to mesh size parameter $l_{eq.}$ Thus, stress-strain relationships were determined for different mesh sizes in accordance with formulas: 5.13 in compression and (5.17 for tension (*Fig. 5.8a-b*). Damage variables (*Fig. 5.9a-b*) were determined with equations eq (5.13 in compression and (5.17 in tension.
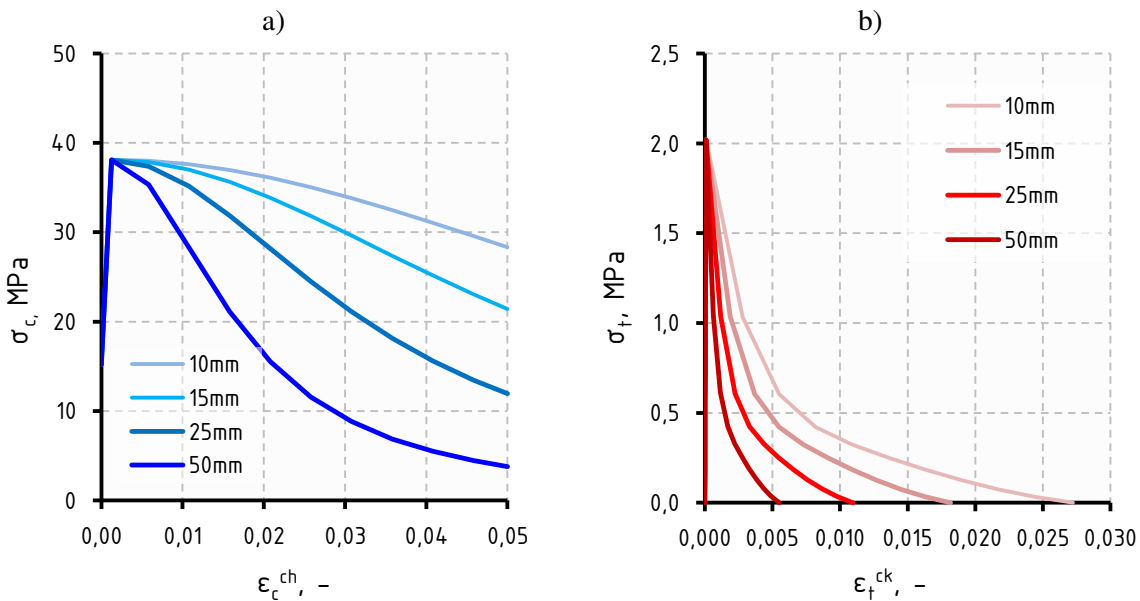
Fig. 5.8.: Uniaxial post-elastic relationships of concrete adopted in the numerical model for a given mesh size a) compression stress - crushing strain b) tension stress - cracking strain
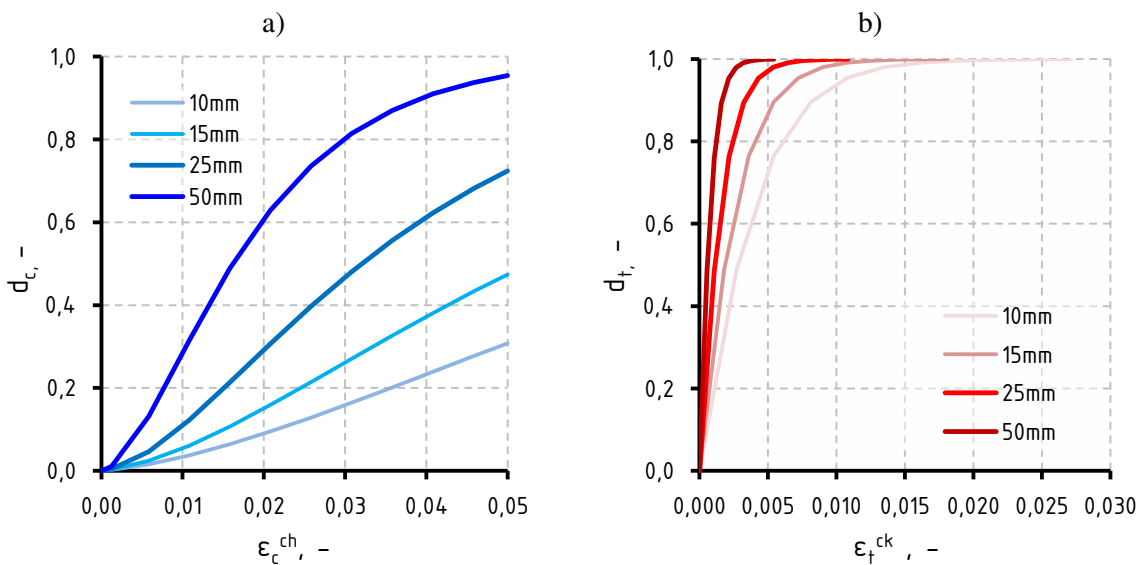
Fig. 5.9.: Uniaxial relationships of concrete adopted in the numerical model for a given mesh size a) compression damage variable - crushing strain b) tension damage variable - cracking strain

It can be noted, that more fine mesh is related to higher values of fracture energy in tension and crushing energy in compression.

5.3.1. CPD CONCRETE MODEL SENSITIVITY STUDY

The main aim is to verify the numerical FEA model as well as to validate adopted material parameters in terms of experimental results. For initial calculations, parameters for the CDP model described in the previous subsection were presented in Table 5.4. The mean Poisson ratio and elastic modulus values were taken directly from the test. The rest of the parameters were adopted based on related literature [2][57][117][137][153]. A sensitivity study was performed to verify how results are affected by changes or uncertainty in input data as well as to confirm the correctness of the adopted literature-based parameters in this type of analysis.

Table 5.4. Direct input data used in the CDP model

Parameter	Symbol	Value	Unit
Dilation angle	ψ	35	$^\circ$
Stress ratio	σ_{b0}/σ_{c0}	1.16	-
Eccentricity	e	0.1	-
Meridian slope	K_c	0.667	-
Viscosity parameter	μ	$0.0001 \div 0.0002$	-

The set of load-deflection curves for various parameters in the case of specimen A1 were shown in Fig. 5.10. There is an agreement in publications for meridian slope K_c which for concrete was set as 0.66 as well as with the value of eccentricity. As shown in Fig. 5.10c, values of eccentricity varying from 0.05 to the value of 0.2 had a negligible effect on load-deflection response. The stress ratio was adopted according to well-known research conducted by Kupfer et al [92]. However, there is some discrepancy when it comes to dilation angle ψ. Values from 5 [139] up to 56 degrees [32] can be found. Wosatko et al. [153] presented an extensive study and explanation for the role of the dilatancy angle. In conclusion, the authors recommend using values not larger than 35 degrees. Load-deflection responses for different dilatation angles were presented in Fig. 5.10a. Higher values of dilatation angle slightly increase the slope of the load-deflection response of the beam. However, a difference in the load level at which plastic strain occurs in bottom reinforcement is unnoticeable. In one of the studies [125], values lower than 25° gives model response (slope) not consistent with RC beam response in the experiment in the higher load values. For this reason, the value of 35 degrees has been chosen as the most common value found in the literature in this type of analysis. In many publications, a low value of viscosity parameter μ is recommended and it stands for the stabilization of results by controlling the convergence of conducted analysis. Here, the value was varying from an initial 0.0001 up to 0.0002 It was increased when premature loss of

convergence was observed especially when the concrete – CFRP bond interface described in the next paragraph was taken into account. In performed analysis, no relevant difference in the whole range of load in the model response has been observed for selected CPD parameters. At this stage, only a slight influence has been observed by directly changing the mechanical properties of concrete like the modulus of elasticity.
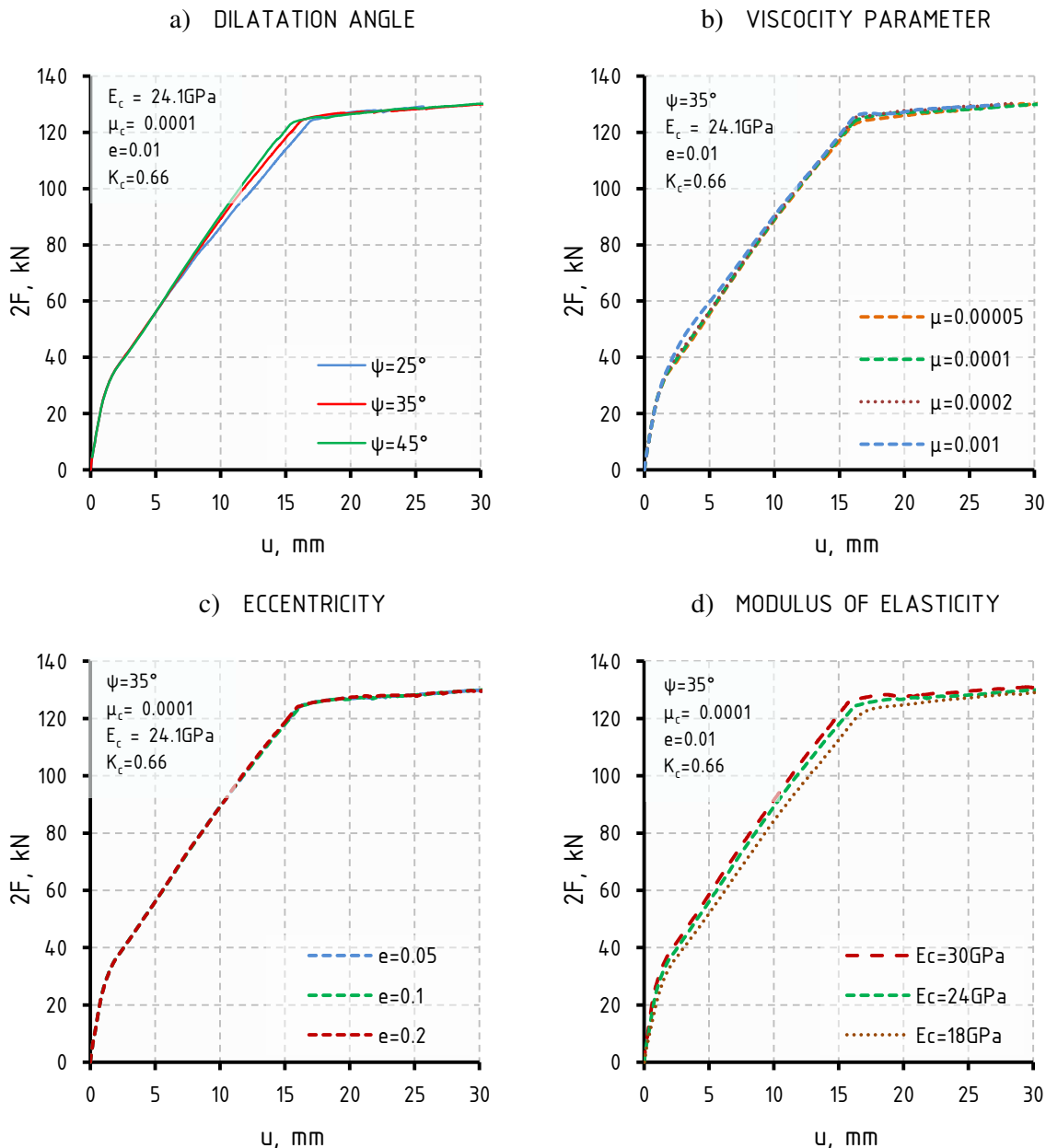
Fig. 5.10.: Comparison of load- mid-span deflection response with mesh size 25mm and selected parameters: dilatation angle a) viscosity parameter b) eccentricity c) elasticity modulus d)

5.3.1. INFLUENCE OF FE SIZE ON CDP MODEL RESPONSE

The next step was to verify the insensitivity of adopted parameters for a post-elastic response of concrete(see Fig. 5.8 - Fig. 5.9) for different mesh sizes in accordance with Alfarah et al. [2].

A comparison of load-deflection curves for selected finite element sizes (15mm, 25mm and 50mm) was presented in Fig. 5.11a. Calculated parameters for concrete show good agreement among load-deflection and moment-curvature responses (Fig. 5.11b) for each mesh size used in the numerical model in the whole load range. The differences between results do not exceed 3%.

a)   b)
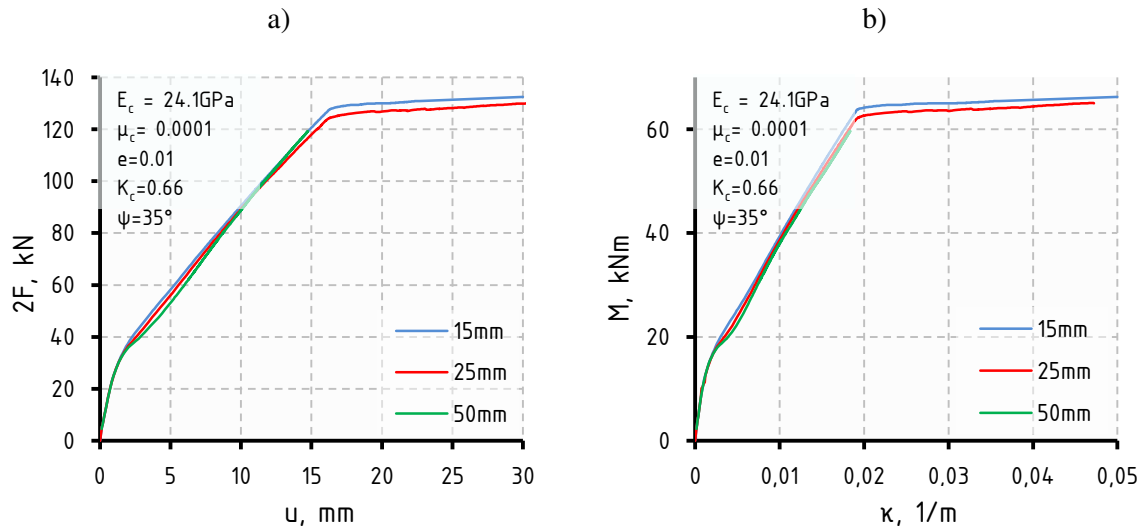
Fig. 5.11.: Load-deflection a) and moment-curvature b) response in relation to the finite element size

Convergence issues have been found in the case of the sample with an FE size of 50mm. This might be due to a dramatic drop in the tension-softening response of concrete when a reasonable load increment has been used. Although load-deflection response and moment-curvature response have been found insensitive for finite element size, a general damage propagation has been inconsistent on finite elements in the case of coarse mesh (*see Fig.: 5.*12).

FE SIZE	DAMAGE VARIABLE IN TENSION (d_t)
EXP	
15mm	
25mm	
50mm	
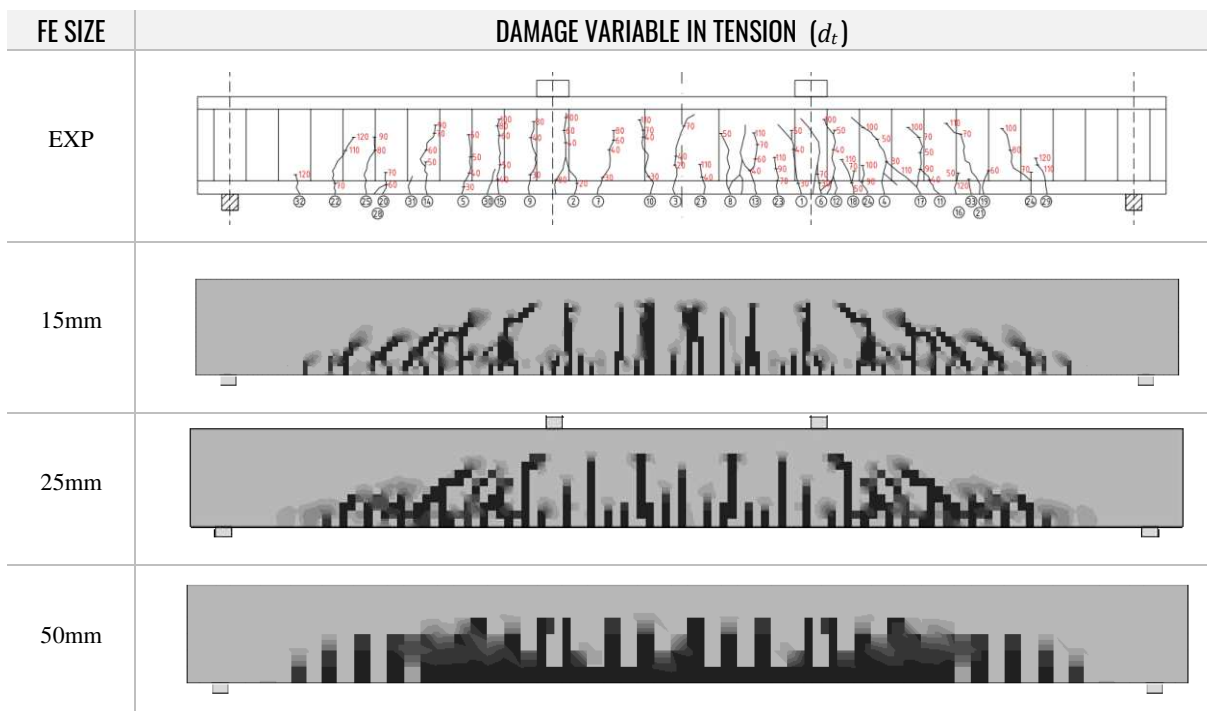
Fig.: 5.12 Comparison of experimental crack pattern and damage variable distribution in tension for different FE sizes at load value of 120kN – specimen A1

Finally, It was decided to use a mesh size of 25mm as a balance between the accuracy of the damage propagation variable and the time consumption of analysis.

5.3.2. VALIDATION OF SELECTED PARAMETERS

At this stage, numerical responses were compared for unstrengthened specimen A1 and strengthened specimen A2 where a perfect bond between concrete and CFRP was assumed. It can be noted that the general post-cracking response is rather similar and relatively good agreement in stiffness in form of the slope was achieved. The difference in derivative calculated between the experimental and numerical load-displacement curves in the range of 5-15mm for specimens A1 and A2 do not exceed 5% and 2% respectively. Using the same mechanical input data based on experimental investigation, the load-deflection response (Fig. 5.13a) and moment-curvature response (Fig. 5.13b) obtained in FEA were confronted with results obtained using the simplified fibre–beam (FB) method described wider in Appendix A

a)   b)
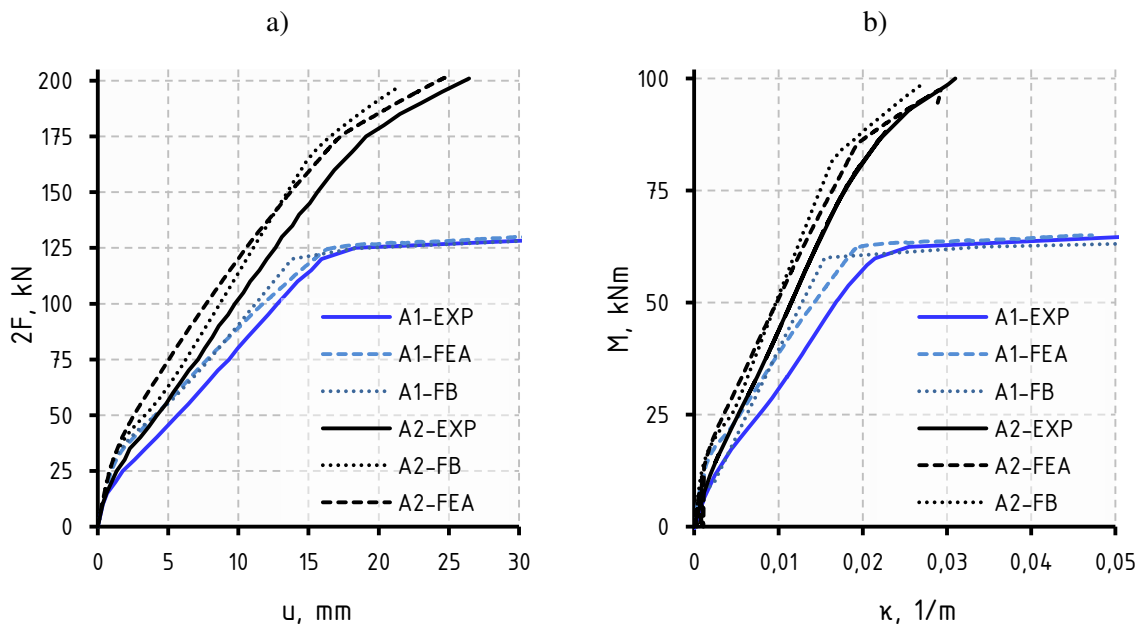
Fig. 5.13.: Comparison of numerical and experimental results a) load-deflection response b) bending moment-curvature response (EXP – experimental results, FB – Fiber beam analysis, FEA – Finite element analysis)

Higher ultimate load values were achieved in numerical calculations - 2% for specimen A1 in FE analysis and 1% lower in the case of the FB method. Due to the lack of delamination in the FE model with perfect bond assumption, only result under specific load value can be compared in the case of specimen A2. It can be noted that in the FB method the slope in load-deflection response is higher in contrast to the FEA. However, simultaneously, relatively better agreement in moment-curvature response can be observed.

A difference between FEA and experimental results can be noted in the load level at which the inelastic response of concrete has begun. Concrete cracking occurred in about 1.5 times higher

load value in numerical simulations in comparison to laboratory tests in both cases. On the one hand, this may be the consequence of the adopted procedure for determining damage variables and post-elastic response that makes results independent from the mesh size. On the other hand, such behaviour can be observed also in other numerical studies on RC beams in bending where the CPD concrete model was adopted [21][58] (see also information in Appendix B). Assuming the same post-elastic response in tension in the FB method similar overestimation of the cracking moment can be observed.

In Fig. 5.14 the mid-span concrete strain response in the compressive zone has been compared for specimens A1 and A2. The difference between the maximal reached strain does not exceed 8% in the case of specimen A1. A higher difference of up to 15% has been observed in the comparison between FEA and experimental results. Strain recorded in the FB method takes similar values as FEA up to 125kN then the difference increases up to 7%.
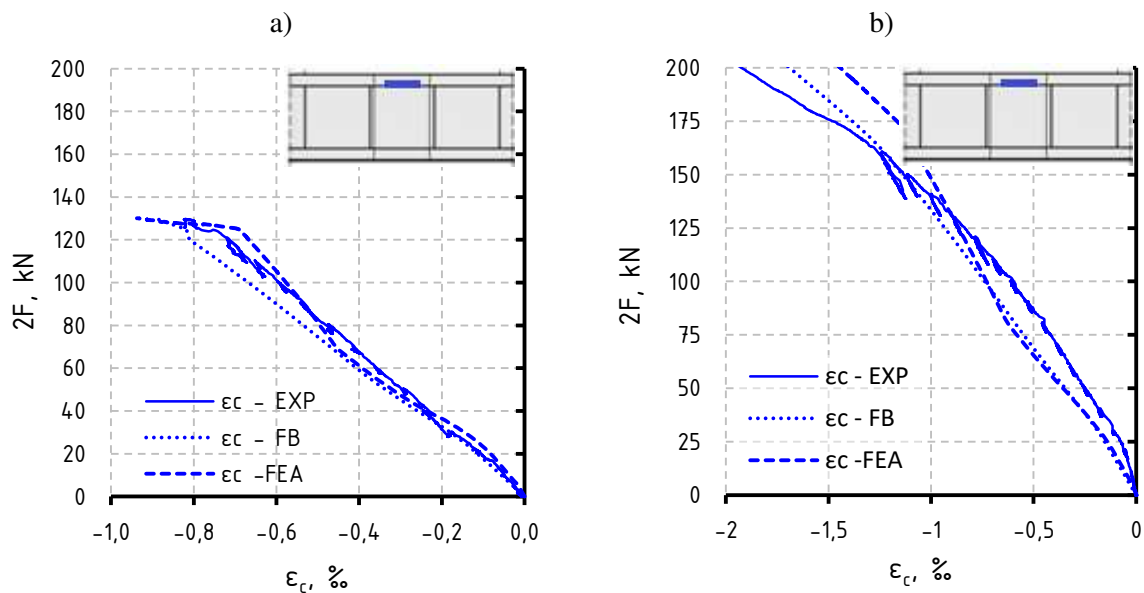
Fig. 5.14.: Mid-span strain comparison measured in a compressive zone of concrete a) in specimen A1 b) in specimen A2

The mid-span strain at CFRP and steel reinforcement for both numerical calculations were compared with laboratory results in figure Fig. 5.15. In the case of FE analysis, both steel and CFRP strain values at ultimate load are about 8% lower than the value measured in the test. The strain value in composite at ultimate load in of fibre–beam analysis, is only about 3.5% higher. However, a clear distinction can be found in strain values after yield strength had been reached in reinforcement. In contrast to FEA and laboratory test, the mid-span zone in the FB method is an exact cross-section where reinforcement undergoes plastic deformation. In the test and FEA, the measured point was located between cracks and between points where plastic deformations of reinforcement occur.

a)   b)
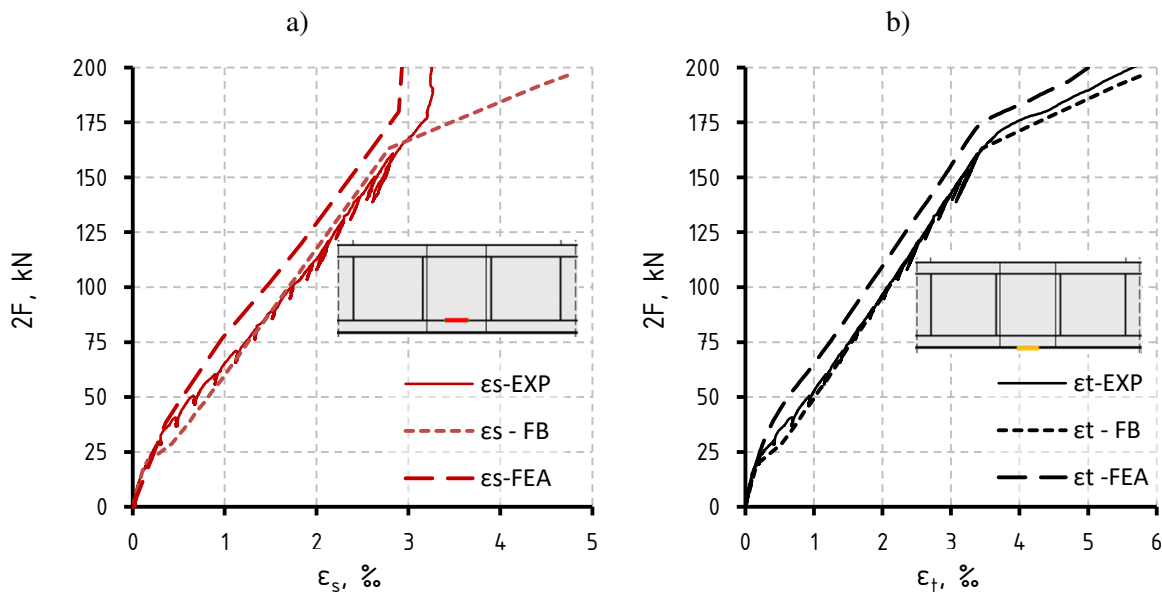
Fig. 5.15.: Mid-span strain history comparison between numerical models and laboratory test of sample A2 measured in steel a) in CFRP composite b)

Considering the minor effect of tension stiffening effect on the ultimate load in some cases [N17] and in results obtained from the FB method (see Appendix A) and obtained agreement in strain response in materials, validation of numerical results was found acceptable given the aim of the study.

5.3.3. BOND BEHAVIOUR OF CFRP - CONCRETE INTERFACE

So far, a perfect bond assumption between concrete and CFRP has been adopted. This is sufficient in the common strain limitation approach. However, it is not always possible to predict a proper failure mode, especially when defects exist in the bond. In this case, behaviour is limited, load is increasing up to the moment when the failure mode not related to debonding occurs. It was also noticed that the perfect bond model overestimates stiffness after concrete cracking [117]. The simplified method of perfect bond assumption was adopted in [52][110][147], and it is usually used as a reference to more complex approaches [21][95][116]. A few basic approaches to modelling concrete - CFRP contact can be distinguished: the use of a predefined crack or cohesive zone model [133]. Here, the second approach with the use of surface-based cohesive behaviour related to cohesive traction–separation law has been adopted. On the whole, a shear traction-separation law of the CFRP–concrete interface in related literature is referred to as the bond-slip law. In traction-separation law, the initial elastic relationship is followed by damage initiation and evolution.

a) Elastic behaviour - before a specific value of ultimate stress in the considered direction is reached, the bond interface provides elastic cohesive behaviour. In the general case, a three-dimensional space traction stress vector consists of the normal, shear and tangent stress components. Each of them corresponds to the related quantity of separation which describes

relative displacements between nodes on bonded surfaces. Those quantities are associated with the stiffness matrix in the following constitutive relation [22][146]:

$$\begin{Bmatrix} \sigma_n \\ \tau_s \\ \tau_t \end{Bmatrix} = \begin{pmatrix} K_{nn} & K_{ns} & K_{nt} \\ K_{sn} & K_{ss} & K_{st} \\ K_{tn} & K_{ts} & K_{tt} \end{pmatrix} \begin{Bmatrix} \delta_n \\ \delta_s \\ \delta_t \end{Bmatrix}$$

(5.22)

where:

σ_n, τ_s, τ_t -   *traction stresses corresponding to normal, shear and transverse stress components*

$\delta_n, \delta_s, \delta_t$ -   *separations refer to normal, shear and transverse stress components*

K_{nn}, K_{ss}, K_{tt} -   *cohesive stiffness components in normal, shear and transverse direction*

K_{nt}, K_{ns}, K_{st} -   *cohesive coupled stiffness components*

A special case of this relationship – uncoupled traction-separation behaviour was adopted which assumes only non-zero values on the main matrix diagonal. In this study, this uncoupled stiffness relation was adopted.

      b) Damage initiation - quadratic nominal stress criterion was assumed for the damage initiation. [115][116][156] In this approach, each stress component contributes to the damage initiation state except compressive normal stress.

$$CSQUADSCRT \; Q = \left\{ \frac{\langle \sigma_n \rangle}{\sigma_n^{max}} \right\}^2 + \left\{ \frac{\tau_s}{\tau_s^{max}} \right\}^2 + \left\{ \frac{\tau_t}{\tau_t^{max}} \right\}^2 = 1$$

(5.23)

      The damage initiation criterion is expressed by the software variable CSQUADSCRT (here denoted as *Q)* describes a stress state intensity at a given point and indicates the start of local damage propagation when the variable reaches the value of 1.

      c) Damage evolution - it describes softening process after damage initiation of the cohesive zone up to the complete failure of the bond corresponding to maximum slip. The softening curve can take different forms whereas exponential and bilinear forms are mostly used in the case of the Concrete – CFRP interface [98]. After degradation is initiated, stress components are correlated with the damage variable CSDMG (here denoted as *D*) which takes value from 0 (no degradation) to 1 (complete local failure):

$$\begin{aligned} \sigma_n &= (1-D)\sigma_n \\ \tau_s &= (1-D)\tau_s \\ \tau_t &= (1-D)\tau_t \end{aligned}$$

(5.24)

From many bond strength models [97], the bilinear function of the bond-slip relationship for externally bonded FRP reinforcement for RC structural members was adopted in this study. This is recommended for design purposes according to [N7][N8]. For the bilinear form of bond-slip law, mentioned linear damage variable is defined as:

$$D = \frac{\delta_m^f(\delta_m - \delta_m^0)}{\delta_m(\delta_m^f - \delta_m^0)}$$

(5.25)

where:

δ_m^f -   *the effective separation at complete failure*

δ_m^0 -   *relative to the effective separation at damage initiation*

The damage variable is based on effective separation that combines normal and shear displacements across the interface:

$$\delta_m = \sqrt{(\langle\delta_n\rangle^2 + \delta_s^2 + \delta_t^2)} \tag{5.26}$$

Sometimes, the parameter of the bond fracture energy G_f is used interchangeably, which is defined as the area under the bond-slip curve (*see Fig. 5.16a*). In the case of bilinear form it can be expressed as:

$$G_f = \int_0^{\delta_f} \tau d\delta = \frac{1}{2}\delta_f \tau_{max} \tag{5.27}$$

For formulas of the bond-slip curve usually displacements symbols $'\delta'$ are replaced by symbol '*s'*. Thus, the bilinear function of each stress component can be expressed by the following equations:

$$\tau(s) = \tau_{max}\left(\frac{s}{s_0}\right) \qquad for\ 0 \leq s \leq s_0 \tag{5.28}$$

$$\tau(s) = \tau_{max}\left(1 - \frac{s - s_0}{s_f - s_0}\right) \qquad for\ s_0 \leq s \leq s_f \tag{5.29}$$

5.3.4. CALIBRATION AND SENSITIVITY STUDY OF CONCRETE - CFRP INTERFACE

As mentioned before, for general isotropic material bond-slip relationship with assumed bilinear form is described by a few quantities: the maximal cohesive failure stress τ_{max} and interchangeably by bond stiffness K and damage initial slip as well as the critical energy release rate G_f and ultimate slip s_f (*see Fig. 5.16a*).
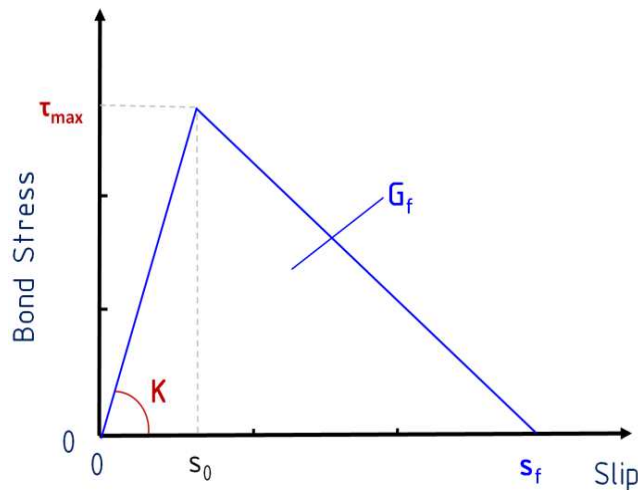
Fig. 5.16.: a) Bilinear stress-slip relationship for EBR with required parameters

The calibration process of the CFRP- concrete interface in terms of the ultimate load was conducted by adjusting interface parameters on specimen A2. It was achieved by the use of trial and error in reference to experimental results. The resulting parameters were summarised in Table 5.5.

Table 5.5. Concrete - CFRP interface parameters used in the model

Parameter	Symbol	Value	Unit
Tensile strength	f_t'	2.37	*MPa*
Width ratio (eq. (2.12)	k_b	0.935	-
Max. shear stress	τ_{max}	2.27	*MPa*
Fracture energy	G_f	163	*N/m*
Ultimate separation	s_f	0.15	*mm*
Normal Stiffness	K_{nn}	$4 \cdot 10^{11}$	*Pa/m*
Shear Stiffness	$K_{ss} = K_{tt}$	$3.85 \cdot 10^{11}$	*Pa/m*

Values of stiffness components were adopted according to Seręga et al. [132] where the normal and tangent stiffness in both directions were assumed to be equal to $4.0 \cdot 10^{11}$ Pa/m and $3.85 \cdot 10^{11}$ Pa/m, respectively. As a starting point, the maximal shear stress and ultimate separation at failure were adopted according to [N8] as the second approach as a 5% mean value and calibrated. Nevertheless, it should be emphasized that after adjusting the bond-slip law to experimental results for specimen A2 and selected FE size, the mesh sensitivity study for traction-separation law in the surface-based contact approach has not been investigated. In Fig. 5.17 and Fig. 5.18 sensitivity study for parameters of bond-slip law was shown. Unlike, the CDP material model, each parameter has a major effect on obtained results in terms of ultimate load. In Fig. 5.17a the effect of maximal shear stress value on ultimate load was analysed for constant fracture energy, which confirmed initial expectations.
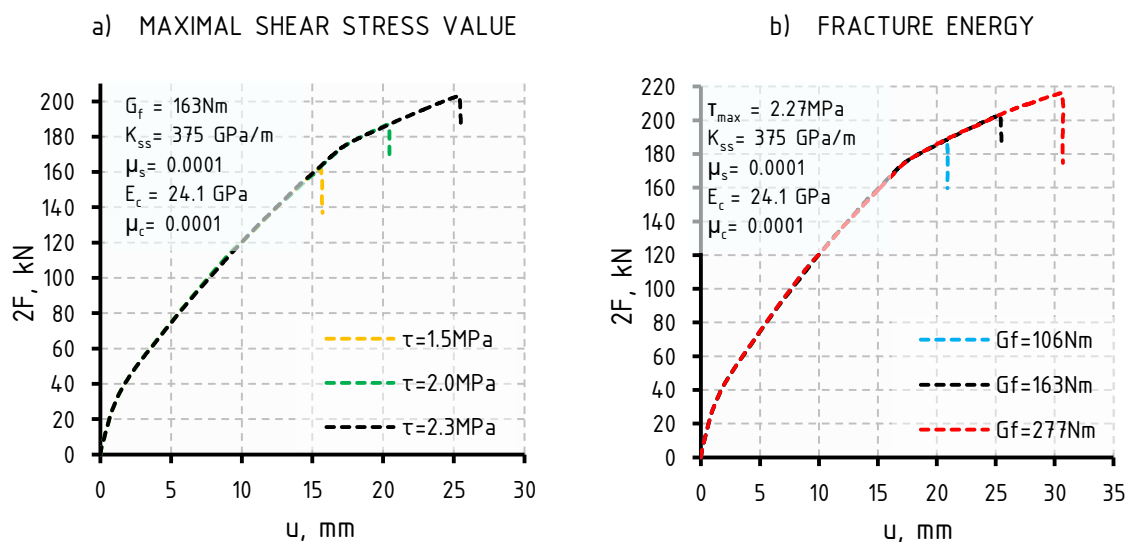
Fig. 5.17.: Comparison of load- mid-span deflection response for various parameters of traction-separation law a) Maximal shear stress, b) fracture energy

By increasing the maximal shear value, the ultimate load increase until debonding. Changes made in maximal shear stress value do not have a linear influence on ultimate load. In reference to

the sample with a maximal allowable shear stress of 2.0MPa, by increasing this value by 15%, the ultimate load increased by about 9% while for decreasing the maximal stress of 25%, only a 9% reduction of the ultimate load has been observed.

In a similar manner increase in fracture energy for a given maximal shear stress value cause also increase in ultimate load (*Fig. 5.17b*). However, In the case of fracture energy, a linear relationship has been found. Fracture energy was controlled by ultimate slip for given stiffness and maximal shear stress. A 70% increase in fracture, energy cause a 70% increase in ultimate load and similarly 65% decrease cause a 65% drop in ultimate load in relation to the specimen with fracture energy of 163Nm.
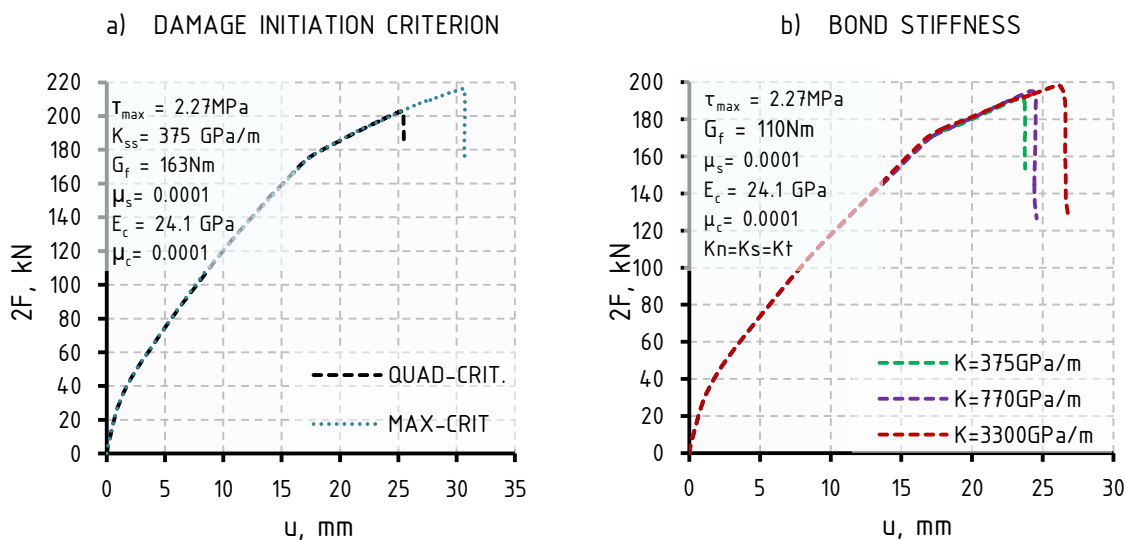
Fig. 5.18.: Comparison of load- mid-span deflection response for various parameters of traction-separation law a) damage initiation criterion b) bond stiffness

The bond stiffness has a minor effect on load-deflection response in the proximity of the considered value of $3.85 \cdot 10^{11}$ Pa/m. An 8% increase in ultimate load was found for ten times of initial value (*see Fig. 5.18*d).

Additionally, another damage initiation criterion has been checked based on absolute maximal stress in each direction (MAX). Nevertheless, because of the higher value of ultimate load obtained using this particular criterion (*Fig. 5.18a*), even lower values of maximal stress or fracture energy should be found to adjust numerical results to the experimental data. Thus, the quadratic nominal stress criterion (QUAD) has been used. No visible difference has been observed in the slope of the load-deflection curve which indicates a lack of influence of parameters on general member stiffness.

5.4. VALIDATION OF BOND BEHAVIOUR ON STRENGTHENED BEAMS WITH DEFECTS

Based on the parameters selected in the previous section, validation of the numerical models in reference to experimental beam specimens with defects was performed. A comparison of the load-deflection responses was presented in Fig. 5.19.
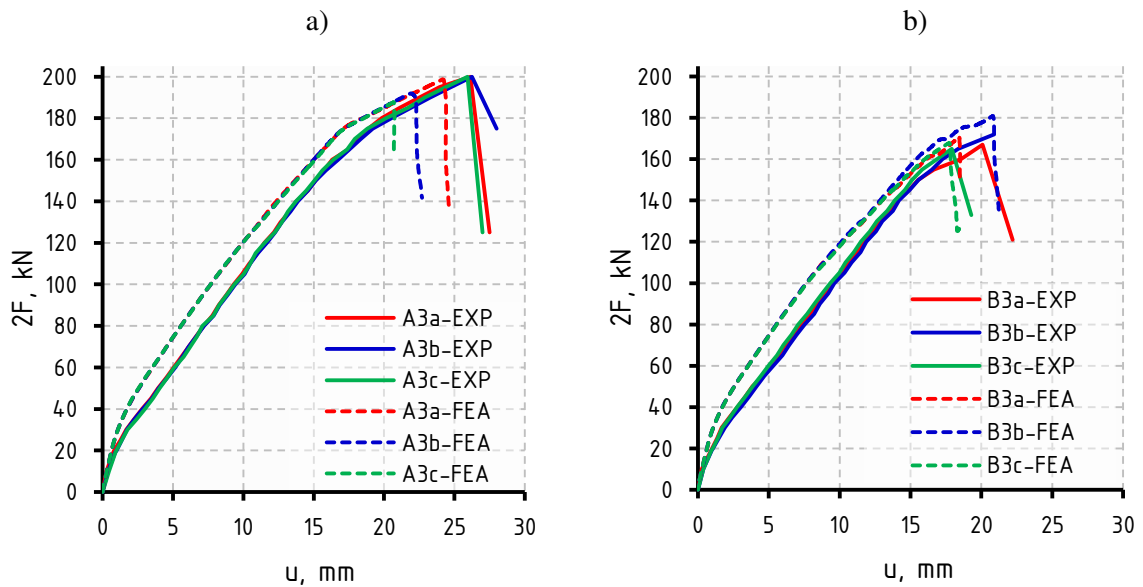
Fig. 5.19.: Validation of a numerical model in load- mid-span deflection response a) for specimens A3a, A3b and A3c b) for specimens B3a, B3b and B3c.

A relatively good agreement for specimens of both series A and B was achieved. In the case of specimens in series A a 1%, 5% and 6% difference in ultimate load was obtained for specimens A3a, A3b and A3c respectively in comparison to experimental data. Similar to the previous analysis, a slight overestimation of the cracking moment can be noticed. Smaller differences (2%, 4% and 2%) in ultimate load were obtained in the case of specimens B3a, B3b and B3c respectively. Higher values of difference were obtained in the numerical study for series B in comparison to experimental data when lower values were obtained for series A (*see Table 5.6*).

Table 5.6. Comparison of ultimate load values between specimens in FE analysis and laboratory tests

SPECIMEN	EXP: Pu [kN]	FEA: Pu [kN]	DIFFERENCE
A1	130	130,08	0,1%
A2	201,3	202,99	0,8%
A3a	200,9	198,70	-1,1%
A3b	201,4	192,01	-4,7%
A3c	199,3	187,71	-5,8%
A6	171,6	161,55	-5,9%
B3a	166,77	170,60	2,3%
B3b	173,8	180,90	4,1%
B3c	164,9	167,80	1,7%

A difference of about 6% in ultimate load in relation to experimental studies was obtained for specimen A6. In this case, the numerical simulation shows slightly different behaviour in terms of stiffness in contrast to a model without a defect after the load had exceeded 80kN (*see Fig. 5.20a*). In contrast to the experimental study, failure of the bond occurs before reinforcement reached its yield strength.

a)   b)
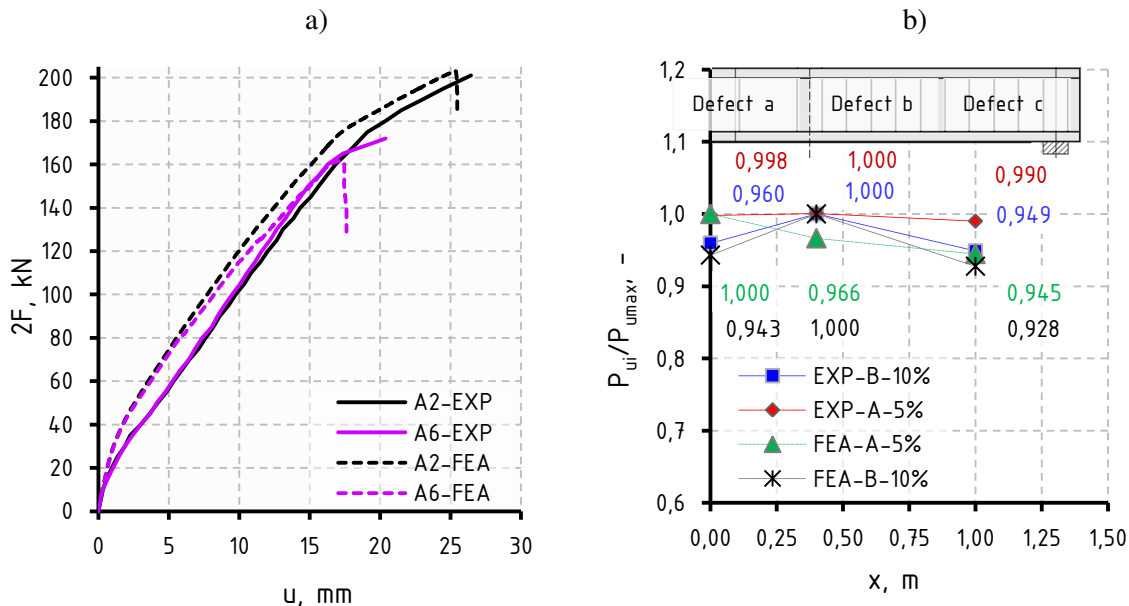
Fig. 5.20.: a) Validation of a numerical model in load- mid-span deflection response specimens A2 and A6 b) comparison of the relationship between relative ultimate load and defect location along the beam for experimental and numerical part

In most cases, simulations confirmed that the highest influence on member capacity in both series has a defect located in the shear span near the anchorage zone - where the lowest values of ultimate load were obtained. Similarly to *Fig. 4.23, in Fig. 5.20* relationship between relative ultimate load (calculated in relation to the highest ultimate load value obtained in a given series) and distance along the half of the beam was presented for numerical and experimental results. According to numerical calculations, the effect of the defects increases with the distance measured from the middle of the span towards the end of the strengthening. The difference between the highest and lowest values of relative ultimate load and as a consequence maximal capacity reduction depending on defect location does not exceed 6% in series A and 8% in series B which is consistent with the experimental part of the work and indicates a relatively small sensitivity of defect location on the flexural capacity for given beam specimens and given percentage of the defect area.

5.5. DAMAGE INITIATION AND EVOLUTION ALONG THE CFRP STRIP

Finite element analysis allows greater insight into the degradation of the bond interface under increasing load. The degradation process measured along the composite up to the failure can

be expressed as a two-dimensional function of the chosen damage initiation criterion. It can be done by retrieving the values at each node of variable Q in subsequent load steps in relation to the distance measured from one end of CFRP to another. Here the quadratic nominal stress criterion was adopted (*see eq. (5.23)*. In other words, the stress-dependent damage initiation criterion - Q, can be recorded along CFRP in each load step and expressed as a function.

Mathematically it can take the form as follows:

$$Q = Q(x, 2F) = \left\{ \frac{\langle \sigma_n \rangle}{\sigma_n^{max}} \right\}^2 + \left\{ \frac{\tau_s}{\tau_s^{max}} \right\}^2 + \left\{ \frac{\tau_t}{\tau_t^{max}} \right\}^2 \qquad (5.30)$$

where:

x -   *the distance measured from one end of CFRP to another*

$2F$ -   *Increasing applied external load value*

The output of the function recorded in the case of reference strengthened specimen A2 up to the peak load was presented in Fig. 5.21.
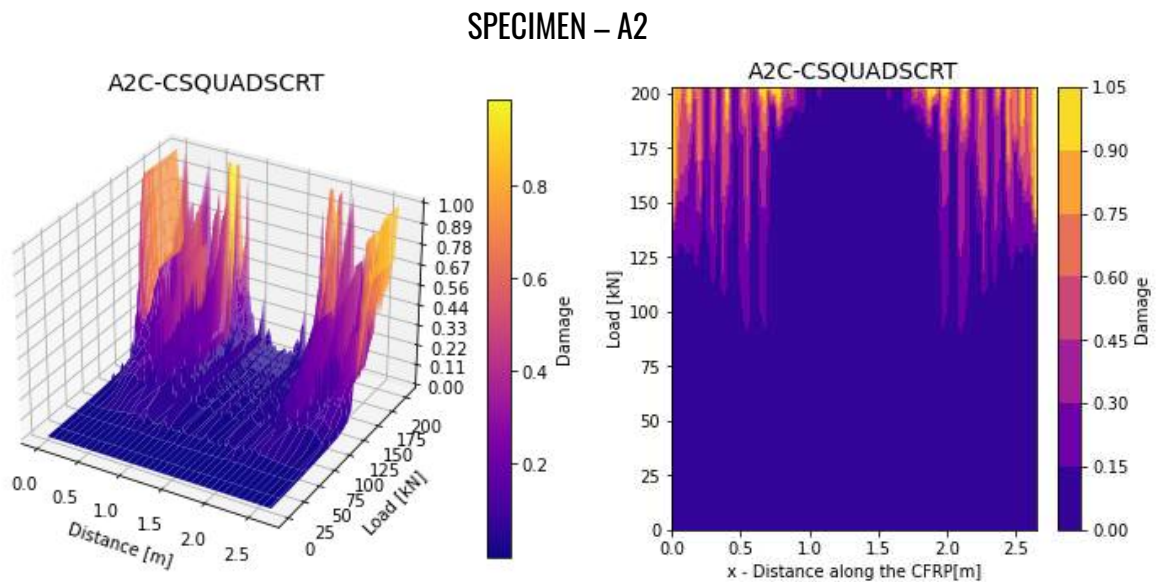
SPECIMEN – A2

Fig. 5.21.: Damage initiation of the bond for a numerical model of specimen A2

It can be noted that the degradation process appears directly under the zone of applied external load at the load value of 90kN. Damage development has a discrete and symmetrical nature at the beginning. This fact can be related to the process of crack opening in concrete, nevertheless, the mid-span zone where crack also occurs remains rather non-affected by the damage. With increasing load, damage initiations proceed towards beam supports and become more intense. At higher load values degradation in the adopted interface model loses its discrete character and becomes fuzzier up to the complete failure at the ends of the composite.

The output of the function of damage initiation variable Q for the rest of the specimens was summarised and shown in Fig. 5.22, Fig. 5.23 and Fig. 5.24.

SPECIMEN – A3a
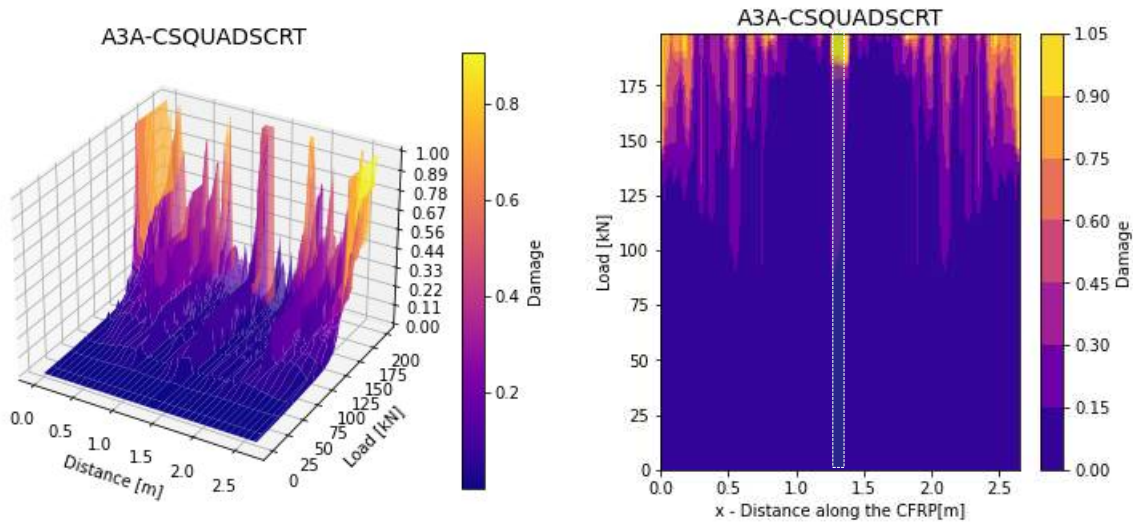
SPECIMEN – A3b
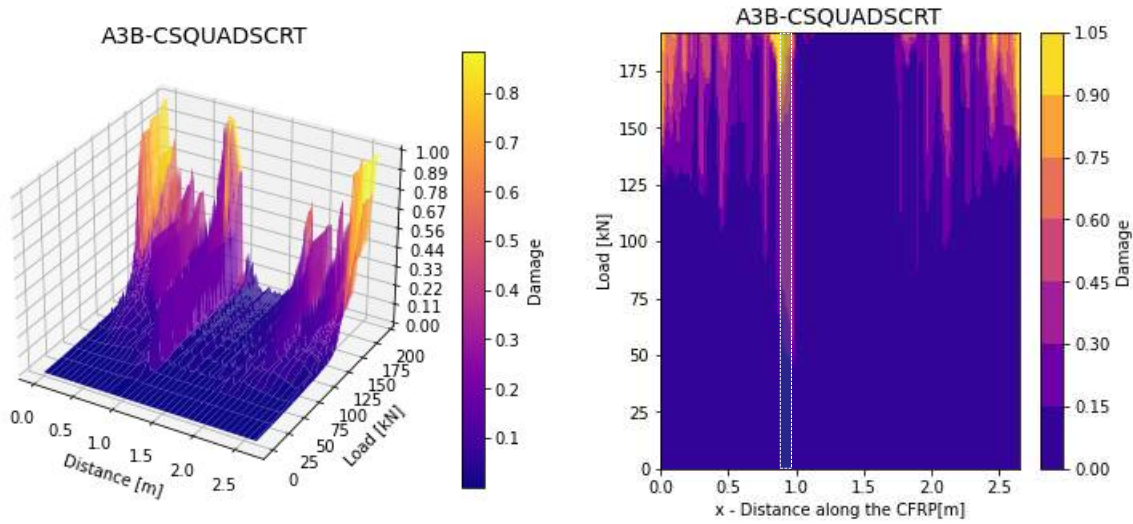
SPECIMEN – A3c
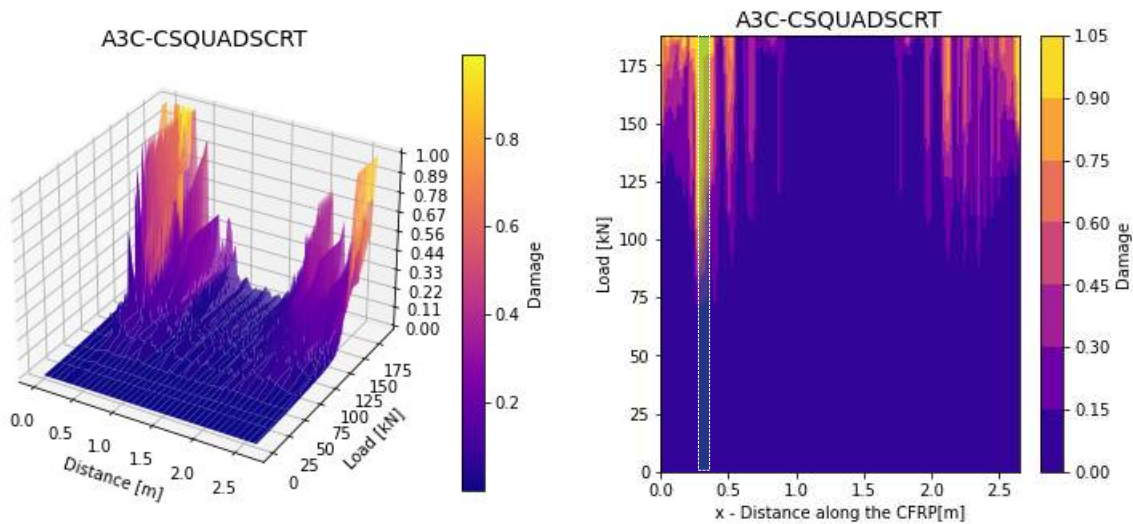
Fig. 5.22 Damage initiation criterion of the bond for selected numerical beams: A3a, A3b, A3c

SPECIMEN – B3a
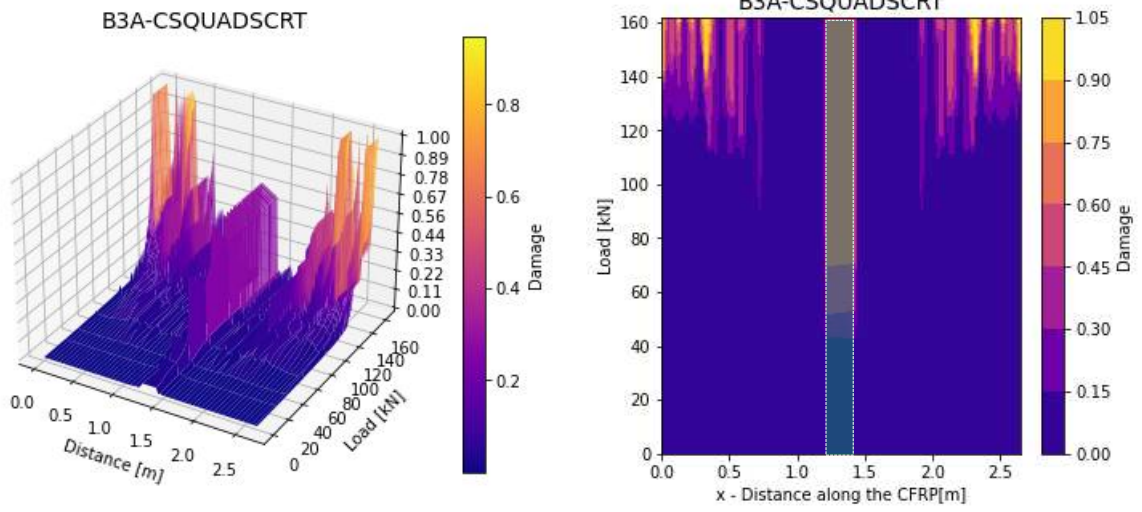
SPECIMEN – B3b
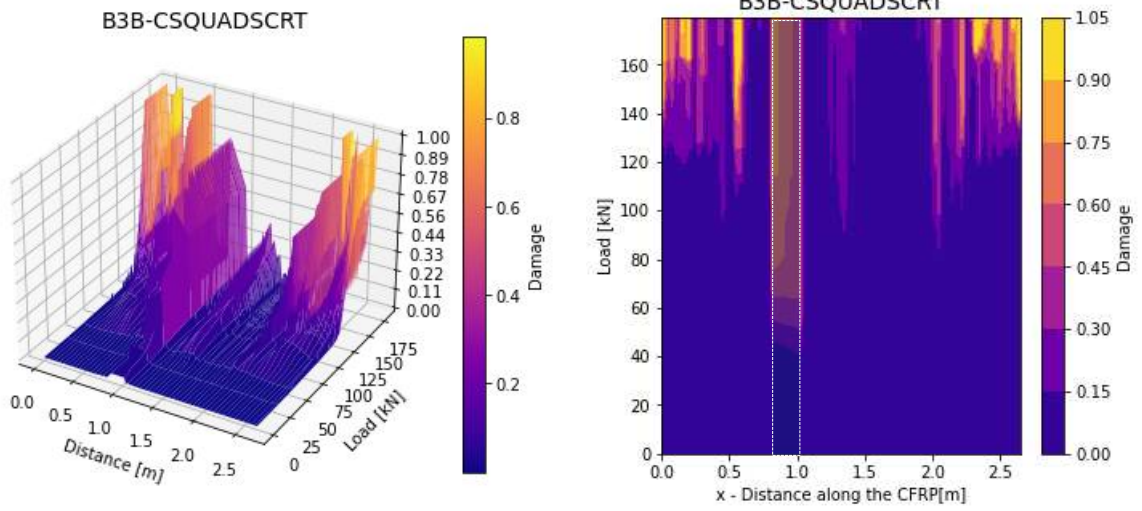
SPECIMEN – B3c
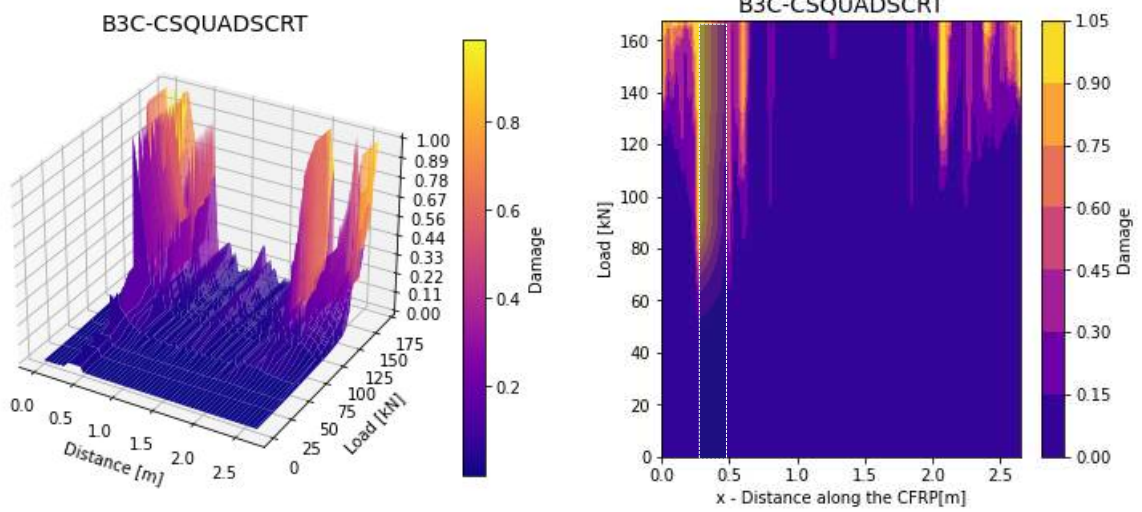
Fig. 5.23 Damage initiation criterion of the bond for selected numerical beams: B3a, B3b, B3c

For numerical convenience, the value of the variable was linearly interpolated over the defect area between the values on both sides in the diagrams, though those interpolated values on the defect area have no physical meaning. In series A, higher values of the Q variable appear under the different load values varying from 50kN to 90 kN. In the case of series B, damage initiation appears a little bit earlier in the range of 40kN to 60kN.

At a higher load level, the stress concentrates closely on the defect in each case. On the whole, the distribution of damage initiation variable Q has also a discrete nature when the defects exist. It seems that local peaks of variable Q are more densely distributed in series A, than those in series B where distribution is more loose and fuzzy but the damage initiation variable seems to be more intense. This may contribute to crack distribution in both series. For specimens, A3b and A3c the symmetry of the stress intensity is disturbed due to an occurrence of the defects in the bond in comparison to specimen A2 without defects. A similar situation takes place in series B for specimens B3b and B3c. Initially, a damage initiation variable takes different values on both sides of the defect. At the same time, higher values occur on the side closer to the beam support. An exception occurs for specimens A3a and B3a with symmetrically located defects where damage initiation variables on both sides are almost equal. Stress distribution, in an outer part of the CFRP split by a defect in shear span for specimens A3cand B3c, reminds the behaviour and stress distribution of specimens used in the shear lap test [154]. In the case of specimen A6 damage initiation criterion increase in the proximity of sides of defects starting at the segment near supports. Lower values of damage initiation variables can be noticed in mid-span located segments.
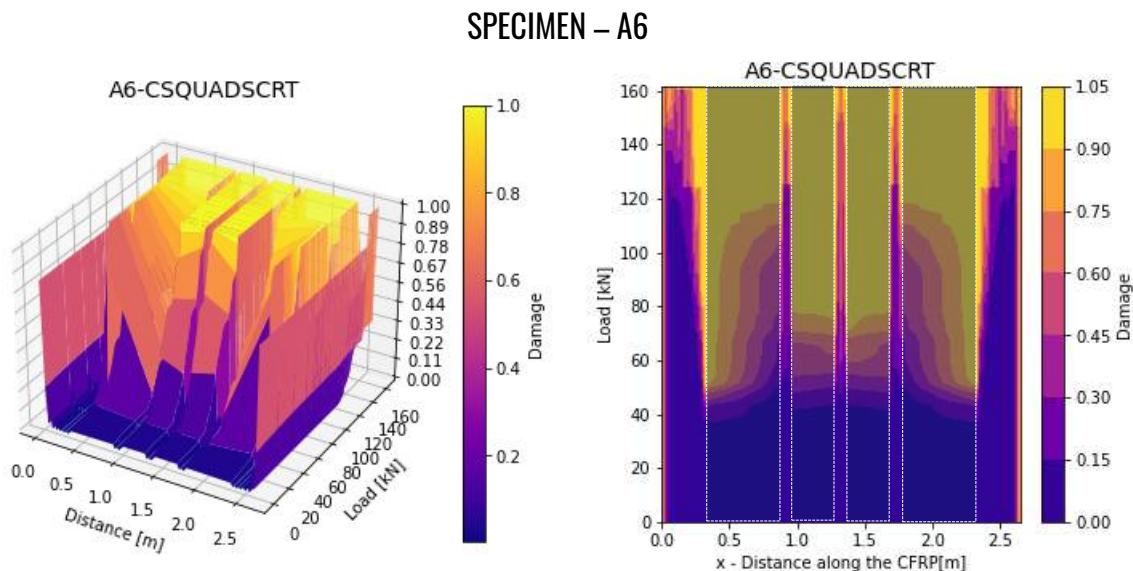
SPECIMEN – A6

Fig. 5.24 Damage evolution of the bond for a numerical model of specimen A6.

In the proximity of the ultimate load, the damage proceeds rapidly. In general, it is expressed via the damage variable *D* in numerical calculations. Propagation of the damage variable for

specimen A2 in the selected timesteps was presented in Fig. 5.25 where the red colour represents damage (*D=1*) and the blue colour represents no damage (*D=0*). The arrows represent the main direction of damage evolution. It can be clearly seen that damage develops from the area of point load towards beam supports up to complete debonding. This behaviour seems to reflect IC debonding failure observed in the laboratory tests, though it has not been started directly from the midspan (cf. Chapter 2.4.1), but under the area of applied external load.

State at loading:

State at ultimate load:

State at the loss of composite action:

Fig. 5.25.: Damage evolution variable D (CDSMG) at the CFRP – concrete interface for specimen A2 in selected load steps

Generally, any significant differences have been observed In damage propagation among the specimens in both series. In contrast to series A, damage in series B was initiated closer to the support. Based on an experimental study in series B concrete cover separation failure mode was observed as a consequence of propagating diagonal crack. A similar observation in numerical models was found where the loss of composite action propagated towards the middle of the span. (*see Fig. 5.26*). Although the whole CFRP – adhesive- concrete interface in form of a bond-slip relationship is some kind of numerical simplification, a coherent failure was observed in simulations with those recorded in an experimental study.

State at loading:

State at ultimate load:
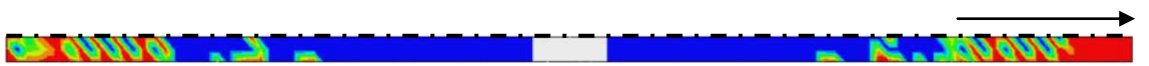
State at the loss of composite action:

Fig. 5.26.: Damage evolution variable D (CDSMG) at the CFRP – concrete interface for specimen B3a in selected load steps

In specimen A6, the damage has been developing at each end of each defect (*see Fig. 5.27*). Nevertheless, loss of composite action was governed by the evolution of damage at the anchorage zone followed by delamination under point load.

State at loading:

State at ultimate load:

State at the loss of composite action:

Fig. 5.27.: Damage variable at the CFRP – concrete interface for specimen A6 in selected load steps

It can be noted that the midspan zone between point loads has not been affected dramatically by the damage in numerical simulations in all types of specimens even if the cracks occur firstly in the middle of the span at loading.

5.6. INFLUENCE OF DEFECT AREA ON FLEXURAL CAPACITY REDUCTION

Thanks to numerical calculations the relationship between defect area to total bonded area ratio on reduction of flexural capacity can be determined in the wider spectrum. To achieve this goal, additional specimens signed as A7 and A8 were introduced. and analysed using the FE method only (*see Fig. 5.28*).

A7 A_{def}/A_{tot} => 30%
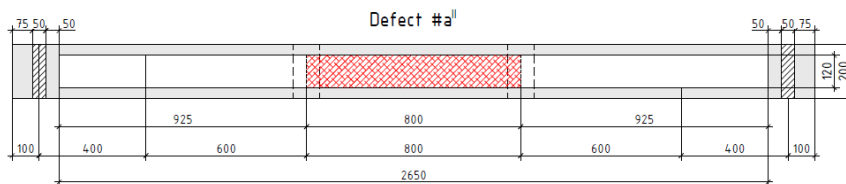
A8 A_{def}/A_{tot} => 42%
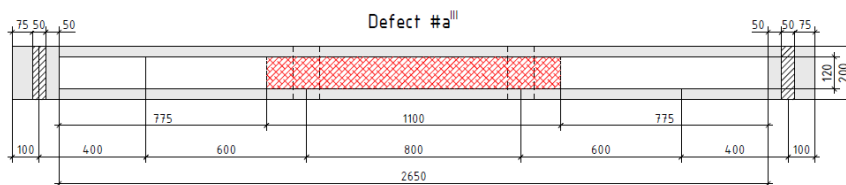
Fig. 5.28 Additional numerical beam specimens signed as A7 and A8

Specimens were based on type A reinforcement with other defect area percentage ratios. Additional numerical specimens were designed with the assumption that the defect always increases its size symmetrically in relation to the mid-span. Ultimate load values of 180kN and 187kN were obtained for specimens A8 and A7 respectively. Based on the set of beam specimens including specimens A7 and A8 as well as specimens analysed previously (A2, A3a and A6) a gradual decrease of

capacity can be observed with increasing defect area (*Fig. 5.29*a). In Fig. 5.29b relationship between maximal CFRP strain in the midspan and defect area ratio was presented. It can be seen clearly, that with the increasing size of the defect, lower values of maximal CFRP strain can be obtained. Assuming zero strain at a 100% defect ratio, a second-order fitting curve can be plotted as an approximation in the whole range.
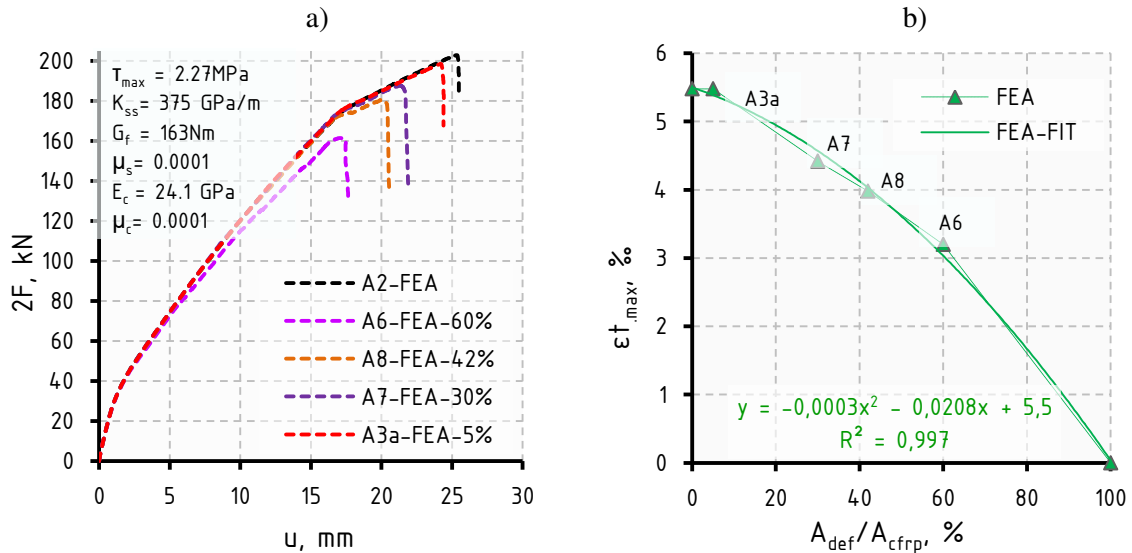
Fig. 5.29.: a) Load – displacement response at midspan zone of specimens
b) Maximal recorded CFRP strain at midspan zone

Similarly, the results allow building a relationship in form of a decreasing strengthening efficiency (*Fig. 5.30a*) and an increasing reduction of relative capacity (*Fig. 5.30b*) with an increasing ratio of defect area to the total bonded area (*see eq (4.2) and (4.3)*).
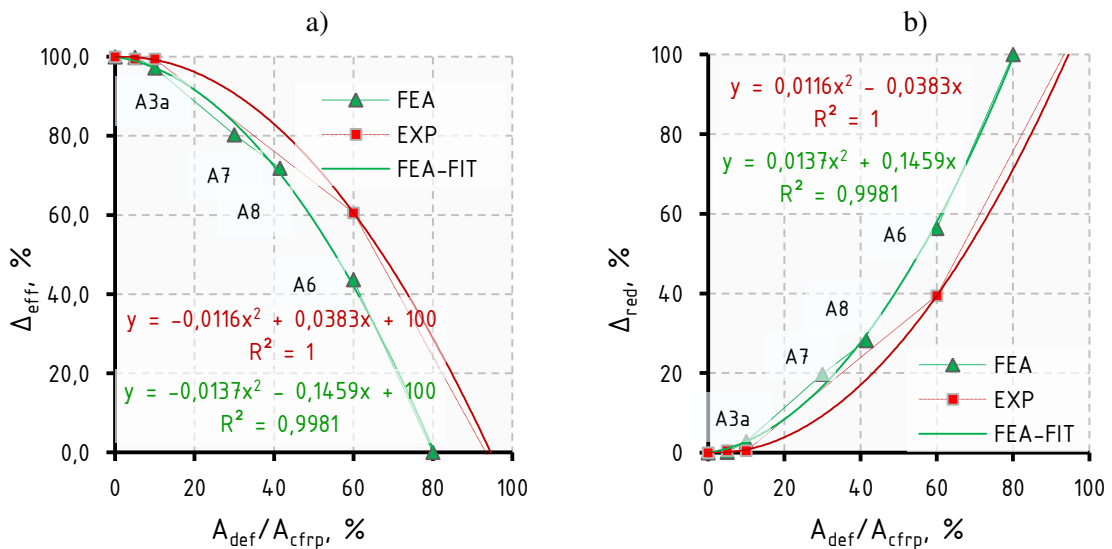
Fig. 5.30.: Strengthening efficiency a) and relative capacity reduction b) in a function of defect area ratio

On one hand, more conservative values of relative capacity reduction were obtained in numerical analysis in comparison to the experimental study. On the other hand, the other effects like friction in propagating defect between concrete – CFRP interface has not been taken into

account in numerical simulations. It also needs to be emphasised that the fitting curve based on least squares and obtained from the experimental study is governed only by one specimen (A6) for higher defect ratios. Nevertheless, numerical study confirms the experimental prediction that reduction of capacity due to the increase of defect ratio can be expressed closely with the use of the parabolic function. It can be noted that according to numerical results, the whole additional capacity given by the installation of the CFRP strip is lost when the defect is about 80% of the total bonded area (lower value than 100%). This means, that for higher defect ratio values, the CFRP strengthening debonds at a load level below the ultimate load flexural capacity of the unstrengthened RC beam.

5.7. CONCLUSIONS FROM NUMERICAL STUDY

Summarizing the presented discussion and analysis, the following conclusion from a numerical study can be formulated:

- Performed numerical analyses indicate that the finite element method can be considered a valuable tool for assessing beams with defects. A good agreement in terms of the ultimate load, as well as strains, has been received after the calibration of materials and the bond-slip models.

- No sensitivity of the CDP model on results with different mesh sizes was observed when proper formulas for determining post-elastic response and damage variables were used. Nevertheless, the cracking moment was rather overestimated in numerical analysis.

- Correct behaviour of damage propagation reflecting failure modes in numerical simulations has been observed and different for both series A and B,

- The numerical simulations show that beam models with surface-based cohesive contact are highly sensitive to maximal shear stress and fracture energy and less sensitive to bond stiffness.

- Lack of cohesive interaction in CFRP – concrete interface occurs to be a sufficient approach for simulating defects in performed analyses,

- Complex stress distribution expressed as damage initiation criterion was cumulated mostly at the border of the defects and can correspond to formulated cracks in the strengthened beam.

- The extended analysis confirmed the experimental prediction of expressing the reduction of flexural capacity of the beam with the increasing defect ratio by the use of the parabolic function (second-order polynomial).

6. SUMMARY

6.1. GENERAL

In this study, an attempt to investigate the influence of the bond defects on the behaviour of the passive strengthened beams with the use of CFRP strip in flexure was made. The research was limited to artificial defects that cause discontinuities in the concrete – CFRP interfaces in three particular locations: in the middle of the span, under point load and in the shear span. Two series of three beams each have been considered. The series differed in the amount of shear reinforcement which was related to expected failure modes.

6.2. CONCLUSIONS FROM THE EXPERIMENTAL PART

Carried out experimental investigations confirm that RC beams strengthened with CFRP with existing defects still exhibit essential residual flexural capacity. The value of existing bending capacity in the case of one-cycle loading strongly depends on the defect area ratio as well as on the properties of the strengthened member. In series A where 5% area defect has been considered, differences of less than 1% of ultimate load value have been observed in comparison to a strengthened RC beam with no defects (reference beams). An experimental study of series A shows that results were insensitive to defect location along the beam at this level of defect ratio. In series B where less shear reinforcement and an increased defect ratio of up to 10% were used, differences between specimens do not exceed 5.1%. Beams in series A show better flexural and more ductile performance than beams in series B. A 15% higher ultimate load has been observed in series A. Moreover, the debonding process occurred after the yield strength of bottom reinforcement was reached in series A in contrast to series B where debonding occurred before. Although, obtained results confirm the results of the numerical study presented by Zhou et al. [156], for assumptions and geometry adopted in the presented study, also defects up to 24000 mm^2 located in the shear span do not affect ultimate load significantly.

Any relevant differences have been observed in the behaviour of strengthened beams in terms of cracks and stiffness among all beams in each series. The defect did not affect the pattern of the cracks recorded on the beams and the existence of the defect remains hidden. In the studied range of defect ratios, any change of predicted failure mode due to defects has been observed. In other words, the failure mode of strengthened beams has not been affected by defects at any location in both series. The 60% defect ratio caused about a 16% decrease in the maximal flexural capacity.

The function of flexural capacity in relation to defect ratio was approximated with the use of a second-order polynomial. For given beam geometry and strengthening, flexural capacity can be estimated according to a determined relationship based on records of bond defects detected along the CFRP. The smallest 5% defect ratio for performed analysis was represented by an artificial defect in size of 120x120mm. That is why, from the non-destructive evaluation point of view, obtained results can indicate roughly the relevance of the required precision range for defects recognition with the use of detection devices and image analysis (*see chapter 1.3.3*).

6.3. CONCLUSIONS TAKEN FROM NUMERICAL SIMULATIONS

The main goal of this study was to verify the possibility of reflecting the proper behaviour of the flexural strengthened members with existing CFRP bond defects in numerical analysis. Secondly, numerical analysis was used to extend the range of laboratory tests. Numerical nonlinear analysis was performed in the ABAQUS software with the use of the concrete damage plasticity material model for concrete, bilinear material model for steel and linear for CFRP. Obtained results for reference RC beam A1 and strengthened specimen A2 with perfect bond assumption, were verified using software developed and calibrated by the author where good agreement between results in both tools has been found. For composite–concrete interface a surface-based cohesive behaviour has been chosen where bilinear bond-slip law has been considered. In performed analysis, constitutive law for bond was calibrated to results obtained in the laboratory tests wherein values from related literature were adopted as starting points. A sensitivity study for various parameters of numerical computations has been conducted.

Performed numerical simulations prove a satisfactory level of analysing the response of the flexural strengthened members with existing defects in the bond. After the calibration process, for smaller (up to 10%) defect ratios, error margins in comparison to laboratory tests do not exceed 6% for the specimens in series A. For specimens of series B, the difference in obtained results does not exceed 4.1%. A difference of up to 6% was obtained in the case of specimen A6 with a larger defect of up to 60% of the total bonded area. A good agreement in ultimate load was obtained regardless of the type of expected failure mode – IC debonding or shear endplate debonding.

In the next step, numerical analyses were used to determine the defect–ultimate load relationship where the size of the midspan defect was set as the main parameter. A good approximation of this relationship has been found by expressing it with the use of close to second-order polynomials. The obtained fitting plots correspond to the laboratory tests. For assumptions made in this study, the capacity loss was found to be proportional to the square of the defect area ratio that exists in the bond. The comparison of experimental and computational results confirms a good predictive performance of the FEM model in terms of the flexural response of CFRP-strengthened RC beams when defects were taken into account.

Given the above, questions asked in section 1.4, were answered and the target aim was achieved. Results indicate that exists some acceptable defects level in terms of the percentage of total bonded area that has a minor effect on the bending moment capacity of the strengthened member. For defects classified in terms of location and considering the size of the defect, a limited relationship to estimate its ultimate load was found. Applied defects do not cause any noticeable change in the failure mode of the beams in the tested range. For given specimens and boundary conditions, numerical simulations show relatively good agreement with those in the experimental study. Thus, the influence of bond defects on the behaviour of RC beams strengthened with CFRP was successfully investigated in the planned limits and range.

6.4. FURTHER RESEARCH

It needs to be emphasised that only a few beam specimens with described geometrical assumptions have been analysed experimentally in this study. Additionally, only beams under increasing monotonic load have been investigated. That is why general conclusions for the whole spectrum of passive CFRP strengthening in flexure with existing defects cannot be formulated without any further research.

According to the study presented here and the study presented by Zhou [156], it seems that a small defect ratio does not affect significantly the ultimate capacity load under monotonic load. However, a similar study should be performed under long-term as well as cyclic or dynamic loads. In those cases, also the defect growth rate in time needs to be investigated which allows for determining the inspection window from the time that the defect has been already detected to the time when the capacity drops beyond acceptable limits.

Considering the above, obtained results in this study may contribute to formulating guidelines and simplified procedures for considering detected defects in assessment procedures for passive strengthened structural members with the use of CFRP strips.

REFERENCES

[1]   ADAMCZYK W., PRZYBYŁA G., KRUCZEK G. i in. *Application of Numerical Procedure for Thermal Diagnostics of the Delamination of Strengthening Material at Concrete Construction*. International Journal of Thermal Sciences, 2019.

[2]   ALFARAH B., ALMANSA-LOPEZ F., OLLER S.: *New Methodology for Calculating Damage Variables Evolution in Plastic Damage Model for RC Structures*. Engineering Structures No. 132 pp. 70-86, 2017

[3]   ARAUJO J.M.: *Simplified procedures for calculation of instantaneous and long-term deflections of reinforced concrete beams,* Engenharia Civili, Numero 24, pp.55-66, 2005

[4]   ARDUINI, M., NANNI, A.: *Behavior of pre-cracked RC beams strengthened with carbon FRP sheets*. Journal of Composites for Construction, 1(2):63-70, 1997.

[5]   BARTOSIK T., KAŁUŻA M.: *Wzmacnianie konstrukcji z betonu materiałami na bazie włókien węglowych, szklanych i aramidowych, rodzaje produktów, zasady projektowania, technologia wykonywania i kontrola jakości robót*, XXI Ogólnopolska Konferencja Warsztat Pracy Projektowania Konstrukcji, Szczyrk, str. 1–38, 2006

[6]   BASCOUL A.*: Load Deflection Diagram of Over-Reinforced Concrete Beams.* Fracture Mechanics of Concrete Structures, Proceedings FRAMCOS-3, Germany 1994.

[7]   BATHE K.J.: *Finite Element Procedures*, Prentice-Hall Inc., New Jersey, 1996.

[8]   BAŽANT, Z.P. & OH, B.H.: *Crack Band Theory for Fracture of Concrete*. Materials and Structures, RILEM 16 (3), pp. 155–177, 1983

[9]   BIAŁOZOR R.: *Zarys problemu termograficznej oceny efektywności zespolenia elementów żelbetowych wzmocnionych kompozytami CFRP.* Gliwice 2019

[10]   BIAŁOZOR R.: *Projektowanie parametryczne jako wspomaganie procesu projektowania konstrukcji*, Nowoczesne projektowanie i realizacja konstrukcji budowlanych, Kraków 2017

[11]   BIRTEL, V., MARK, P., *Parameterised finite Element Modelling of RC Beam Shear Failure*, ABAQUS Users' Conference. 95-108, 2006

[12]   BODZAK P.: *Wpływ gatunku stali zbrojenia głównego na nośność na zginanie i graniczne odkształcenia kompozytu przy wzmacnianiu taśmami CFRP*, Przegląd Budowlany, nr 11, str. 47-51, 2017.

[13]   BONENBERG W., GIEDROWICZ M., RADZISZEWSKI K.: *Współczesne Projektowanie Parametryczne w Architekturze*. Wydawnictwo Politechniki Poznańskiej, Poznań, 2019

[14]   BRENA S.F., BRAMBLETT R.M., BENOUAICH M.A., et al.: *Use of Carbon fiber Reinforced Polymer Composites to Increase the Flexural Capacity of Reinforced Concrete Beams*, Research Report 1776-1, Texas Department of Transportation, Texas, April 2001.

[15]   CACHO D.V.: *Structural strengthening design based on TR55 & Eurocode 2*. Corporate Technical Dept. – SIKA Services AG. April 2016.

[16]   CAPRANI C.: *Structural Analysis III The Moment Area Method – Mohr's Theorems, Dublin Institute of Technology*, Lecture Notes, Dublin, 2007

[17]   CHEN J.F., TENG J.G.: *Anchorage Strength Models For FRP And Steel Plates Bonded to Concrete*. Journal of Structural Engineering, pp. 784-791 July 2001

[18]   CHEN G.M., TENG J.G., CHEN J.F.: *finite-Element Modeling of Intermediate Crack Debonding in FRP-Plated RC Beams*, Journal Of Composites For Construction pp. 339-353, June 2011

[19]   CICHOCKI M.: *Odkształcalność i nośność zarysowanych belek żelbetowych wzmocnionych taśmami kompozytowymi CFRP*, Inżynieria i Budownictwo, R. 55, nr 12, str. 698-703, 1999.

[20]   CICHOCKI M.: *Uwarunkowania wytrzymałościowe wzmacniania zarysowanych dźwigarów żelbetowych taśmami z włókien węglowych*, Inżynieria i Budownictwo, R. 57, nr 10, str. 571-575, 2001.

[21]   COHEN M., Numerical *Analysis of Debonding Mechanisms of Externally Bonded FRP Reinforcement in RC Beams*, PhD thesis, Waterloo, Ontario, Canada, 2018.

[22]   COHEN M., MONTELEONE A., POTAPENKO S.: *finite element analysis of intermediate crack debonding in fiber-reinforced polymer strengthened reinforced concrete beams*. Canadian Journal of Civil Engineering, May 2018.

[23]   CORVAGLIA P., LARGO A.: *IRT survey for the quality control of FRP reinforced R.C. structures*, 9th International Conference on Quantitative InfraRed Thermography, Krakow, 2008.

[24]   COOK R.D., et al.: *Concepts And Applications of finite Element Analysis*, 4th Edition, John Wiley & Sons, Inc, 2002.

[25]   CZADERSKI C.: *Strengthening of Reinforced Concrete Members by Prestressed, Externally Bonded Reinforcement With Gradient Anchorage,* PhD thesis, ETH Zurich, Switzerland, 2012.

[26]   CZADERSKI C., MEIER U.: *EBR Strengthening Technique for Concrete, LongTerm Behaviour and Historical Survey*, Polymers 10, 77, 2018.

[27]   CZKWIANIANC A., KAMIŃSKA M.: *Metoda nieliniowej analizy żelbetowych elementów prętowych*, Studies of civil engineering, no. 36, KILiW, IPPT, Warsaw 1992.

[28]   DEBNEY P.: *Computational Engineering*, IStrutE Guide, The Institute of Structural Engineers, London, 2020

[29]   DELANEY J., KARBHARI V.M.: *Defect Criticality in FRP Strengthening*, 8th International Symposium on fiber Reinforced Polymer Reinforcement for Reinforced Concrete Structures, University of Patras, Greece, July 16-18, 2007

[30]   DELPAK R., SHIH J.K.C., HU C. W AND TANN D. B.: *Detection of air blisters and crack propagation in FRP strengthened concrete elements using infrared thermography*, InfraMation - The Thermographers Conference, 2002.

[31]   DELPAK R., SHIH J.K.C., ANDREOU E., HU C. W AND TANN D. B.: *Thermographic Blister Detection in FRP Strengthened RC Elements and Degradation Effects on Section Performance in FRP Composites in Civil Engineering*, Elsevier, pp. 1135-1142, 2001.

[32]   DEMIR A., OZTURK H., DOK G.: *3D Numerical Modeling of RC Deep Beam Behaviour by Nonlinear Finite Element Analysis*, *DISASTER SCIENCE AND ENGINEERING* p. 13-18, 2(1), 2016

[33] DERKOWSKI W.: *Opportunities and risks arising from the properties of FRP materials used for structural strengthening,* Procedia Engineering 108 (2015) pp. 371 – 379

[34] DERKOWSKI W., ZYCH T.: *Nowoczesne materiały kompozytowe do wzmacniania konstrukcji budowlanych,* Czasopismo Techniczne, Wyd. Politechniki Krakowskiej, 2004.

[35] DERKOWSKI W.: *Fatigue Life of Reinforced Concrete Beams Under Bendig Strengthened with Composite Materials,* Archives of Civil And Mechanical Engineering Vol. VI No.4, Cracow, 2006

[36] DERKOWSKI W., WALCZAK R.: *Possibilities of Increasing Effectiveness of RC Structure Strengthening with FRP Materials*. Materials 2021, 14, 1387.

[37] DOMIN J., GÓRSKI M., BIAŁECKI R et al.: *Wheeled Robot Dedicated to the Evaluation of the Technical Condition of Large-Dimension Engineering Structures,* Robotics, *9*(2), 2020.

[38] EKENEL, M. AND MYERS, J.J.: *Nondestructive Evaluation of RC Structures Strengthened with FRP Laminates Containing Near-Surface Defects in the form of Delaminations*. Science and Engineering of Composite Materials. 14(4): 299–315, 2007.

[39] FINCKH W.: *Influence of Member-Specific Effects on the Design of Reinforced Concrete Members Strengthened Using CFRP Strips.* PhD Thesis, TECHNISCHE UNIVERSITAT MUNCHEN, 2012

[40] FU B., et al.: *Effect of Load Distribution on IC Debonding in FRP-Strengthened RC Beams: Full-Scale Experiments*, Composite Structures, January 2018

[41] GAO B., LEUNG C.K.T., KIM J.K.: *Prediction of Concrete Cover Separation Failure For RC Beams Strengthened with CFRP Strips.* Engineering Structures, No. 27, pp.177-189, September 2005.

[42] GÓRSKI M*.: Doświadczalno-teoretyczne podstawy wzmacniania elementów żelbetowych poddanych zginaniu, ścinaniu i skręcaniu z zastosowaniem nakładek zbrojonych włóknami węglowymi*. Rozprawa doktorska. Gliwice, 2005.

[43] GÓRSKI M., KRZYWOŃ R.: *Modelowanie numeryczne elementów wzmocnionych nakładkami FRP*. Materiały kompozytowe w budownictwie mostowym. Referaty z konferencji naukowo-technicznej. Łódź : Wydaw. Politechniki Łódzkiej, 2006, s. 17-24.

[44] GÓRSKI M., CASTRO-GOMES J., KRZYWOŃ R. I IN.: *Handbook - fibrous composite materials in the strengthening of structures*, Tipografia da Universidade da Beira Interior, Covilha, Portugal, 2016.

[45] GÓRSKI M., KOTALA M., BIAŁOZOR R.: *Rodzaje i właściwości zbrojenia niemetalicznego. Innowacyjne i współczesne rozwiązania w budownictwie*. Konstrukcje żelbetowe. XXXIII Ogólnopolskie Warsztaty Pracy Projektanta Konstrukcji, Szczyrk, 6-9 marca 2018 roku. T. 2, Wykłady. Red. Radosław Jasiński. Gliwice : Polski Związek Inżynierów i Techników Budownictwa. Oddział w Gliwicach, 2018, s. 45-90

[46] GÓRSKI M., KRZYWOŃ R., BIAŁOZOR R. I IN.*: IRT research on influence of long term loads on defects In FRP strengthened RC beams*. 64 Konferencja Naukowa Komitetu Inżynierii Lądowej i Wodnej PAN oraz Komitetu Nauki PZITB. Krynica 2018.

[47] GÓRSKI M., KRZYWOŃ R.: *Obliczanie wzmocnień z wykorzystaniem taśm i mat zbrojonych włóknami wysokiej wytrzymałości*. XXIX Ogólnopolskie Warsztaty Pracy

Projektanta Konstrukcji, Szczyrk, 26-29 marca 2014 roku. T. 1, Wykłady. Polski Związek Inżynierów i Techników Budownictwa. Oddział w Gliwicach, 2014, s. 285-342

[48] GULVANESSIAN H., CALGARO JA., MILAN H.: *Designer's Guide to EN 1990: Eurocode: Basis of Structural Design,* T. Telford, London. 2012.

[49] HAMED A., et al.: *Flexural Strengthening of Preloaded Reinforced Concrete Continuous Beams: an Experimental Investigation,* Alexandria Engineering Journal, 558, pp.207-216, 2019

[50] HESLEHURS R.B.: Defects and Damage in Composite Materials and Structures, CRC Press Taylor Francis Group, 2014.

[51] HIRIYUR B.: T2D2 - *An AI Revolution in Structural Health Assessment.* Thornton Tomasetti CORE studio Brochure, September 2019

[52] HOFSTETTER G., MESCHKE G.: *Numerical Modeling of Concrete Cracking*. CISM International Centre for Mechanical Sciences, vol 532. Springer, Vienna

[53] HOLLAWAY L., TENG J.G.: *Strengthening and rehabilitation of civil infrastructures using fibre-reinforced polymer (FRP) composites*. Woodhead Publishing Limited and CRC Press LLC, 2008

[54] HOLZENKÄMPFER, P.: *Ingenieurmodelle des Verbunds geklebter Bewehrung für Betonbauteile*. Dissertation. Technische Universität Braunschweig, Institut für Baustoffe, Massivbau und Brand-schutz, Braunschweig, 1994.

[55] HORDIJK D.A.: *Local Approach to Fatigue of Concrete,* PhD Thesis, Delft University of Technology, 1991

[56] IOVINELLA I., PROTA A., ZAZZOTTI C.: *Influence of Surface Roughness on the Bond of FRP Laminates to Concrete,* Construction and Building Materials 40, pp. 533–542, 2013

[57] JABŁOŃSKI Ł., HALICKA A.: *Influence of Surface Based Cohesive Parameters on Static Performance of Concrete Composite T-Shaped Beams*, MATEC Web of Conferences 262, 08003 (2019), Krznica 2018,

[58] JANKOWIAK I.: *Weryfikacja doświadczalna modeli numerycznych belek żelbetowych wzmocnionych taśmami FRP,* Inżynieria i Budownictwo nr 10, 2007.

[59] JANKOWIAK T., ŁODYGOWSKI T.: *Identification of Parameters of Concrete Damage Plasticity Constitutive Model,* Foundations of Civil and environmental engineering No. 6, pp. 53-69, 2005.

[60] JAWDHARI A., HARIK I.*: Simulation of Delamination Failures in RC Members Strengthened with CFRP Rod Panels and CFRP Laminates*. Journal of the American Concrete Institute, XII, 2018.

[61] KAISER H., KARBHARI V.M.: *Identification of Potential Defects in the Rehabilitation of Concrete Structures with FRP Composites,* Int. J. of Materials & Product Technology, Vol. 19, No. 6, pp. 498–520, 2003.

[62] KALAYCI A.S., YALIM B., MIRMIRAN A.: *Effect of Untreated Surface Disbonds on Performance of FRP-Retrofitted Concrete Beams*. Journal of Composites for Construction 13, pp. 476-485, 2009.

[63]   KAŁUŻA M.: *Wybrane problemy wzmacniania konstrukcji żelbetowych sprężonymi taśmami z włókien węglowych*, Zeszyty Naukowe Politechniki Śląskiej, zeszyt 102, Gliwice, 2004, str. 93–20

[64]   KAŁUŻA M., BARTOSIK T.: *Wzmacnianie konstrukcji budowlanych taśmami i matami FRP – zagadnienia technologiczne*. XXIX Ogólnopolskie Warsztaty Pracy Projektanta Konstrukcji, Szczyrk, 26-29 marca. T. 2, Wykłady. Polski Związek Inżynierów i Techników Budownictwa. Oddział w Gliwicach, pp. 173-212, 2014.

[65]   KAŁUŻA M., AJDUKIEWICZ A.: *Comparison of Behaviour of Concrete Beams with Passive and Active Strengthening by Means of CFRP Strips*. Architecture Civil Engineering Environment – ACEE 2/2008, str. 51–64

[66]   KAMIŃSKA M.E., KOTYNIA R.: *Obliczeniowe określanie nośności żelbetowych belek wzmocnionych taśmami CFRP*, Inżynieria i Budownictwa, nr 11, str. 620-625, 2000.

[67]   KAMIŃSKA M.E., KOTYNIA R.: *Doświadczalne badania żelbetowych belek wzmocnionych taśmami CFRP*, Badania doświadczalne elementów i konstrukcji betonowych, Z. 9, Wyd. Kat. Bud. Bet. PŁ, Łódź, 2000.

[68]   KARBHARI V.M., KAISER H., NAVADA R, et al.: *Methods for Detecting Defects in Composite Rehabilitated Concrete Structure - Final Report SPR 336,* University of California, San Diego, 2005

[69]   KARBHARI V.M., ZHAO L.: *Issues related to composite plating and environmental exposure effects on composite-concrete interface in external strengthening*., Composite Structures Vol. 40, pp 293-304, 1998.

[70]   KARBHARI V.M.: *Durability of Composites for Civil Structural Applications,* Woodhead Publishing Limited*,* 2007

[71]   KARBHARI VM, NAVADA R.: *Investigation of Durability and Surface Preparation Associated Defect Criticality of Composites Bonded to Concrete*. Composites Part A: Applied Science and Manufacturing, 39(6) pp. 997-1006, 2008;

[72]   KIM Y.J., HEFFERNAN P.J.: *Fatigue Behavior of Externally Strengthened Concrete Beams with Fiber-Reinforced Polymers: State of the Art,* Journal of Composites for Construction No. 12 pp.246-256, 2008,

[73]   KISHI, N., ZHANG, G., AND MIKAMI, H.: *Numerical cracking and debonding analysis of RC beams reinforced with FRP sheet*. J. Compos. Constr., 96, 2005, pp 507–514.

[74]   KLAMER E. L.*: Influence of temperature on concrete beams strengthened in flexure with CFRP*. PhD Thesis. Eindhoven: Technische Universiteit Eindhoven, 2009.

[75]   KORENTZ J.: *Ścieżki Równowagi statycznej belek żelbetowych wzmacnianych taśmami z włókien węglowych*, JCEEA, t. XXXIV, z. 64 (3/I/17), lipiec-wrzesień, pp. 213-222, 2017

[76]   KO H., SATO Y.: *Bond Stress-Slip Relationship between FRP Sheet and Concrete under Cyclic Load*, JOURNAL OF COMPOSITES FOR CONSTRUCTION, 11(4), pp. 419-426, 2007.

[77]   KOTYNIA R.: *Wzmacnianie żelbetowych belek na ścinanie za pomocą kompozytów polimerowych*, Zeszyty Naukowe, Nr 1106, Łódź, 2011.

[78]   KOTYNIA R, BAKY HA, NEALE KW, EBEAD UA.: *Flexural strengthening of RC beams with externally bonded CFRP systems: Test results and 3-D nonlinear FE analysis*.

Journal of Composites for Construction 2008; 10.1061/(ASCE)1090-0268(2008)12:2, pp. 190–201.

[79]   KOTYNIA R.: *FRP Composites For Flexural Strengthening of Concrete Structures Theory, Testing, Design*, Lodz University of Technology, Łódź, Poland, 2019

[80]   KOTYNIA R.: *Przyczepność zbrojenia kompozytowego do betonu w żelbetowych elementach wzmocnionych za pomocą materiałów kompozytowych CFRP*. Badania doświadczalne elementów i konstrukcji betonowych, Z. 16, Wyd. Kat. Bud. Bet. PŁ, Łódź, 2008.

[81]   KOTYNIA, R.: *Debonding Phenomena in FRP – Strengthened Concrete Members*. Brittle Matrix Composites 8, 2006.

[82]   KOTYNIA R.: *Wpływ ukształtowania zewnętrznego zbrojenia kompozytowego CFRP na efektywność wzmocnienia belek żelbetowych*, Inżynieria i Budownictwo, R. 61, nr 1, str. 27-31, 2005.

[83]   KOTYNIA R., KAMIŃSKA M.E.: *Odkształcalność i sposób zniszczenia żelbetowych belek wzmocnionych na zginanie materiałami CFRP*, Badania doświadczalne elementów i konstrukcji betonowych, Z. 13, Wyd. Kat. Bud. Bet. PŁ, Łódź, 2003.

[84]   KOTYNIA R, LASEK K..: *Efektywność wzmocnienia zginanych elementów żelbetowych przy użyciu naprężonych kompozytów CFRP – stan wiedzy w dziedzinie badań doświadczalnych*, Przegląd Budowlany, nr 9, str. 38-42, 2018.

[85]   KOTYNIA R, LASEK K..: *Efektywność zastosowania wstępnie naprężonych taśm CFRP do wzmacniania belek żelbetowych na zginanie.* Badania doświadczalne elementów i konstrukcji betonowych, Z. 21, Wyd. Kat. Bud. Bet. PŁ, Łódź, 2018.

[86]   KOWAL M.: *Wzmacnianie elementów stalowych kompozytami FRP*, Rozprawa doktorska, Politechnika Lubelska, Lublin, 2015.

[87]   KRZYWOŃ R.: *Zasady projektowania konstrukcji z zewnętrznym zbrojeniem niemetalicznym. Innowacyjne i współczesne rozwiązania w budownictwie*. Konstrukcje żelbetowe. XXXIII Ogólnopolskie Warsztaty Pracy Projektanta Konstrukcji, Szczyrk, 6-9 marca,. T. 3, Wykłady. Red. Radosław Jasiński. Gliwice 2018.

[88]   KRZYWOŃ R.: *Behaviour of EBR FRP strengthened beams exposed to elevated temperature. Analytical models and new concepts in concrete and masonry structures*. AMCM'2017. 9th International Conference, Gliwice, June 5-7, 2017.

[89]   KRZYWOŃ R., GÓRSKI M., DAWCZYŃSKI S.: *Features of SRP tapes against CFRP composites used for strengthening of concrete structures*, International Conference on Analytical Models and New Concepts in Concrete and Masonry Structures AMCM'2017.

[90]   KRZYWOŃ R., GÓRSKI M., DAWCZYŃSKI S.: *Long-term comparative tests of RC beams strengthened with CFRP strip and SRP tape*. Proceedings of the International Conference on Engineering. ICEUBI2015 Engineering for Society, Covilha, Portugal, 2-4 December 2015.

[91]   KUBICA J., GALMAN I.: *Comparison of Two ways of AAC Block Masonry Strengthening Using CFRP Strips - Diagonal Compression Test.* Procedia Engineering 193 pp. 42 – 49, 2017.

[92]   KUPFER H., HILSDORF H., RUSCH H.: *Behaviour of Concrete Under Biaxial Stresses*, ACI JOURNAL, pp. 656-666, 1969

[93]   KUSA E., KAMIŃSKI M.: *Badania ugięć belek żelbetowych wzmacnianych taśmami węglowymi CFRP*. Materiały Budowlane, No.3, pp. 38-39, 2013

[94]   LEE J., FENVES G.L.: *Plastic-damage Model for Cycling Loading of Concrete Structures*. Eng Mech 124(8):892-900, 1998

[95]   LEZGY-NAZARGAH M., DEZEHANGAH M., SEPEHRINIA M.: *The effects of different FRP/concrete bond-slip laws on the 3D nonlinear FE modeling of retrofitted RC beams - A sensitivity analysis*, Steel and Composite Structures, July 2018.

[96]   LI G., ZHANG A., GUO Y.: *Effect of Preload Level on Flexural Load-carrying Capacity of RC Beams Strengthened by Externally Bonded FRP Sheets,* The Open Civil Engineering Journal, 2015, 9 pp.426-434, 2015

[97]   LU X.Z., TENG J.G., YE L.P., JIANG J.J.*: Intermediate Crack Debonding in FRP-Strengthened RC Beams: FE Analysis and Strength Model*, Journal of Composites for Construction • April 2007.

[98]   LU X.Z., TENG J.G., YE L.P., JIANG J.J.: *Bond–slip models for FRP sheets/plates bonded to concrete*. Engineering Structures, 27(6):920-937, May 2005.

[99]   LUBLINER J, OLIVER J, OLLER S., ONATE E.: *A Plastic-Damage Model for Concrete*. Solids Struct 25(3):299-326, 1989

[100] ŁAGODA M.: *Wzmacnianie Konstrukcji Mostowych Kompozytami Polimerowymi,* Polska Akademia Nauk KILIWIPPT, Warszawa, 2012

[101] ŁAGODA M.: *Zalecenia dotyczące wzmacniania konstrukcji mostowych przez przyklejanie zbrojenia zewnętrznego*. IBDIM. Warszawa, 2002

[102] ŁAKOTA, W., BUDA-OŻÓG, L., KLICH, R.: *Badania dynamiczne w ocenie stanu belek żelbetowych i wzmocnionych taśmami CFRP*, Inżynieria i Budownictwo, R. 63, nr 4, str. 213-216, 2007.

[103] MAERZ N., GALECKI G., NANNI A.*: Experimental non-destructive testing of FRP materials, installation, and performance*, Dallas county bridge, Missouri, USA. Proceedings of the 16th World Conference on Nondestructive Testing (2004, Montreal, Canada), NDT (Non-Destructive Testing) c/o Bongiovanni Research & Technology, Inc., Sep 2004.

[104] MAJEWSKI S.: Mechanika betonu konstrukcyjnego w ujęciu sprężysto-plastycznym, Wydawnictwo Politechniki Śląskiej, Gliwice, 2003

[105] MASHREI M.A., MAKKI J.S., SULTAN A.A: Flexural Strengthening of Reinforced Concrete Beams Using Carbon Fiber Reinforced Polymer (CFRP) Sheets with Grooves, Latin American Journal of Solids and Structures, 16(4), e176, 2019.

[106] MARI A.R., OLLER E., BAIRAN J.M et al.: *Simplified Method for the Calculation of Long-Term Deflections in FRP-Strengthened Reinforced Concrete Beams,* vol. 45, Issue 1, pp. 1368-1376, 2013

[107] MEIER U.: *Strengthening of structures using carbon fibre/epoxy composites*, Construction Building Materials 9 (6)/1995, str. 341–351

[108] MEIER U., KOTYNIA R.: *Wzmacnianie konstrukcji żelbetowych naprężonymi materiałami kompozytowymi FRP*, Inżynieria i Budownictwo 11/2006, str. 596–599

[109]   MILOVANOVIĆ B., PECUR I.: Review of Active IR Thermography for Detection and Characterization of Defects in Reinforced Concrete, Journal of Imaging No.02, 2016.

[110]   MROZEK M.: *Numeryczna symulacja wzmacniania matami CFRP Konstrukcji murowych z cegły*, Rozprawa Doktorska, Politechnika Śląska Styczeń 2012.

[111]   MTENGA P.V., LIMERICK R.L., TAWfiQ K.S.: *IRT Evaluation of Bond Layer Thickness for CFRP Bonded to Concrete*, 2018

[112]   MUSIAŁ M.: *Badanie doświadczalne częstotliwości własnych i ugięć belek żelbetowych wzmocnionych taśmami CFRP*. Materiał Budowlane, nr 9 str. 68-69, 2016.

[113]   NAGRODZKA-GODYCKA K.: *Badanie właściwości betonu i żelbetu w warunkach laboratoryjnych*, Arkady, Warszawa, 1999.

[114]   NIEDERMEIER R., ZLICH K.: *Zugkraftdeckung bei klebearmierten Bauteilen*, Ernst & Sohn · Beton- und Stahlbetonbau 96, Heft 12, 2001.

[115]   NGUYEN H.T, KIM S.E.: *Finite Element Modeling of Push-out Tests For Large Stud Shear Connectors*, Journal of Constructional Steel Research No. 65 pp. 1909-1920, 2009.

[116]   OBAIDAT Y.T.: *Structural Retrofitting of Concrete Beams Using FRP - Debonding Issues,* PhD Thesis, Lund University, Sweden, 2011

[117]   OBAIDAT Y.T., HEYDEN S., DAHLBLOM O.: *The effect of CFRP and CFRP/concrete interface models when modeling retrofitted RC beams with FEM*., Composite Structures no. 92, Elsevier, pp. 1391-1398, 2010.

[118]   OEHLERS D.J., VISINTIN P., LUCAS W.: *Flexural Strength and Ductility of FRP-Plated RC Beams: Fundamental Mechanics Incorporating Local and Global IC Debonding*, Journal of Composites for Construction, 20(2), 2015.

[119]   PASCOE J.A.: *Slow-growth Damage Tolerance for fatigue after impact in FRP composites: Why current research won't get us there,* Theoretical and Applied Fracture Mechanics 116, Elsevier, 2021

[120]   PIĄTEK B.: *Nowa technologia wzmacniania konstrukcji betonowych naprężanymi taśmami CFRP*, Rozprawa doktorska, Politechnika Rzeszowska, 2017

[121]   PIĄTEK B., SIWOWSKI T.: *Investigation of strengthening effectiveness of reinforced concrete bridge with prestressed CFRP strips*, Drogi i Mosty 15/2016, str. 301–314

[122]   PIEKARCZYK A.: Lokalizacja wad struktury betonu w konstrukcji. XXIX Ogólnopolskie Warsztaty Pracy Projektanta Konstrukcji, Szczyrk, 26-29 marca 2014 roku. T. 3, Wykłady. Polski Związek Inżynierów i Techników Budownictwa. Oddział w Gliwicach, 2014, s. 1-82.

[123]   PLEVRIS N, TRIANTAFILLOU TC.: *Time-Dependent Behavior of RC Members Strengthened with FRP Laminates*. Journal of Structural Engineering ASCE, 120(3):1016-1042, 1994

[124]   QIN R., LAU D., TAM L. et al.: *Experimental Investigation on Interfacial Defect Criticality of FRP-Confined Concrete Columns*. Sensors 19, 468, 2019.

[125]   REWERS I.: *Numerical Analysis of RC beam with High Strength Steel Reinforcement Using CDP Model*, IOP Conf. Series: Materials Science and Engineering 471, 2019

[126] RIBOLLA E.M., SPADA A. HAJIDEHI M.R. et al..: Ultrasonic inspection for the detection of debonding in CFRP-reinforced concrete. Structure and Infrastructure Engineering, Taylor & Francis Group, Published online, October 2017.

[127] ROCCO C., et al.: *Size Effect And Boundary Conditions in the Brazilian Test: Experimental Verification,* Materials And Structures, Vol. 32, pp. 210-217, 1999

[128] S&P C-Laminate – Product Technical Card of FRP System.TDS.PL-PL.V1 - 01.2019

[129] SARKER M.M., HADIGHEH S.A., DIAS-DA-COSTA D.: *Non-Destructive Evaluation Techniques for Identification of Interfacial Cracking in FRP-Concrete Connections*, The 8th International Conference on Structural Health Monitoring of Intelligent Infrastructure, Brisbane, Australia. 5-8 December 2017

[130] SAYED-AHMED E.Y. BAKAY R. SHRIVE N.G.: *Bond Strength of FRP Laminates to Concrete: State-of-the-Art Review*, Electronic Journal of Structural Engineering, No. 9, pp 45-61, 2009.

[131] SEIM W., HORMAN M., KARBHARI V., SEIBLE F.: *External FRP post-strengthening of scaled concrete slabs.* J Compos Construct 5(2):67–75, 2001

[132] SERĘGA S., KOTYNIA R., LASEK K.: *Obliczeniowa analiza belek żelbetowych wzmocnionych naprężonymi taśmami CFRP.* Czasopismo Inżynierii Lądowej, Środowiska i Architektury Journal Of Civil Engineering, Environment And Architecture JCEEA, T. XXXIII, Z. 63 (1/I/16), Styczeń-Marzec 2016, pp. 279-287

[133] Da SILVA, L. F. M., Campilho, R. D. S. G.: *Advances in Numerical Modeling of Adhesive Joints.* SpringerBriefs in Applied Sciences and Technology. Computational Mechanics, 2012.

[134] SHARDAKOV I.N., BYKOV A.A., SHESTAKOV A.P.: *Delamination Of Carbon Fiber Strengthening Layer From Concrete Beam During Deformation (Infrared Thermography)*, Frattura ed Integrita Strutturale, 38 (2016), 331-338.

[135] SIWOWSKI T.: *Mosty z kompozytów FRP – Kształtowanie, Projektowanie, Badania.* Wydawnictwo Naukowe PWN, Wyd. 1, 2018.

[136] SIWOWSKI T., RADOMSKI W.: *Pierwsze krajowe zastosowanie taśm kompozytowych do wzmocnienia mostu.* Inżynieria i Budownictwo 7/1998, str. 382–388.

[137] ŚLEDZISZEWSKI K.: *Praca Stalowo-Betonowej Belki Zespolonej z Uwzględnieniem Zarysowania Płyty,* PhD Thesis, Politechnika Lubelksa, Wydział Budownictwa i Architektury, Lublin, Poland, 2015.

[138] SOARES S., SENA-CRUZ J., CRUZ J.R et al.: *Influence of Surface Preparation Method on the Bond Behaviour of Externally Bonded CFRP Reinforcements in Concrete*. Materials 12, 414, 2019

[139] SZCZECINA M., WINNICKI A.: *Selected Aspects of Computer Modeling of Reinforced Concrete Structures Structures*, Archives of Civil Engineering, Vol. LXII, Issue 1, 2016

[140] TAILLADE F. I IN.: *Nondestructive Evaluation of FRP Strengthening Systems Bonded on RC Structures Using Pulsed Stimulated Infrared Thermography*, In : Infrared Thermography, Chapter 9, InTech, pp. 193-208, 2012

[141] TENG J.G., SMITH S.T., CHEN J.F.:Intermediate Crack-Induced Debonding in RC Beams and Slabs, Construction and Building Materials, Volume 17, Issues 6-7, pp. 447-462, 2003.

[142] TAUCER F., SPACONE E., FILIPPOU F.C: *A Fiber Beam-Column Element For Seismic Response Analysis of Reinforced Concrete Structures*, Report No. UCB/EERC-91/17, Earthquake Engineering Research Center, College of Engineering, University of California, Berkeley, December 1991.

[143] THÉROUX L. D., DUMOULIN J., MALDAGUE X.: *Active Thermal Shearography And Infrared Thermography Applied to NDT of Reinforced Concrete Structure by Glued CFRP*, 7th European Workshop on Structural Health Monitoring, July 8-11, 2014. La Cité, Nantes, France.

[144] TIMOSHENKO S.: *History of strength of materials*. New York: McGraw-Hill, 1953

[145] TRAPKO T.: *The Effect of High Temperature on the Performance of CFRP and FRCM Confined Concrete Elements,* Composites: Part B 54 pp. 138–145, 2013

[146] TURON A., DAVILA C.G., CAMANHO P.P., et al: *An Engineering Solution for solving Mesh Size Effects in the Simulation of Delamination with Cohesive Zone Models* Engineering Fracture Mechanics, Vol. 74, No. 10, pp. 1665-1682, 2007.

[147] URBAŃSKA D., MARCINCZAK K.: *Porównanie Wyników Badań Żelbetowych Wzmocnionych na Ścinanie z Analizami Numerycznymi*, Materiały Budowlane nr 529, 9 pp.74-75, 2016.

[148] VALLAZZI M.R., GRINZATO E., PELLEGRINO C.: *IR Thermography For Interface Analysis of FRP Laminates Externally Bonded to RC Beams*, Materials and Structures, 42, pp.25-34, 2009.

[149] VOLPE NATIONAL TRANSPORTATION SYSTEMS CENTER.: *Damage Tolerance Assessment - Handbook. Volume I: Introduction, Fracture Mechanics, Fatigue Crack Propagation,*Cambridge, USA, 1993.

[150] WAN, B.; JIANG, C.; WU, Y.-F. *Effect of defects in externally bonded FRP reinforced concrete*. Constr. Build. Mater. 172, pp. 63–76. 2018.

[151] WAUGH R.: *Development of Infrared Techniques for Practical Defect Identification in Bonded Joints*, Springer International Publishing, Switzerland, 2016,

[152] WENWEI W., GUO L.: *Experimental Study and Analysis of RC Beams Strengthened with CFRP Laminates Under Sustaining Load*, International Journal of Solids and Structures 43, 1372–1387, 2005.

[153] WOSATKO A., WINNICKI A., POLAK M.A., et al: *Role of dilatancy angle in plasticity-based models of concrete*, Archives of Civil and Mechanical Engineering 19, pp. 1-16, 2019.

[154] YAO, J., TENG, J.G.: *Plate End Debonding in FRP-plated RC Beams - I: Experiments*. Engineering Structures 29: 2457–2471, 2007

[155] YAZDANI N., BENEBERU E., RIAD M.: *Nondestructive Evaluation of FRP-Concrete Interface Bond due to Surface Defects*, Advances in Civil Engineering, Hindawi, Volume 2019, pp. 1-10.

[156] ZHOU A., QIN R., FEO L., et al: *Investigation on interfacial defect criticality of FRP-bonded concrete beams*, Composites Part B, 113, pp. 80-90, 2017.

[157] ZHOU H.: *Behaviour of FRP-to-Concrete Bonded Joints Under Cyclic and Thermal Loading,* PhD thesis, The University of Queensland, 2018.

[158] ZIENKIEWICZ O.C., TAYLOR R.L.: *The finite Element Method*, Volumes 1-3, fifth Edition, Butterworth Heinemann, 2000.

[159] ZOGHI M.: *The International Handbook of FRP Composites in Civil Engineering*, CRC Press, Taylor & Francis Group, Boca Raton, 2014.

CODES AND GUIDELINES

[N1] ACI 440.1R-08 (2008), Guide for the Design and Construction of Externally Bonded FRP Systems for Strengthening Concrete Structures, ACI Committee 440, American Concrete Institute (ACI)

[N2] ASTM D3039 / D3039M-17, Standard Test Method for Tensile Properties of Polymer Matrix Composite Materials, ASTM International, West Conshohocken, PA, 2017, www.astm.org

[N3] ASTM D638 − 14, Standard Test Method for Tensile Properties of Plastics, ASTM International, West Conshohocken, PA, www.astm.org

[N4] EN 1992-1-1: Eurocode 2: Design of concrete structures - Part 1-1: General rules and rules for buildings, 2004.

[N5] fiB Bulletin 14. Externally Bonded FRP Reinforcement For RC Structures. Federation Internationale du Beton. Technical Report, 2001.

[N6] fiB Bulletin 40. FRP Reinforcement in RC Structures. Federation Internationale du Beton. Technical Report, 2007.

[N7] fiB Bulletin 65. Model Code 2010 - final draft, Volume 1. Federation Internationale du Beton. Technical Report, 2010.

[N8] fiB Bulletin 90. Externally applied FRP reinforcement for concrete structures. Federation Internationale du Beton. Technical Report, 2019.

[N9] CNR-DT 200 R1/2013, (2014), Guide for the Design and Construction of Externally Bonded FRP Systems for Strengthening Existing Structures, National Research Council, Italy 2013

[N10] CSA-S806-02 (2002), Design and Construction of Building Components with Fibre-Reinforced Polymers, Canadian Standards Association, Ontario

[N11] CSA-S6-06 (2006), - Canadian Highway Bridge Design Code, Canadian Standards Association, Ontario

[N12] ISO 1920-4:2020 - Testing of concrete — Part 4: Strength of hardened concrete

[N13] JSCE (2001). "Recommendations for Upgrading of Concrete Structures with Use of Continuous fiber Sheets", Japan Society of Civil Engineers, Tokyo, Japan

[N14] JRC Science for Policy Report. Prospect for new guidance in the design on FRP. Support to the implementation, harmonization and failure development of the Eurocodes. 2016.

[N15] JSCE (1997), Recommendation for Design and Construction of Concrete Structures Using Continuous fiber Reinforcing Materials, Research Committee on Continuous fiber Reinforcing Materials, Japan Society of Civil Engineers, Tokyo

[N16] PN-EN 12390-2:2019 Testing hardened concrete - Part 2: Making and curing specimens for strength tests

[N17] TR55 Design Guidance For Strengthening Concrete Structures Using fibre Composite Materials, Third edition, Report of a Concrete Society Committee, 2012

[N18] TR57 Strengthening Concrete Structures With fibre Composite Materials: Acceptance, Inspection And Monitoring, Report of a Concrete Society Committee, 2003.

[N19] TR59 Strengthening Influence of tension stiffening on deflection of reinforced concrete structures, Report of a Concrete Society Committee, 2004.

APPENDIX A – DEVELOPED TOOL FOR ANALYSIS VERIFICATION

A.1 - DESCRIPTION

The software was developed by author using Python programming language to control numerical nonlinear analyses using the fibre beam concept where more complex material models were adopted (see Fig.A. 0.1).
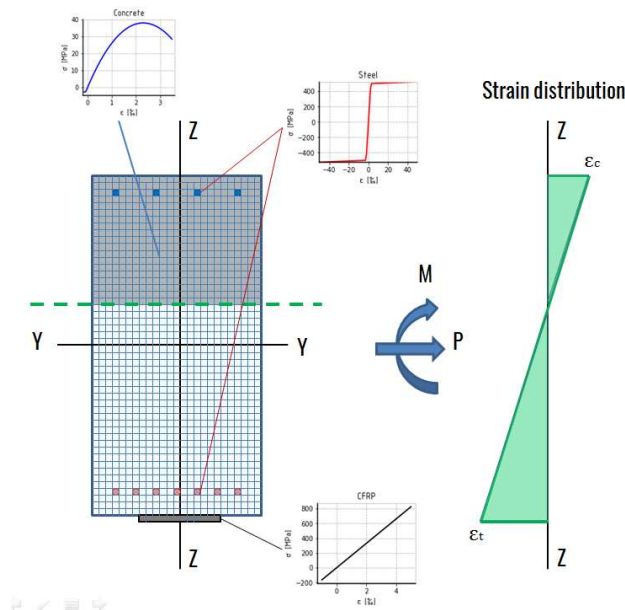
Fig.A. 0.1 Materials scheme and strain distribution in RC cross-section divided into fibres under bending and axial force

It is based on the following assumptions:

- consideration is limited to normal stress only
- plain section principle was adopted in the whole load range
- a perfect bond between concrete and reinforcement as well as concrete and CFRP was assumed
- the nonlinear uniaxial stress-strain relationships for concrete and steel for each diameter obtained in experimental data were adopted
- the stress-strain relationships for CFRP obtained in experimental data were adopted,

Table A.0.1. Input parameters for numerical cross-section procedure

Geometry	
External Load	P_{ext} – axial force*, M_{ext} – bending moment
Cross-section geometry**	b – width, h- height, ct – top cover, cb – bottom cover
Steel geometry	n – reinforcement number, φ – rebar diameter, φ_s – stirrup diameter
CFRP geometry	b_f – CFRP width, t_f – CFRP thickness

*   *optional, here N=0kN,*
**   *rectangular section*

Table A.0.2. Input relationships of materials

Material properties	
Concrete	$\sigma_c = \sigma_c(\varepsilon_c)$
Steel	$\sigma_f = \sigma_f(\varepsilon_f)$
CFRP	$\sigma_s = \sigma_s(\varepsilon_s)$

The numerical procedure starts by calculating the initial strain distribution for a given load increment and the considered RC section geometry(*see Table A.0.1*) as well as for assumed material stress-strain relationships (*see Table A.0.2*). Based on the plain section assumption the linear distribution of strain along the section (*see Fig.A. 0.2*) can be written:

$$\varepsilon(z) = az + b = \kappa z + \varepsilon_0 \tag{A.0.1}$$

where:

a, b -   linear function parameters
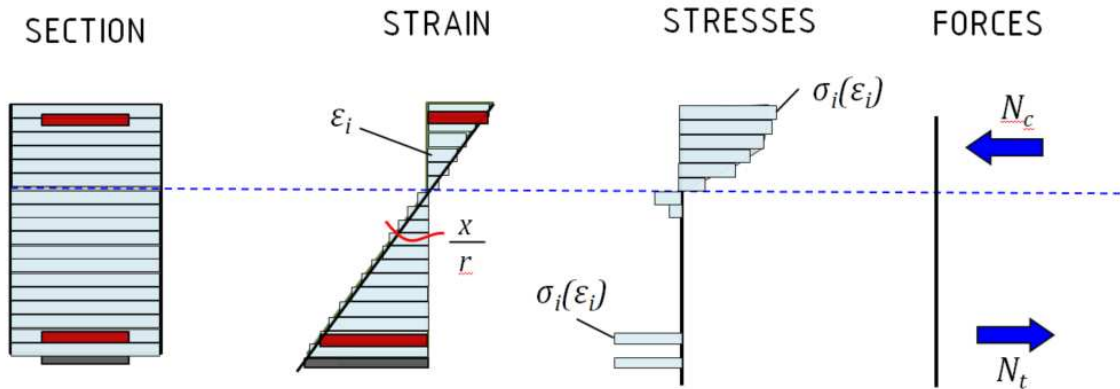
κ -   curvature

Fig.A. 0.2 Stress and strain distribution in RC cross-section divided into fibres

Initially, b=0 is considered. By changing curvature, received strain distribution allows calculating strain value in each fibre. Based on material constitutive relationships (steel, concrete, CFRP separately) and fibre cross-section area, the stress in fibres is calculated for a given strain value. Then, internal forces from stress distribution are determined and the condition of forces equilibrium acting on the section is checked:

$$|P_{ext} - N_{int}| \leq \delta_N \tag{A.0.2}$$

$$N_{int} = N_c + N_t = \sum_{i=1}^{n_{strip}} A_{ci}\sigma(\varepsilon_{ci}) + \sum_{k=1}^{m} A_{sk}\sigma(\varepsilon_{sk}) + A_f\sigma(\varepsilon_f) \tag{A.0.3}$$

$$|M_{ext} - M_{int}| \leq \delta_M \qquad \text{(A.0.4)}$$

$$M_{int} = \sum_{i=1}^{n_{strip}} A_{ci}\sigma(\varepsilon_{ci})(y_g - y_i) + \sum_{k=1}^{m} A_{sk}\sigma(\varepsilon_{sk})(y_g - d_i) + A_f\sigma(\varepsilon_f)(y_g - y_f)$$

$$\text{(A.0.5)}$$

where:

δ_N, δ_M -   *assumed iteration accuracy parameters*

A_{ci}, A_{sk} -   *a cross-section area of i - concrete strip, k - reinforcement row*

If equilibrium is not achieved, the curvature is modified and the procedure is repeated as long as the balance of external and internal forces will be met. Once is achieved, the next load increment is considered. Ultimate load is obtained when strain limits value in concrete, steel, or composite is reached (*see Table A.0.3*).

Table A.0.3. Adopted strain limits values

Strain limits	
CONCRETE	in Compression: $\varepsilon_{c.lim} = \varepsilon_{cu2} = 0.0035$
STEEL	in Compression/Tension $\varepsilon_{s.lim} = 0.01$
CFRP	in Tension $\varepsilon_{f.lim} = 0.005 \div 0.006$

By recording strain data for each load (bending moment) increment up to the ultimate load, the moment-curvature relationship can be plotted. In this study, this relationship was used to compare with experimental results.

A.2 - ADOPTED MATERIAL MODELS
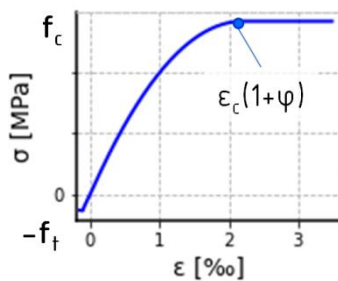
Concrete – EC2	Steel – Bilinear Model	CFRP – Linear Model
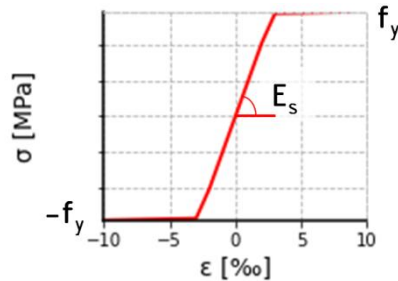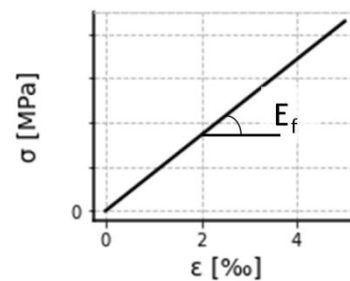
Parameters:

$\varepsilon_{c0}, f_c, f_{ct}, E_c, \varphi$ f_y, E_s, E_{sh} E_f

CFRP strengthening was implemented as optional. If strengthening influence is investigated, the linear response is considered for CFRP material where the only value of modulus of elasticity is required. For steel, the bilinear stress-strain relationship was adopted. Mathematically, positive values of the strain in the steel material model are described by yield strength, modulus of elasticity and hardening modulus. It can be expressed via the following equation:

$$\sigma_s = \begin{cases} \varepsilon_i E_s \; for \; \varepsilon_i < f_y/E_s \\ f_y + (\varepsilon_i - f_y/E_s)E_{sh} \; for \; \varepsilon_i > f_y/E_s \end{cases} \qquad (A.0.6)$$

Concrete response for concrete section design was adopted according to EC2 and [3] :
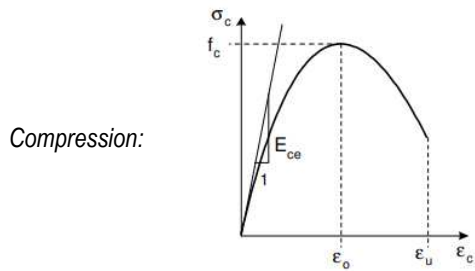
Compression:

$$for \; 0 \leq \varepsilon_{ci} \leq \varepsilon_{c2}$$
$$\sigma_{cc} = f_c \left[1 - \left(1 - \frac{\varepsilon_{ci}}{\varepsilon_{c0}} \right)^n \right]$$

$$for \; \varepsilon_{c2} \leq \varepsilon_{ci} \leq \varepsilon_{cu}$$
$$\sigma_{cc} = f_c$$

$$(A.0.7)$$

Tension
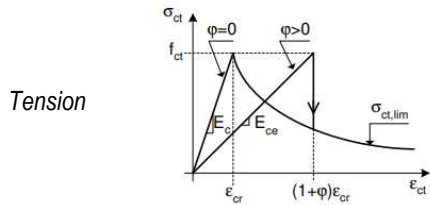
$$\sigma_{ct} = \begin{cases} \varepsilon_i E_{ce} \; for \; \varepsilon_{ci} < f_{ct}/E_{ce} \\ 0 \; for \; \varepsilon_{ci} > f_{ct}/E_{ce} \end{cases} \qquad (A.0.8)$$

where:

ε_i -   compressive strain at point i
k = $E_{ce}\varepsilon_{c0}/f_c$
ε_{c0} = $\varepsilon_0(1 + \varphi)$

An increase in total strain in case of long-term effects like a creep can be included in the calculation based on the concept of increasing ε_0 strain value [3] and introducing effective modulus of elasticity related via creep coefficient:

$$E_{ce} = \frac{E_c}{1 + \varphi} \qquad (A.0.9)$$

A.3 - DEFLECTION CALCULATION

For the calculation of the deflection, the tool uses the moment-area method [14] based on Mohr's theorems [16] relating rotations, curvatures and deflections. Calculation of deflection requires obtained previously moment-curvature response of the analysed beam in bending in the given section. The numerical procedure starts from the plot of the bending moment diagram along the beam for the given length and chosen load configuration. If each bending moment value is referenced to the curvature value, a curvature diagram along the beam can be determined with the use of the bending moment diagram. Calculations of rotations and as a consequence deflections (equations A.0.10 ÷ A.0.12) at any point may be calculated using numerical integration of expression under integral based on the curvature diagram (see Fig. A.0.4). For numerical integration trapezoidal rule was adopted.
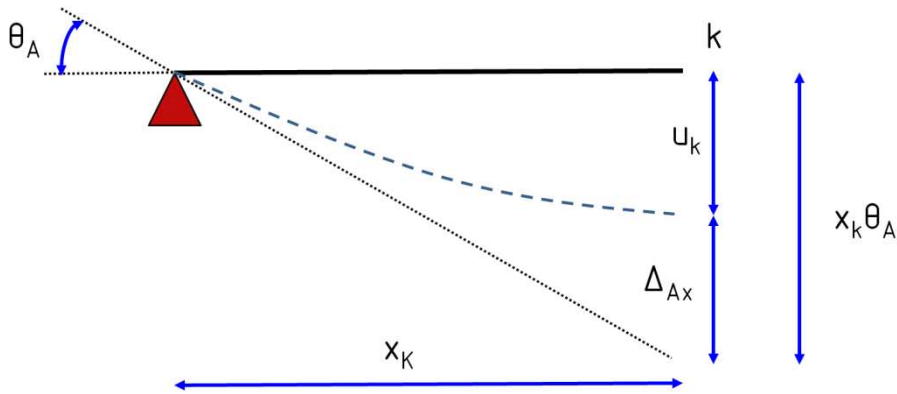
Fig. A.0.3 Rotation and deflection relationship (based on [6])

$$u_k = \theta_A x_k - \Delta_{Ax} \tag{A.0.10}$$

$$\theta_A = \frac{\Delta_{AB}}{L} = \frac{1}{L} \int_A^B \frac{M}{EI} \cdot \overline{x_{\iota B}} \, dx = \frac{1}{L} \sum_{i=1}^{n} x_{iB} \cdot A_i \tag{A.0.11}$$

$$\Delta_{Ax} = \int_A^k \frac{M}{EI} \cdot \overline{x_{\iota k}} \, dx = \sum_{i=1}^{n} x_{ik} \cdot A_i \tag{A.0.12}$$

where:

θ_A -   Rotation at support A

x_{ik}, x_{iB} -   Distance to a given point of integration from support A, Distance from support B

Load – deflection response of a simply supported beam can be obtained in the following steps:

1) Calculation of moment-curvature response in the considered load range,

2) Determine the bending moment diagram along the beam considering boundary and load conditions,

3) Determine the curvature diagram along the beam based on the moment-curvature response

4) Numerical integration of curvature diagram by dividing it into a finite number of segments and calculating the area, centroid and the first moment of area of each segment about point k and point A,

5) Calculate deflection based on geometrical relationships of rotations and tangents.
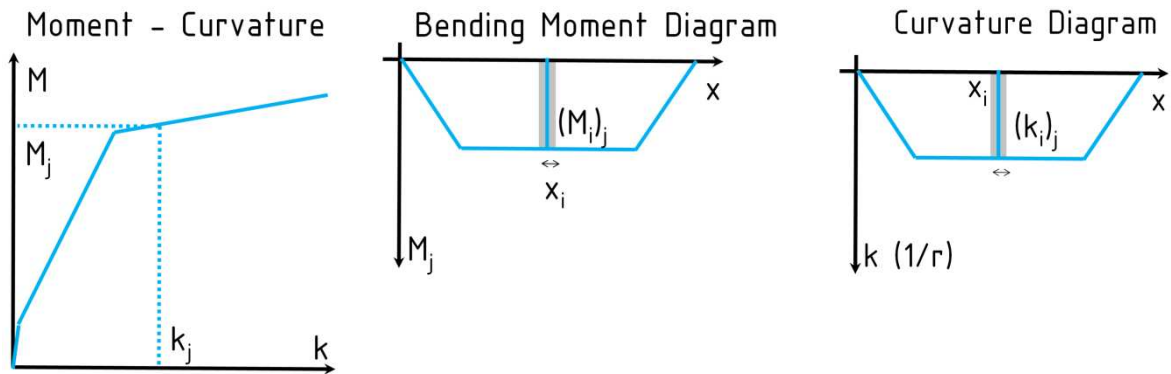
Fig. A.0.4 Deflection calculation concept based on (based on [6])

The tension stiffening effect is represented through optional concrete tension softening (stress-strain diagram) after crack formation. In Fig. A 0.5 set of load-deflection curves was compared for the beam model (described in the numerical part of this study) without tensile strength (NC), with the only elastic response (0) and with tension softening in the post-elastic response taken into account.
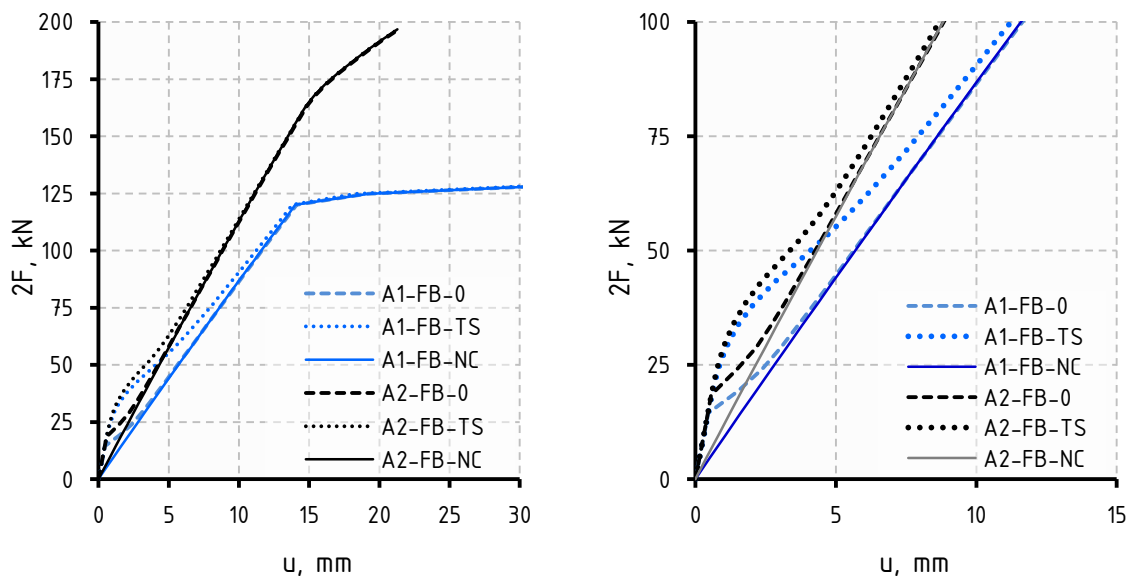
Fig. A 0.5.: Comparison of load-deflection curves: NC – Concrete carries no tension, TS - Tension Stiffening, 0 – Linear behaviour of concrete up to tensile strength a) overall response b) zoom at an early stage of loading

127

Although response at the early stage varies between models, there is no significant difference in overall response and ultimate load value.

A.4 - MODEL VALIDATION

The tool prepared according to the rules presented above can be used to compare moment-curvature and load-deflection response, as well as strain at steel, concrete and composite obtained in the experimental study. Here, three different specimens based on available literature were selected to verify the correctness of the proposed tool and its predictive ability [58][67][83][89]. Specimens vary in terms of length, cross-section dimensions, concrete as well as steel and CFRP reinforcement. Specimens were tested in a four-point bending test with different point load configurations (*see* Fig. A.0.6). The experimental setup for each beam was presented in Fig. A.0.7 and material properties were summarised in Table A.0.4.

a) Krzywoń et. al [89]
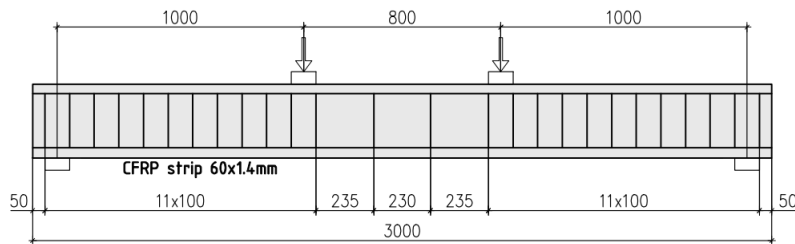
b) Kamińska, Kotynia (2000) [67]
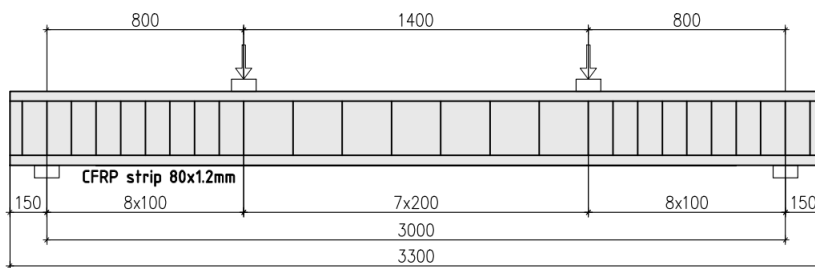
c) Kotynia, Kamińska (2003) [83]
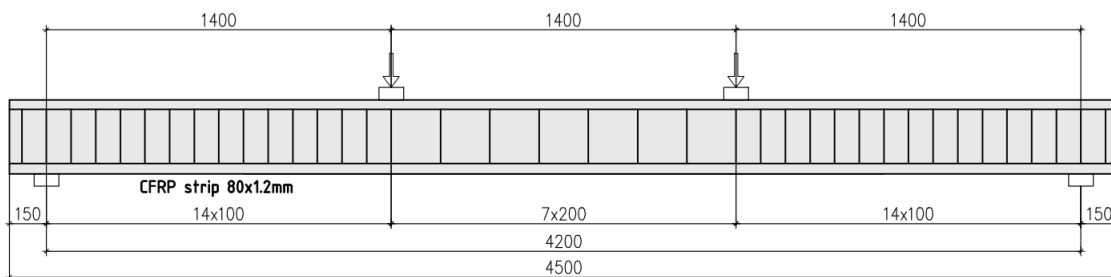
Fig. A.0.6 Experimental setup for verified beam specimens
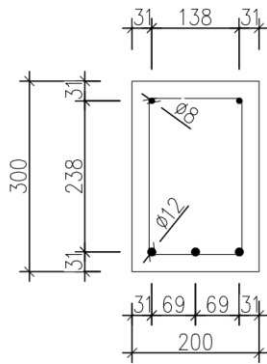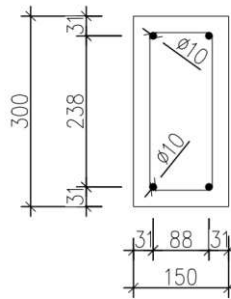
a) Krzywoń et. al [89]   b) Kamińska, Kotynia (2000) [67]   c) Kotynia, Kamińska (2003) [83]
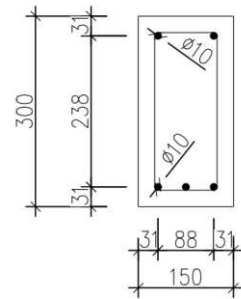
Fig. A.0.7 Cross-sections for selected beams used invalidation

Table A.0.4. Input material parameters of considered specimens

Material	Parameters	Krzywoń et. al [89]	Kotynia, Kamińska (2003) [83]	Kamińska, Kotynia (2000) [67]
CONCRETE	ε_{c_1}, mm/m	0.0022	0.0022	0.0022
	f_c, MPa	44.7	32.3	28.5
	f_{ct}, MPa	3.20	2.80	2.73
	E_c, GPa	31.0	22.7	23.4
	φ, ---	0	0	0
STEEL	f_y, MPa	570	(493)/(524)	421
	f_t, MPa	660.8	(688-126) (647-115)	651
	E_s, GPa	200.7	(215)(209)	199.5
CFRP	E_f, GPa	171.2 (60x1.4)	172 (80x1.2)	171.9(80x1.2)

Based on available data from a study conducted by Krzywoń et al. [89], load-deflection curves of strengthened and non-strengthened RC beams (Fig. A.0.8a) were compared. Good agreement in curves close to the ultimate load can be found. The difference in ultimate load does not exceed 1% and 4% relatively for strengthened and non-strengthened beams. A little underestimation of stiffness can be noted just after the load value related to the cracking moment. Similar behaviour comparing composite strain at midspan as a function of load (Fig. A.0.8b) in the case of the strengthened beam can be found.
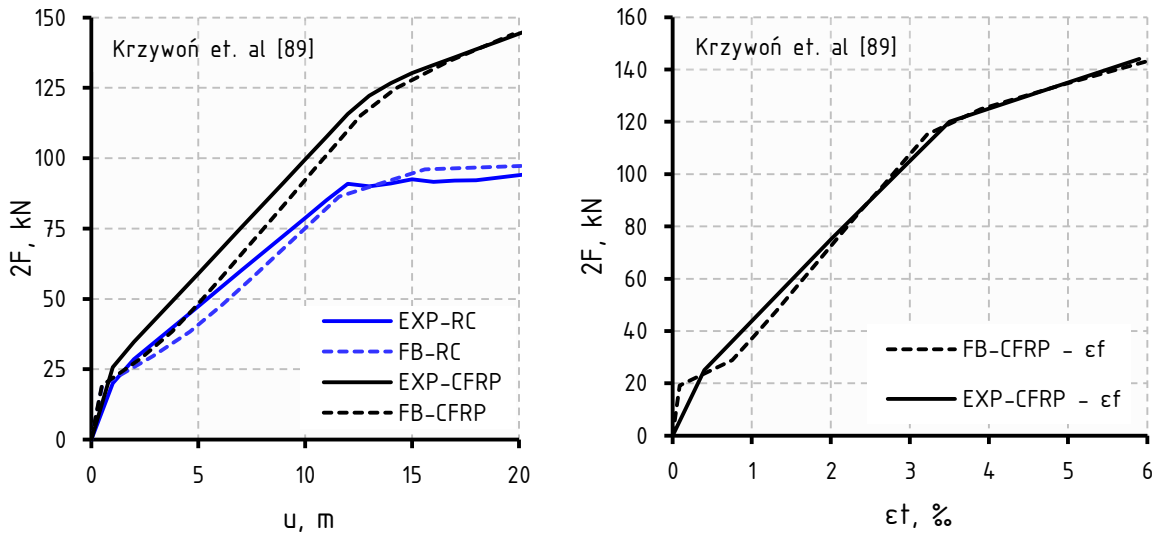
Fig. A.0.8.: Comparison of experimental and fibre-beam analysis results of mid-span load-deflection response a) and mid-span composite strain of CFRP strengthened RC beam b)

More relevant differences were observed when specimen B0-04/S in accordance with the study conducted by Kaminska and Kotynia was analysed (*see Fig. A.0.9a and b*). About a 12% difference in the value of strain referring to the ultimate bending moment was noted.
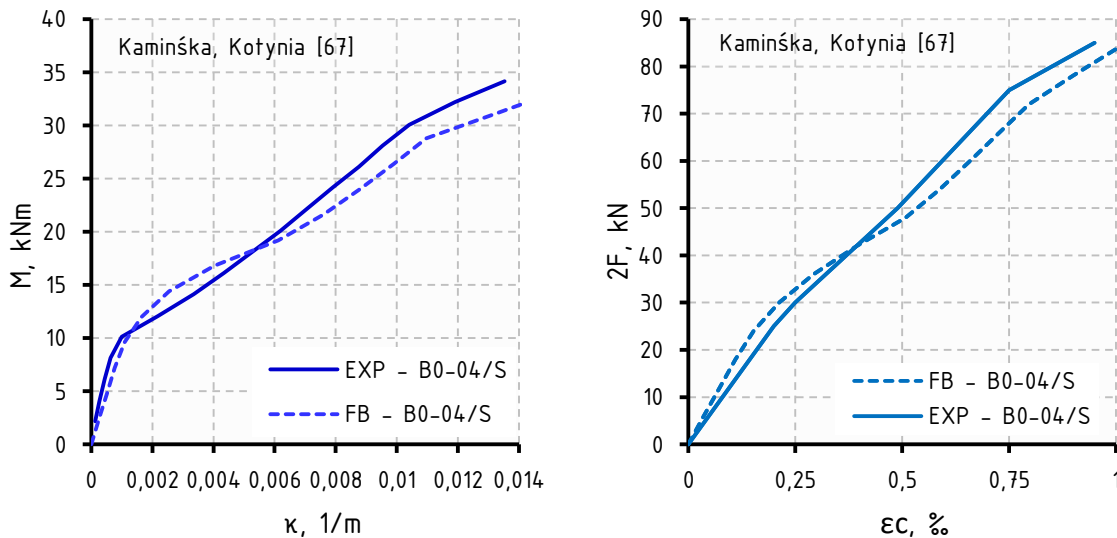
Fig. A.0.9.: Comparison of experimental and fibre-beam analysis results of mid-span load-deflection response a) and mid-span compressive strain of concrete b)

For the next comparison, another sample of the experimental study performed by the same research team [83] has been chosen (specimen B-08/S). Good agreement is obtained results of the ultimate load can be observed in both the load-deflection curve as well as CFRP strain response (*see Fig. A.0.10a* and *b*). A similar disturbance can be noted in the proximity of the cracking load. This is related to the lack of tension stiffening effect after cracking load and sudden drop of stress down to zero value.
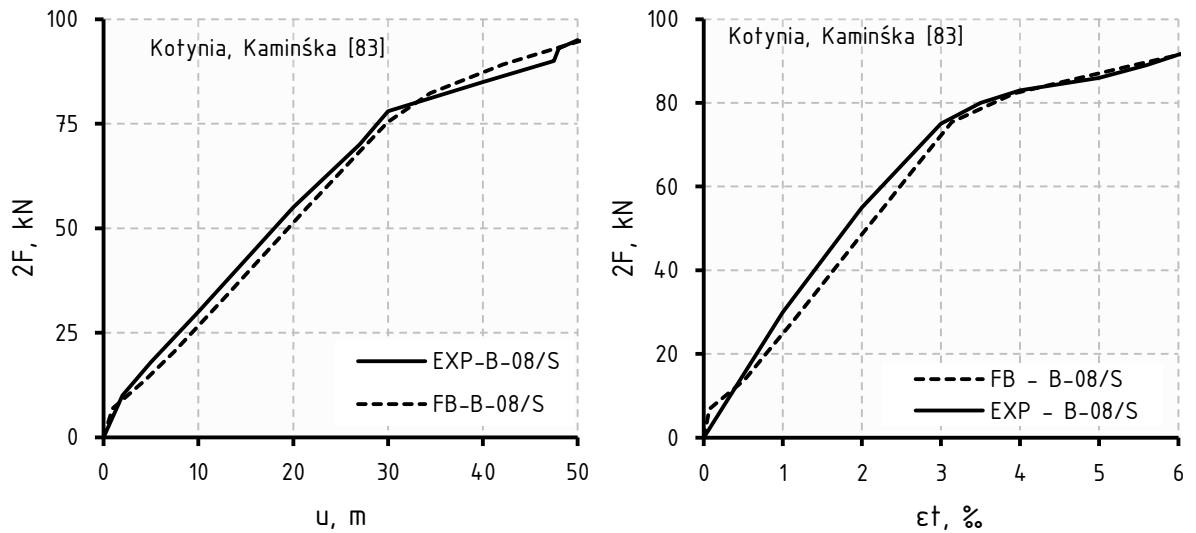
Fig. A.0.10.: Comparison of experimental and fibre-beam analysis results of mid-span load-deflection response a) and mid-span composite strain of CFRP strengthened RC beam   b)

Based on the relatively good agreement of results obtained from fibre–beam analysis in comparison to available data from different experimental studies can be concluded that the developed tool has been properly prepared and have the predictive potential for studies of reinforced concrete beams both non-strengthened and strengthened (with perfect bond assumption) subjected to monotonic load. The tool also has great potential for even designing purposes, and various effects of analysis can be additionally developed. More information about source code can be found at [E1].

[E1]	Bialozor R.: Beams in Bending in Python, Online source code repository, *https://github.com/rbialozor/phD* [online] (available: January 2022).

APPENDIX B – INITIAL VERIFICATION OF THE CDP MODEL

To initial verification of the CDP model, available in literature laboratory results of RC beams strengthened with CFRP were recreated in numerical analysis. Following analysis based on results obtained at Łódz University of Technology. Beam signed as B-04/S and its material investigation have been chosen [66][67]. The beam geometry and material properties were presented in Fig. B.0.1 and Table B.0.1.
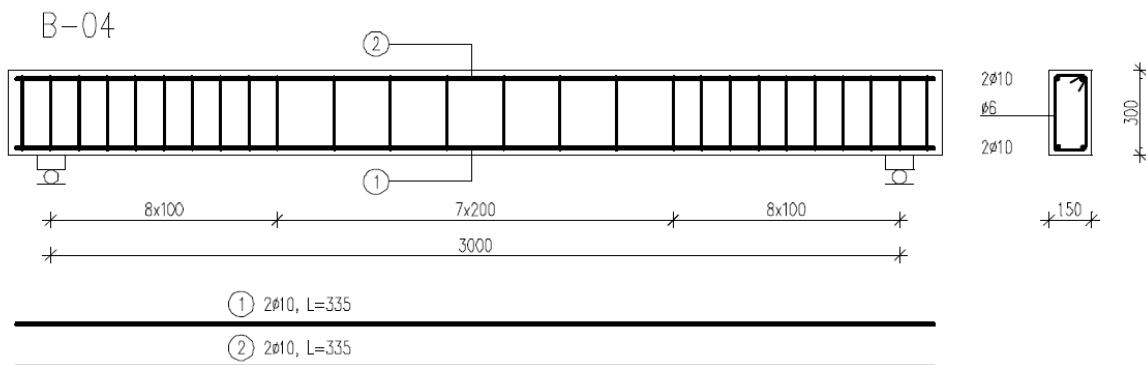
Fig. B.0.1.: Geometry and reinforcement data of specimen B-04/S [66][67]

Table B.0.1. Input material data and parameters for the CPD model

Concrete								
E_0, GPa	v	ψ, °	σ_{b0}/σ_{c0}	e	K_c	μ	f_c, MPa	f_{ctsp}, MPa
23.40	0.2	35	1.16	0.1	0.667	0.001	28.4	2.8

Steel					
	E_s, GPa	f_y, MPa	f_t, MPa	ε_t, ‰	-
Φ10	199	421	651	-	-
	E_s, GPa	f_y, MPa	f_t, MPa	ε_t, ‰	-
Φ6	207	437	501	-	-

CFRP						
E, GPa	v	ε_{pu}, ‰	f_p, MPa	t, mm	b, mm	-
171.5	0.3	17.1	2915	1.2	80	-

Stress-strain relationship and damage variables for concrete tension and compression were calculated according to the procedure in chapter 5.
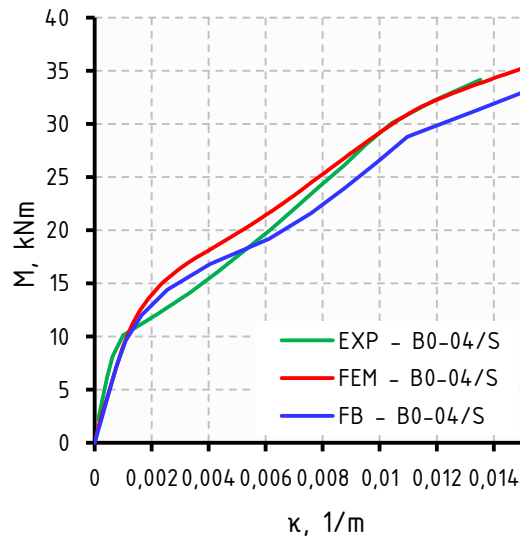
*Fig. B.0.2.: Comparison of the moment-curvature response of specimen B-04/S
(based on data from [66][67])*

Moment – curvature response for the considered specimen received from the numerical study was presented in Fig. B.0.2. Good agreement in terms of the ultimate load has been obtained. A slight overestimation of the cracking moment has been observed in both FE and FB methods Comparable crack pattern in form of damage variable in tension has been observed (*see Fig. B.0.3*). The range of crack patterns along the beam is also coherent with the experiment.
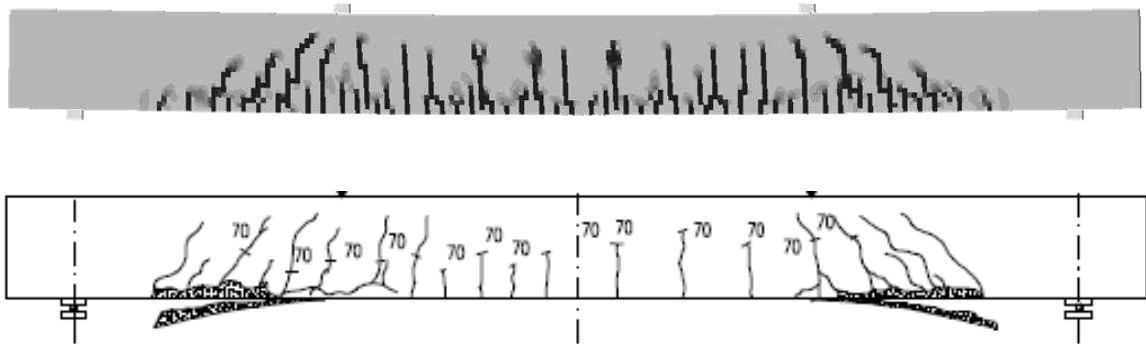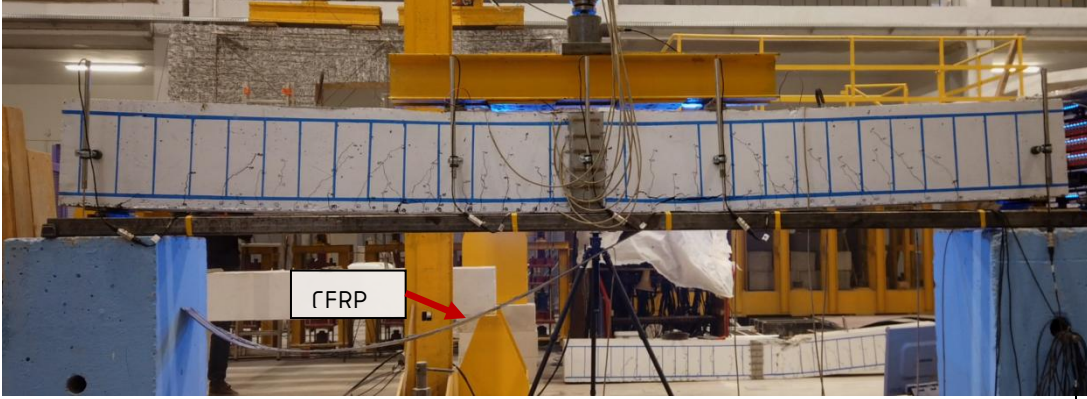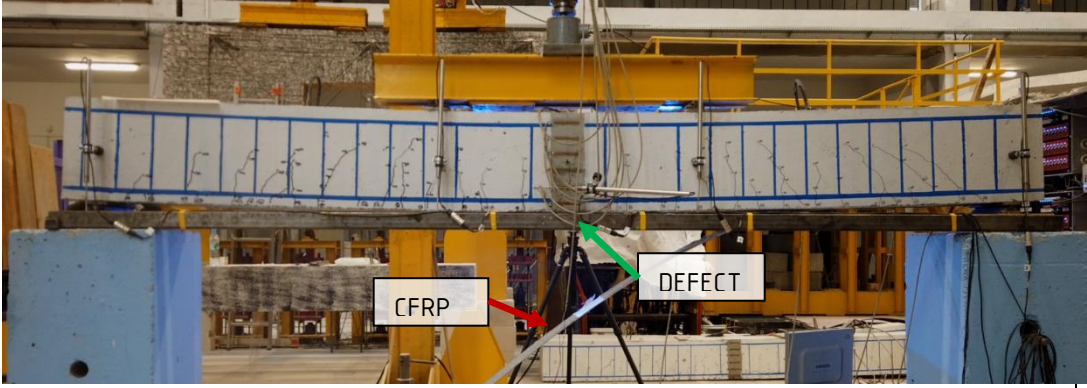
Fig. B.0.3.: Comparison of the crack pattern obtained in an experimental study [66] with damage variable in the numerical model

APPENDIX C – FAILURE MODES OF TESTED STRENGTHENED BEAMS

A2 (IC)	
A3a (IC)	
A3b (IC)	
A3c (IC)	

B3a (CSS)	
B3b (CSS)	
B3c (CSS)	
A6 (IC)	
IC - Intermediate crack debonding, CSS - concrete cover separation	
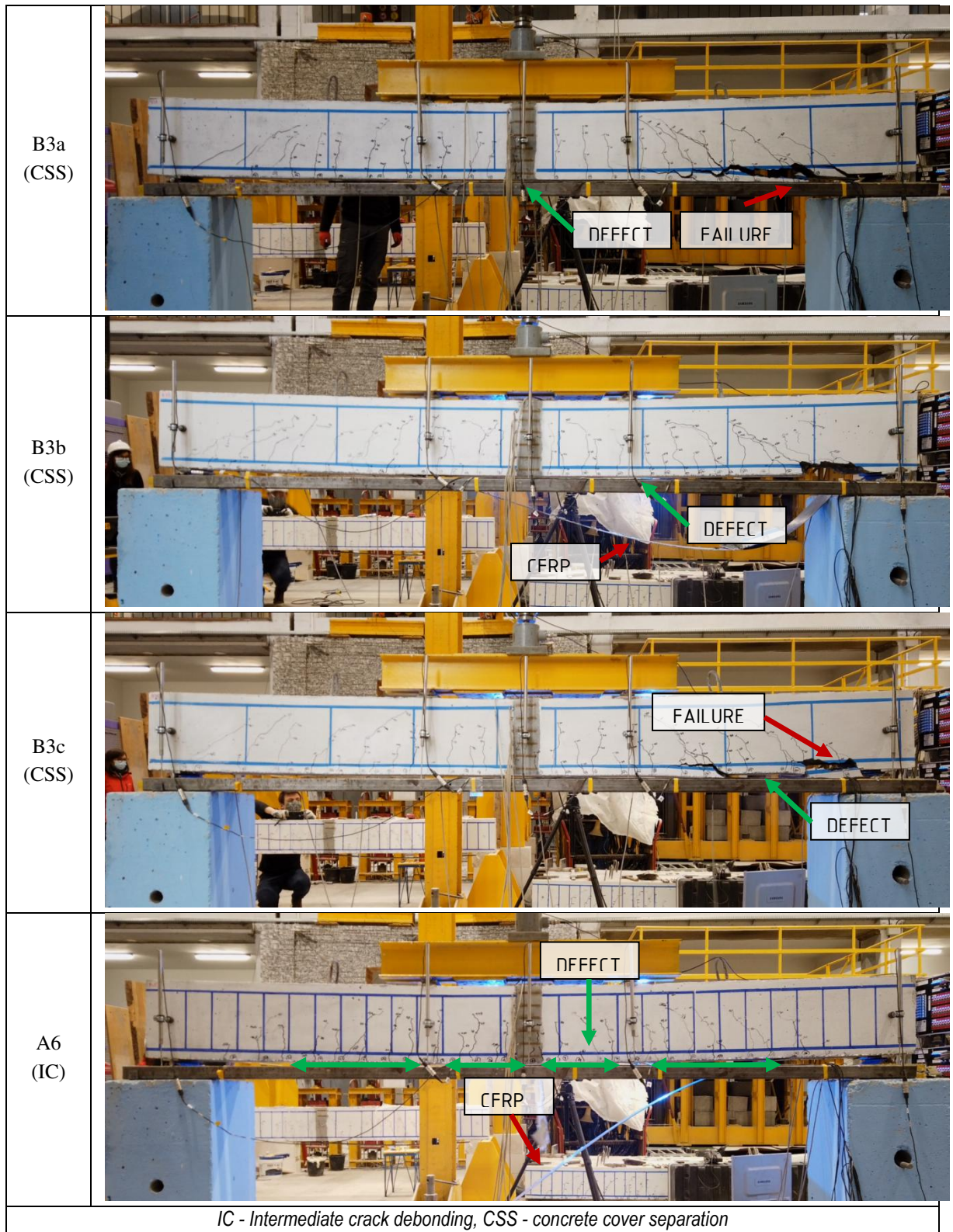
Fig. C.0.1.: List of failure modes of beam specimens recorded in the experimental study with suggested theoretical identification (in brackets)

APPENDIX D – STRAIN DIC RESULTS

Beam - A1
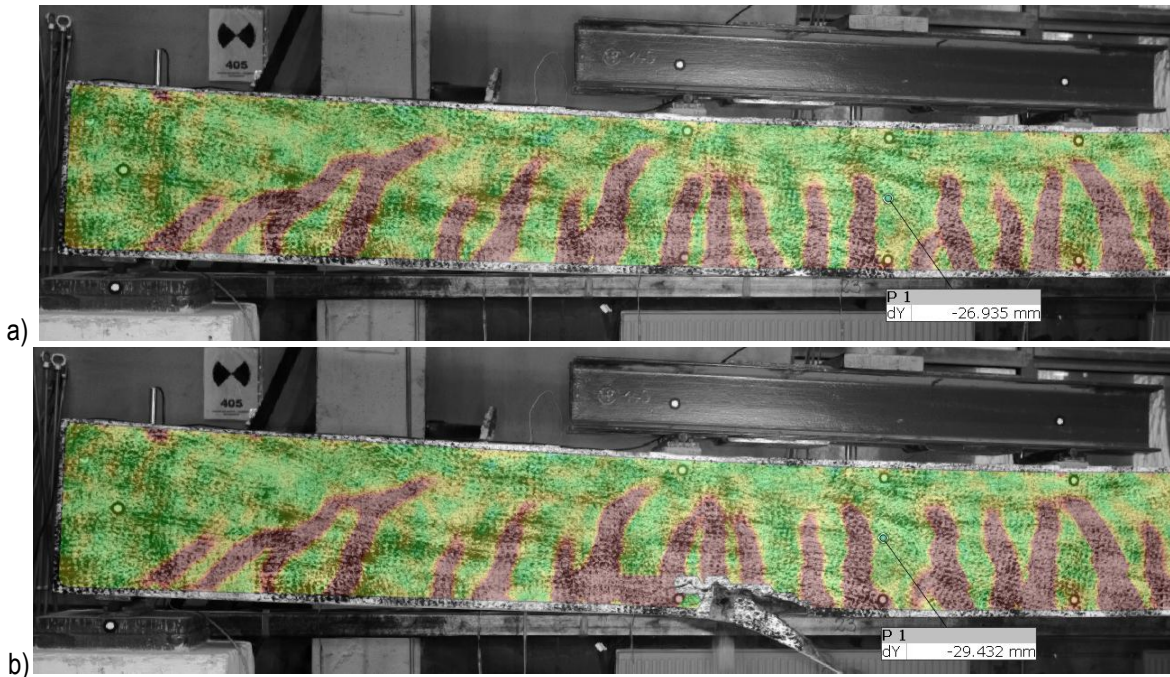
Fig. D.0.1 Strain ε_1 distribution in specimen A1 a) before and b) after failure

Beam – A2
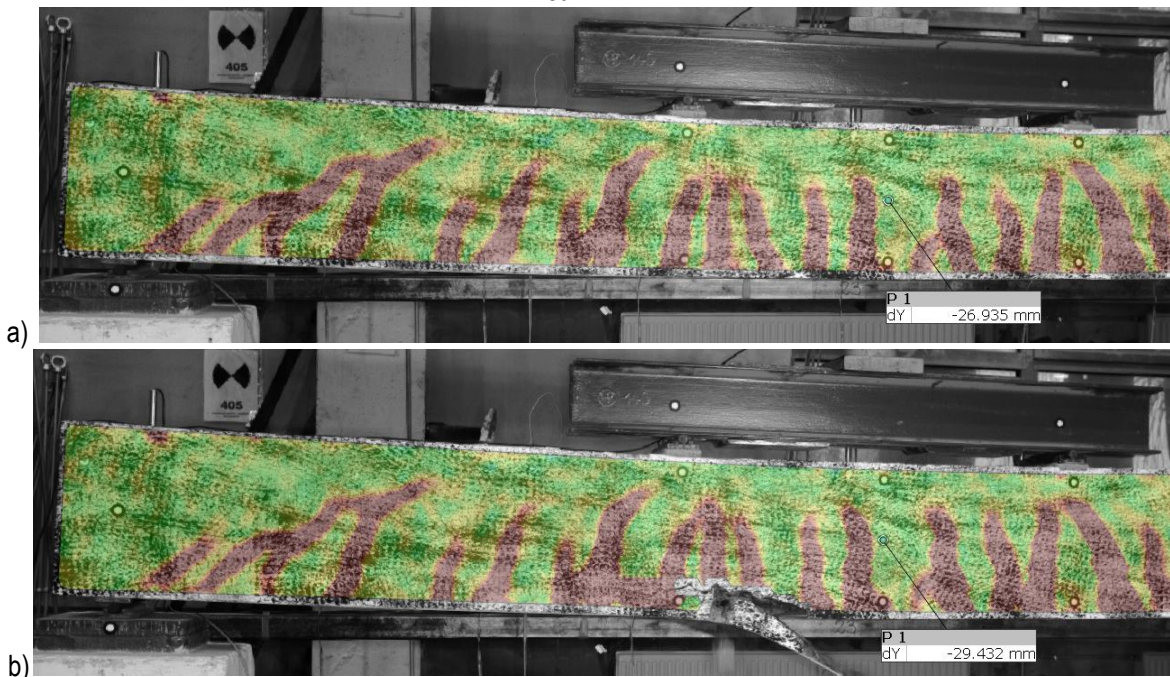
Fig. D.0.2 Strain ε_1 distribution in specimen A2 a) before and b) after failure

Beam – A3a
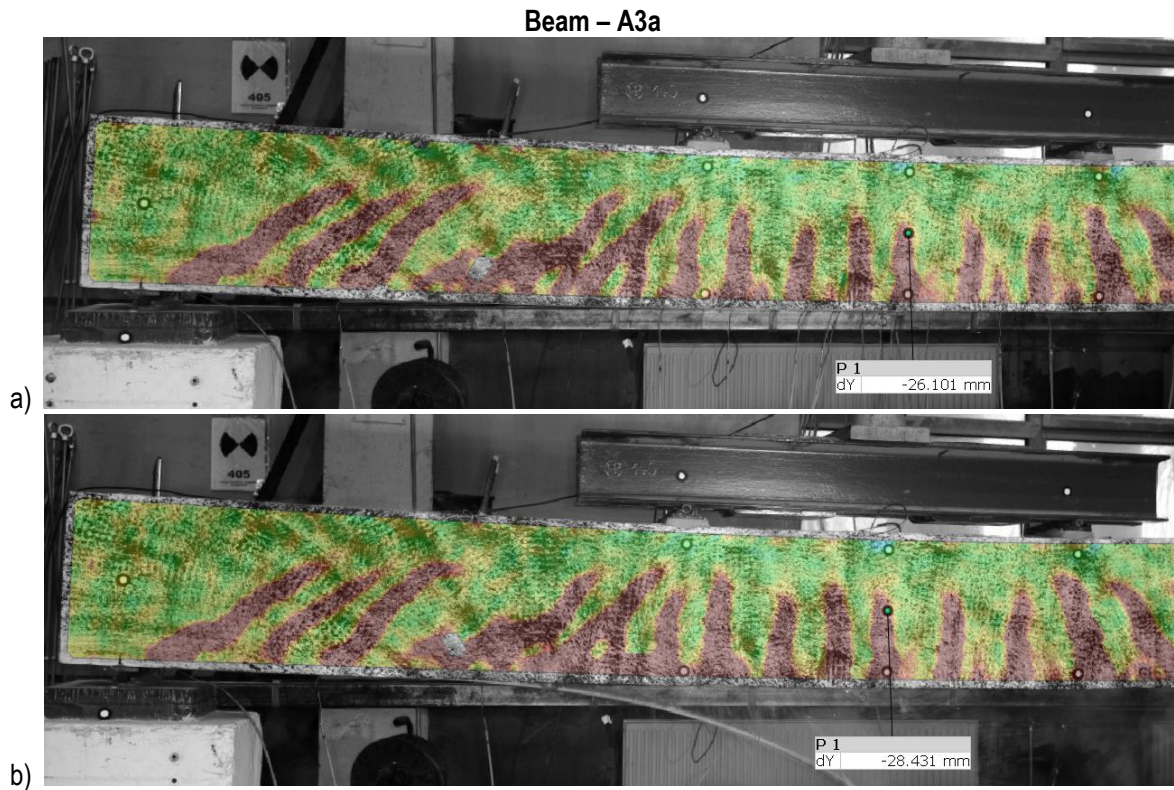
Fig. D.0.3 Strain ε_1 distribution in specimen A3a a) before and b) after failure

Beam – A3b
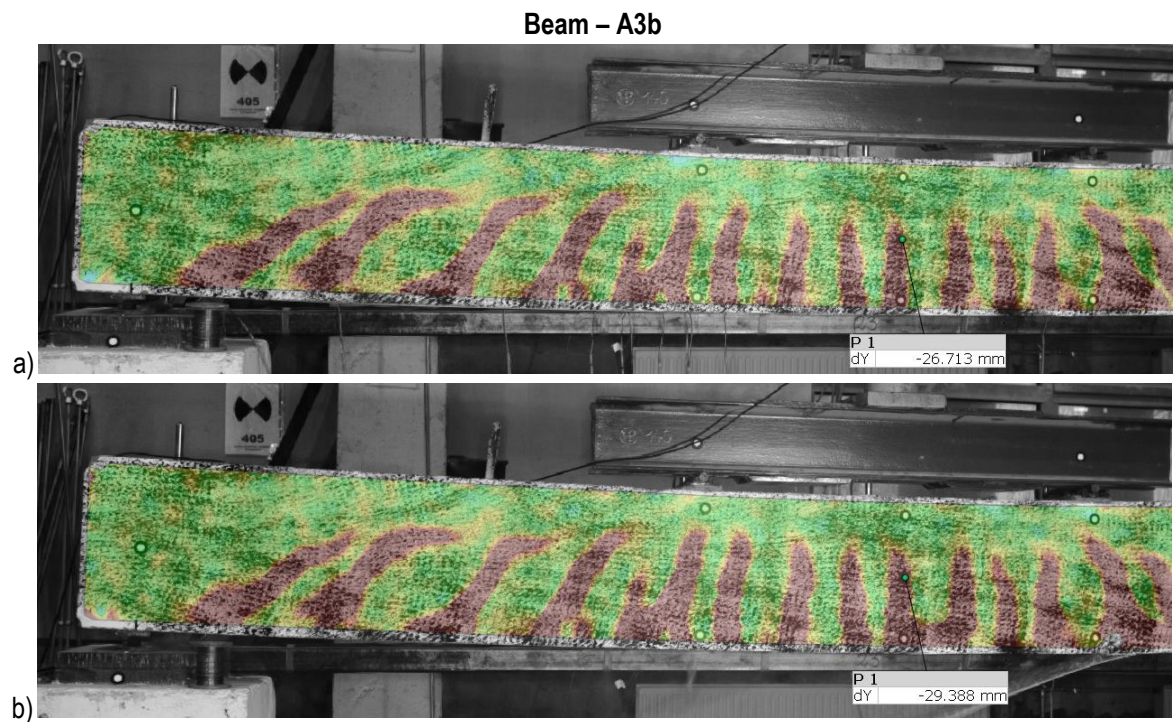
Fig. D.0.4 Strain ε_1 distribution in specimen A3b a) before and b) after failure

Beam – B3a
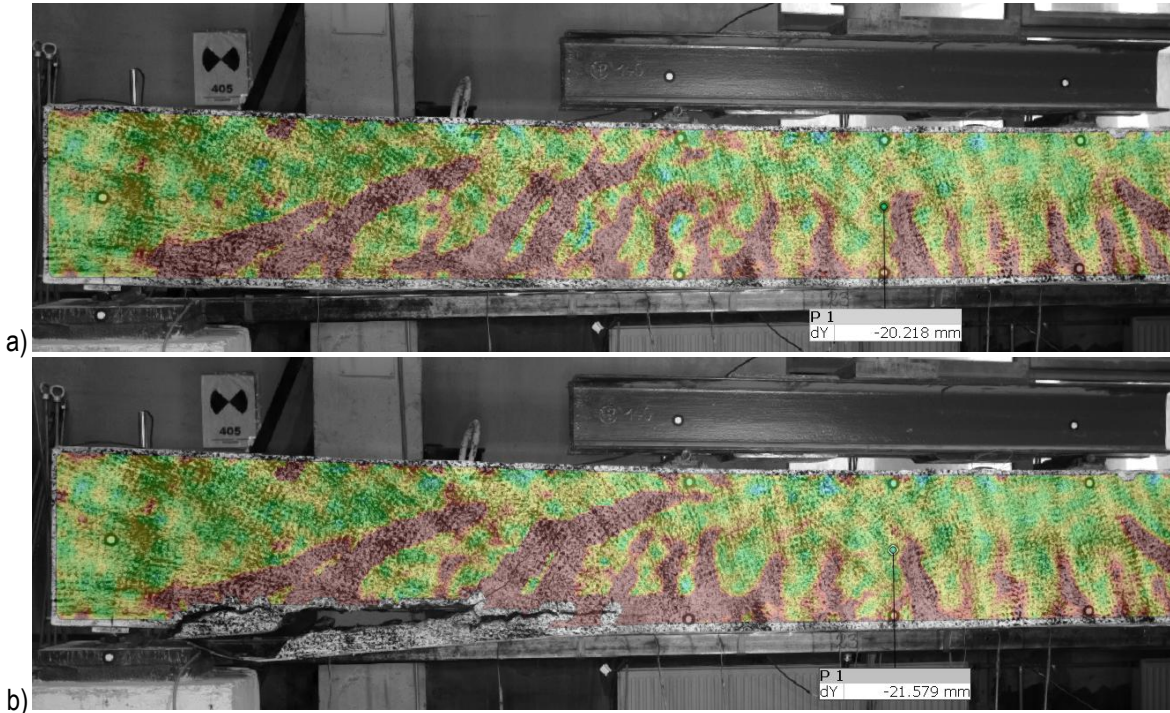
Fig. D.0.5 Strain ε₁ distribution in specimen B3a a) before and b) after failure

Beam – B3b
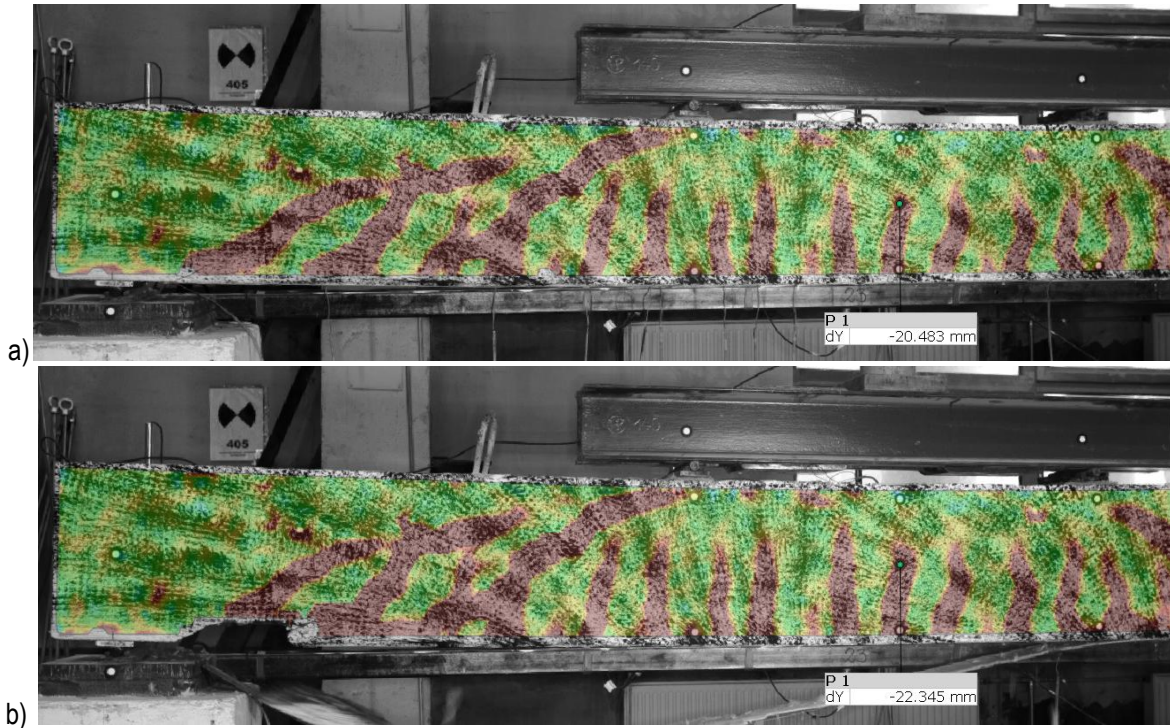
Fig. D.0.6 Strain ε₁ distribution in specimen B3b a) before and b) after failure

Beam – A6
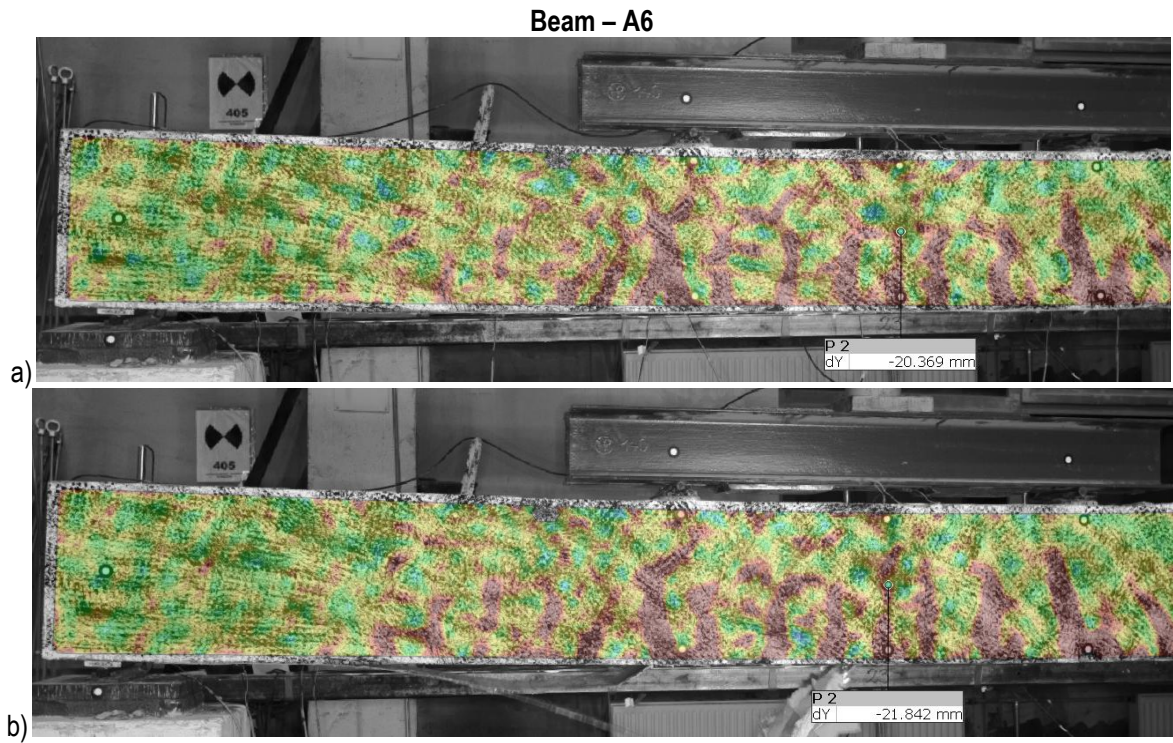
Fig. D.0.7 Strain ε_1 distribution in specimen A6 a) before and b) after failure

LIST OF FIGURES

LIST OF TABLES